Deutsches Zentrum
für Luft- und Raumfahrt
German Aerospace Center

Universität Bremen

Finite Element Model Correlation and Evaluation of the Design of a Structural Support for the DLR Shell Lander.

Master thesis

Presented to the Faculty 04 - Production Engineering

Universität Bremen

In the partial fulfilment of the requirement for the degree of

Master of Science

In

SPACE ENGINEERING

By

Pushya Subramanyam

3124749

Universität Bremen

Supervisor:

Prof. Dr.-Ing. Andreas Rittweger

Institute of Space Systems

DLR, Bremen

Supervisor:

Christian Grimm MSc., MSc.

Institute of Space Systems

DLR, Bremen

June, 2020

Universität Bremen

The following declarations are to be included in every exemplar of the Bachelor's and Master's Thesis

Name: **Pushya Subramanyam** Enrolment number: **3124749**

Declaration of copyright

Hereby I declare that my Master's Thesis was written without external support and that I did not use any other sources and auxiliary means than those quoted. All statements which are literally or analogously taken from other publications have been identified as quotations.

Date: Signature 

Declaration with regard to publishing theses

Two years after the final degree, the thesis will be submitted to the University of Bremen archive and stored there permanently.

Storage includes:

1) Master's Theses with a local or regional reference, as well as 10 % of all theses from every subject and year
2) Bachelor's Theses: The first and last Bachelor degrees from every subject and year

☒ I agree that for research purposes third parties can look into my thesis stored in the University archive.

☐ I agree that for research purposes third parties can look into my thesis stored in the University archive after a period of 30 years (in line with §7 para. 2 BremArchivG).

☐ I do not agree that for research purposes third parties can look into my thesis stored in the University archive.

Date: Signature 

Declaration

Acknowledgement

I wish to express my sincere thanks to Universität Bremen and DLR, Institute of Space Systems, Bremen for providing the opportunity and for making it possible for me to have a Master degree in Space Engineering.

My sincere thanks to Prof.Dr.Andreas Rittweger for being a wonderful mentor and inspiring me to develop my interest on structural design and analysis even further. It is he who also insisted me to get in contact with Dr.Lars Witte, another mentor I cannot thank enough for being so very kind. My greatest regards to him for finding time in answering the mails and giving me an opportunity to work on my Master Thesis and my Master Project at the Institute of Space Systems, DLR.

My deepest gratitude to my supervisor Mr.Christian Grimm for patiently guiding and giving excellent inputs at every step. My heartfelt thanks for being a great source of motivation throughout the work, without who the success of this work might not have been possible. I would also like to thank Dr.Marco Scharringhausen, the kindest person who has guided and helped me in many ways throughout my studies.

I also wish to express my immeasurable thanks to my parents and my friends for being the strongest pillar of support through out my life. They have always encouraged me to take a step forward towards my goals, each time I felt otherwise.

Lastly, my regards to this beautiful land of Earth for giving me the knowledge not only about Space Engineering but also about life as one of the Indian quote says $Vidhya\ Dhanam,\ Maha\ Dhanam$ which translates to $Knowledge\ shared\ is\ the\ biggest\ charity$. Additionally my little regards to the whole Universe for resonating the Space-time continuum in positive vibration around me.

Abstract

The current work is a correlation between models of finite element analysis and laboratory test models. The second task of this work involves the evaluation of the design of a rigid interface frame requirement for a concept study of an asteroid lander -a freely falling scientific object. The lander in consideration is similar in size, shape and mass to that of the Mobile Asteroid Surface Scout (MASCOT). The development of the lander concept has led to the requirement of having an outer protective covering (cushion) that acts as an energy absorber in order to protect the internal instruments when impacted on a hard surface. This cushion is a sandwich panel with aluminum honeycomb core and Dyneema composite face sheet. The advancement on study of cushion geometry has opened to two models. The efficiency of the cushion as energy absorber is experimented at DLR laboratory with test setups for different impact conditions. Major difference in the surface on which the cushion impact considered, is on a flat surface target and a penetrator target. The performance of the cushion is also tested by varying the number of face sheets glued over the core. Crash analysis by finite element model of the cushion is developed for the laboratory test condition and the properties of the core and the face sheet is optimised. These finite element models are correlated with laboratory test condition for the first model of the cushion. On impact, cushion absorbs energy up to its absorption capacity. The load transfer results in the deflection of the sandwich cushion panel. A possible solution to over come this deflection was to provide a rigid frame support. The frame is designed with the requirement to accommodate a load cell to measure the impact force and to provide attachment points between the cushion and the housing. An evaluation on the provision of the frame to prevent the bending is predicted with the second model of the cushion.

Keywords: Asteroid landers, Damping system, Energy absorbers, Dynamic impact analysis, LS Dyna, *MAT_126, *MAT_054, CATIA V5.

Contents

List of Figures

List of Tables

1 Introduction

"Exploration is in our nature, we began as wanderers and we are wanderers still."
— Carl Sagan

1.1 Motivation

Curiosity on exploring the lands farther away from Earth or human reach is one of the main driving force for constant improvement of current space technology to explore and widen the horizon of our knowledge on the existence of extra-terrestrial life or to understand the surface characteristics of the target object or to learn the atmospheric constituents and its changes. This work is yet another concept study on an exploration and landing system such as the *Landers*.

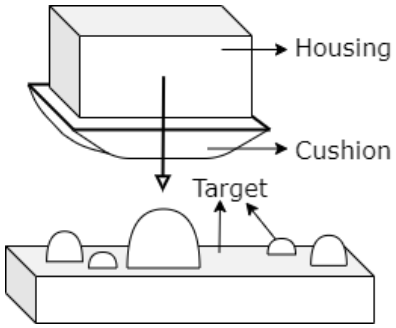

Figure 1: Concept study of lander under free fall on a relatively large celestial object which has higher surface gravity. The lander has a housing protected with a shell covering (cushion) falling on an target surface.

The study of the lander in this work are for exploring relatively large celestial objects such as an asteroid. The model concept in consideration is a generic instrument carrier similar to that of the Mobile Asteroid Surface Scout (MASCOT). MASCOT as such did not require a damping system since its was used for exploring objects of lower surface gravity and therefore was under low impact velocity.[18]. When landers are dropped towards the object in study, impact forces are apparent at touchdown. Severity of impact can vary depending on surface gravity of the target object, lander mass and velocity of decent. If the landers are dropped on relatively large celestial objects which has relatively higher surface gravity, the lander is under higher velocity of impact that further results in higher shock load in the system.[6]. To reduce the transfer of shock loads on the lander a possible solution investigated by the DLR Institute of Space Systems in Bremen is to accommodate an outer protective covering (cushion) that acts as an energy absorber in order to protect the internal instruments on impact. The figure 1 depicts a lander under free fall condition, falling on a surface which could be a flat surface or on an obstacle. It shows a housing that carries the scientific instruments, provided with a cushion and the terrain of the target surface. The different possibilities on which the lander could fall on, is a flat surface or an obstacle that could penetrate through the cushion. The concept of cushion and its

geometry has a series of development which is discussed in section 1.2. The current work is based on the study of the cushion for these impact conditions. Multiple laboratory tests are carried out and a impact velocity 4m/s is seen. These studies are to be FEA setup and a correlation of the laboratory tests are to be carried out.

1.2 Challenges and Difficulties

The first concept of the cushion was chosen based on the concept of MASCOT-1.[6] The cushion model was decided to be placed all sides of the housing to account for the ambiguity of landing orientation. Once at rest the cushion would unfold, uncovering the housing for the instruments to execute their tasks.[6] Figure 2 shows early design concept of the shell covering. The cushion was chosen to be given on all sides of the housing which then unfolds. The unfolding of the cushion is seem on the left. The cushion geometry of this concept is referred as *Model 1*. A FEA model for the laboratory tests conducted on this model of cushion is to be correlated.

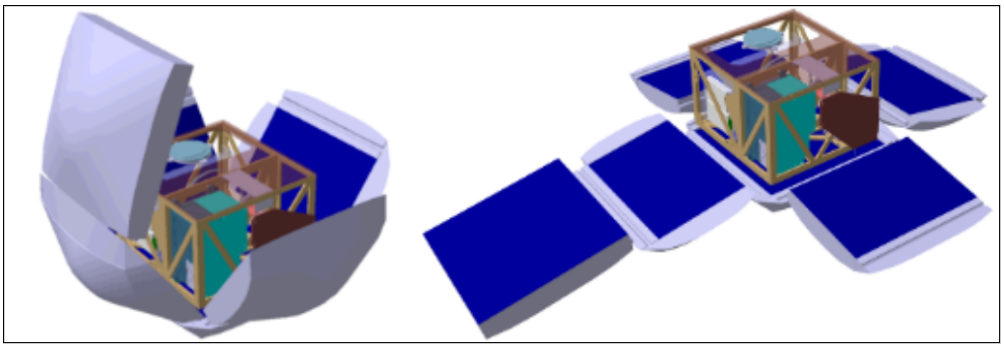

Figure 2: Early design concept of the cushion model 1. The cushion is given on all sides of the housing. The unfolding process of cushion is also shown.[6]

In the first model of the cushion- Model1, cushion blocks are required even at the corers of the housing. The strong axis of the cushion block was place at 45°to the central axis of the housing at the corners to accomplish the fact of placing the honeycomb cells in the energy absorbing direction. Although there were cushion elements at the corners, the damping effect was mostly due to the attachment and not the cushion itself.[18] Figure 3 shows the sectional cut out of the cushion Model 1 given on all sides of the housing. The arrow highlights the geometry of the cushion. The side edges of the cushion model 1 is a straight cut that is fixed to the corner block of the cushion. The placement of the cushion with corner block at 45°is also illustrated. A correlation of the results seen on the laboratory test performed on this geometry is considered in the current work.

Developing this concept further, the geometry of the cushion was improved to reduce the number of cushion elements and to have the damping effect at the corners by the cushion.[6]. Figure 4 shows the advancement of the cushion geometry with fewer cushion block. The corner blocks of the cushion are compensated by the geometry. This cushion model is referred as *Model 2*. A relative change in the cushion geometry

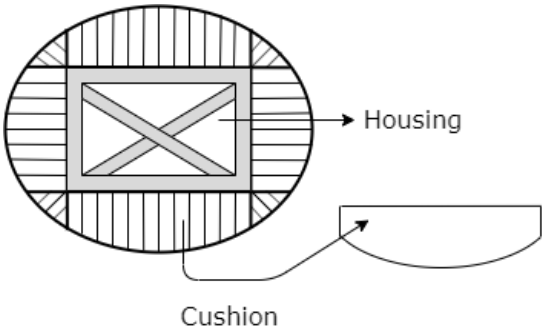

Figure 3: Sectional cut out of cushion and housing with cushion Model 1 when given on all sides of the housing. The geometry of cushion model 1 is highlighted. (*reproduced based on* [18])

can be made by comparison of figure 3 and figure 4.

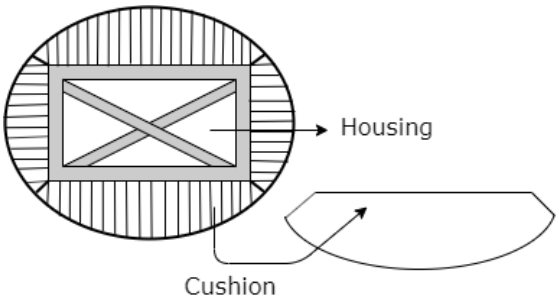

Figure 4: Sectional cut out of cushion and housing with cushion Model 2 when given on all sides of the housing. The geometry of cushion model 2 is highlighted. (*reproduced based on* [6])

The final development of the cushion concept has been to provide the cushion on one side of the housing. This is to reduce the overall mass and volume and to decrease the complexity with the unfolding of the fully covered cushion. This lander system will be a horizontal direction stabilized system that include instruments for attitude control.[6]. Furthermore to accommodate for the reactions seen due to impact, a frame is to be designed as an interface between the housing and cushion model 2.

Since the laboratory test were conducted for cushion geometry model 1, a correlation with FEA model is to be carried out with model 1. The laboratory test with model 2 and frame support will be performed in the future and hence a prediction is to be given for the setup with model 2.

1.3 Problem Statement

The laboratory testing of the concept of a special kind of damping system considered in the DLR shell lander project, are experimented at Landing and Mobility laboratory

test facility (LAMA) in the DLR institute with a pendulum system. The housing of lander is similar in size, shape, mass to that of MASCOT. MASCOT has a size of 300mm x 300mm x 200mm and weighs 10 kg and falls with a velocity of 4m/s.[6].

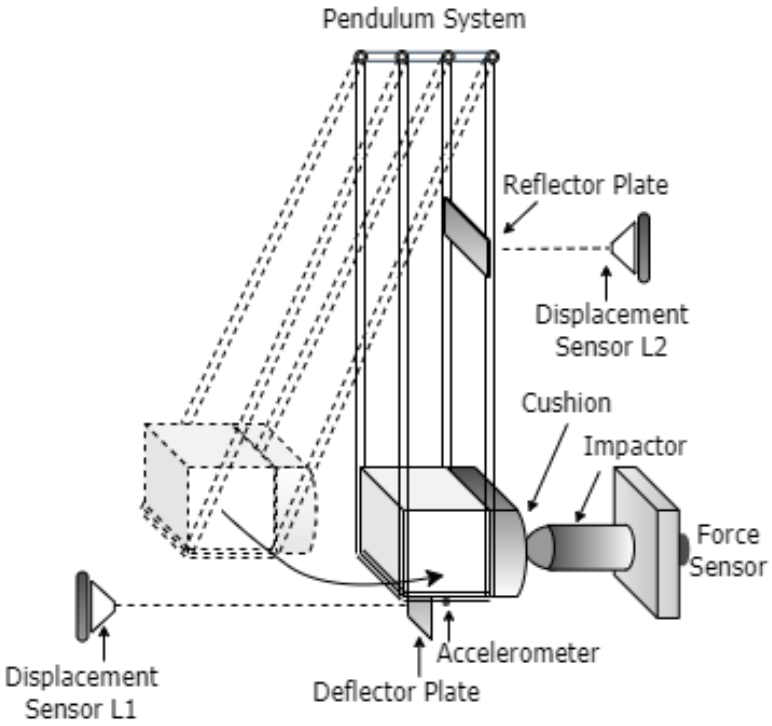

Figure 5: Pendulum test setup as used during laboratory impact tests. The setup for the shell lander is shown with different sensors placed at different positions for recording the required values. (Based on [6])

The pendulum setup is depicted in figure 5 that executes the requirement of a free fall of the lander on a surfaces. The laboratory setup is designed with the cushion being held on parallel arms of a rigid pendulum. At the start of laboratory testing the arms of the pendulum along with the cushion is held rigidly. An target is fixed firmly to one of the walls. The target is positioned such that it impinges the cushion at the centre when the arms are released from stationary state to follow the oscillatory motion of the pendulum system. [6].

During laboratory testing, different sensors are used to record the desired values. These sensors are placed at different point on the pendulum system. Two displacement sensors are used to measure the relative displacement of the arms of the pendulum and the cushion. The sensor arrangement and the pendulum system is illustrated in figure 5. One laser-deflector plate combination L1 is placed opposite to the target, which measures the cushion displacement. Another laser-deflector plate combination L2 is placed above the target wall to measure the displacement of the rigid arms of the pendulum. The displacement measured by L1 is interpolated to obtain velocity of the system. A force sensor is placed behind the mounting wall of target to measure the

impact forces on the cushion. Accelerometer is placed below the cushion to measure the acceleration of motion.

The laboratory tests are conducted with different impact condition and for different sandwich components of the cushion setup. These laboratory tests record values of displacement, velocity, force and acceleration. Finite element models are to be setup such that the results from these laboratory test condition can be correlated. The FEA model should provide a reliable finite element analysis setup for future studies. These formulation is discussed in the next section.

1.4 Thesis Statement

A correlation of results between FEA model and laboratory test model will provide a better understanding of the cushion as energy absorbers. Setting up the finite element model (FEM) requires an understanding of meshing of components and defining the material properties of the component. A reliable FEA model of the cushion and a free fall condition is to be set up.

The outer protective covering is referred as *Cushion* throughout the thesis. It is a sandwich structure made of aluminum honeycomb *Core* with faces on top and bottom of the core. The sandwich construction and the deformation behaviour is discussed in chapter 3. A composite face referred as *Face sheet* is glued on the bottom of the core and a base support referred as *Ground plate* is assembled on top. The ground plate also helps to attach the cushion to the housing. The housing that carries all the instruments is simulated as a mass dummy referred as *Mass plate*, having a mass equivalent to 10 kg.

Figure 6: The laboratory set up of the cushion and housing is shown on the left and an equivalent system for correlation is created as shown on the right. The model of the housing is simplified to a mass plate in the FE analysis. The cushion model shown here is of cushion geometry-Model 1.

Figure 6 illustrates the model setup of the first concept of the cushion model 1. This design is adopted for the *correlation* of the laboratory test results. Correlation of model 1 is considered for two types of impacting surface and varying the number of composite face sheet layers used. Figure 7 depicts the model setup of model 2 for the *prediction* of results of the cushion. The difference in geometry of the cushion model 1 and model 2 can be noticed in these figures. The housing of the lander is formulated

as a rigid *Mass plate* in both the setups. The lander is a horizontal direction stabilised system and hence cushion is provided only on one side of the housing as per the final development of the concept.

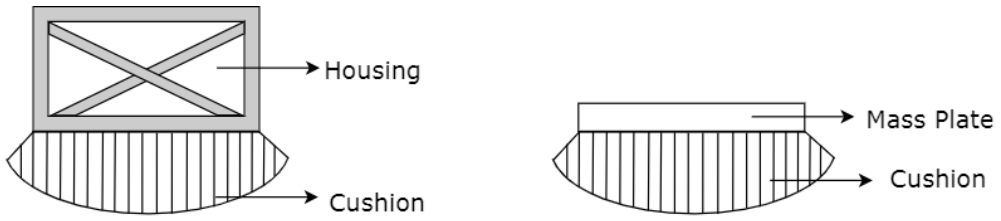

Figure 7: The laboratory set up of the cushion and housing is shown on the left and an equivalent system for correlation is created as shown on the right. The model of the housing is simplified to a mass plate in the FE analysis. The cushion model shown here is of cushion geometry-Model 2.

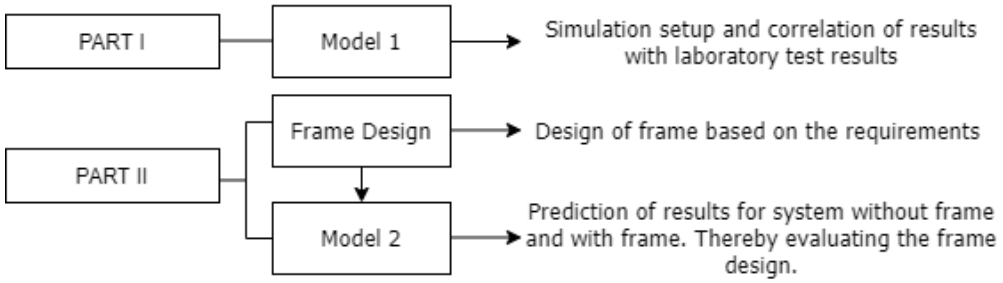

Figure 8: The whole scope of this thesis is broken down into a two part in the flow chart. The first part is the simulation set up and correlation of laboratory test of model 1, the second is the designing of frame and evaluation and prediction of results for model 2 when considered with frame is described.

The scope of this thesis can be divided into two main parts as shown in figure 8. The first part is the simulation set up and correlation of laboratory test of model 1, the second is the designing of frame. The is to be designed as a rigid structure to support the housing and to offer resistance to bending of the cushion. The frame is then applied to model 2 and prediction of results for model 2 when considered without a frame and with frame can be compared. This comparison would then evaluate the frame requirement and its design.

Considering the FEA model as an ideal condition and the variation with the accuracy of material properties defined for FEA models, a percentage change in the values of ± 20 % or more can be expected for the reasons discussed in later chapters.

1.5 Outline

The concept development, laboratory testing method and thesis statement were discussed in the previous sections. Further on, Chapter 2 gives a discussion on the state of art and a comparison and limitations of previous works in relation to the current work. Chapter 3 has a theoretical approach in understanding the deformation mechanics of the sandwich elements that is the core and the face sheet in subsections 3.1.1 and 3.1.2 respectively. These discussion leads to better understanding of the material behaviour and there by assisting in the approximation of the parametric values in the FEA models. The material formulation for the FEA model of the core and face sheet is discussed in section 3.2. The approximation carried out for the material card *MAT_126 of the core properties in subsection 3.2.1 is in relation with discussions in subsection 3.1.1. Similarly the discussion of material card *MAT_054 for the face sheet is discussed in subsection 3.2.2 in relation with subsection 3.1.2.

Chapter 4 is the correlation of the FEA model and the laboratory test model of cushion model 1 for different impact condition and different sandwich components. The model with cushion model 1 with one layer of Dyneema face sheet with penetrator type target is discussed in section 4.1. The first variation with this model considered is with the type of target. Section 4.2 correlates model with cushion model 1 with one layer of Dyneema face sheet with flat surface impact. The other variation considered for correlation is with the number of layers of the face sheet. Section 4.3 discusses the model set up and correlation for cushion geometry 1 with two layer of Dyneema face sheet and penetrator type of target. A summary of the codes required for setting up the model is given in the appendix.

Chapter 5 is the evaluation of frame and prediction of the results for the cushion model 2. Evaluation of frame is started with the FEA model setup for model 2 with standoffs placed in between the mass plate and cushion to predict the maximum deflection when a frame is not used. This discussion is carried out in section 5.1. Based on the requirement of a frame, the design of a rigid interface structure is carried out in section 5.1.1. The next task considered is to perform analysis for model 2 when the cushion is supported with the frame. In the section 5.2, the prediction of the results and a comparison of cushion model 2 without frame and with frame is performed. Similar results as for done for correlation is predicted for cushion model 2. Results of Impact depth, velocity, acceleration and force is compared and tabulated.

Chapter 6 gives a final discussion and summary of the results. Section 6.1 discussed the results obtained from correlation of the cushion model 1 and section 6.2 gives the summary on evaluation of frame and prediction of results for the cushion model 2. Final future scope of the current work is discussed in Chapter 7.

2 State of the Art

'If you want to find the secrets of the universe, think in terms of energy, frequency and vibration.'
— Nicola Tesla

The deep dark sky has millions of objects shining, that seems so close to reach yet so far to understand. Just considering the closest celestial object to Earth, the Moon is so very different from Earth in terms of its content, pressure variation, temperature, gravity, terrains and size. Studying these objects requires sophisticated instrument and instrument carrier. One of such scientific carriers are *Landers* that are dropped on the surface of object in study. A simple classification of a lander can be an *Orbiter Lander* which are usually provided with propulsion systems and GNC systems for soft landing, and a *Carry-on Lander* which on the other hand are usually dropped without any active or passive system of guidance towards the object in study.[6]

This work is a study on a concept of small body lander, in particular a lander that would be dropped on an asteroid. Since asteroids are smaller objects when compared to planets, the surface environment of an asteroid is without atmosphere and of very low gravity. Some of the different terrains observed so far on small bodies are hard terrains as seen on *Vesta* and icy surfaces seen as such on *Ceres*. Carry-on landers when dropped on such surfaces sustain impact forces that could potentially damage the instruments. Hence, current work deals with the study of a protective shell covering made of a sandwich panel that acts as dampers by absorbing the impact forces and thereby protecting the internal instruments.

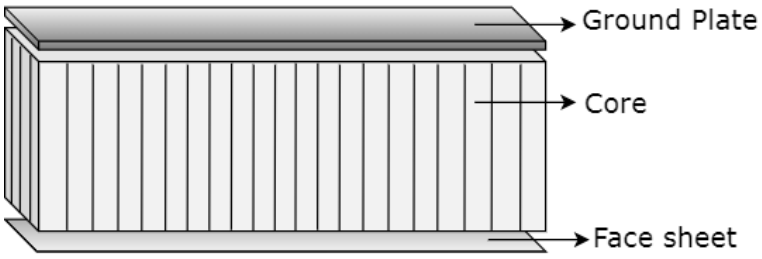

Figure 9: Components of a cushion made like a sandwich structure with a honeycomb core and ground plate and face sheet as the faces placed on either sides of the core.

The protective covering- cushion as seen in section 1.4 is made of a sandwich structure. A sandwich panel has a core structure with faces placed on either side of the core. Figure 9 shows the basic composition setup of the cushion as a sandwich construction. The cushion is built up with a faces, a support ground plate on one side of the core and thin face sheet layers on the other side. The core is made of aluminum honeycomb cells, the ground plate is a solid aluminum plate and the face sheet is a composite

material of Dyneema fibres and epoxy resin.

Mechanism of deformation and the energy absorbing capacity of this sandwich structure will define the performance of the cushion. A better understanding of a sandwich panel and the components of the cushion is explained in chapter 3. The previous works done so far are in relation to these conditions. The next section discusses the input from previous works and a limitation on its application to the current work.

2.1 Literature review

The book by *L.Gibson and M.Ashby* in reference [5] is a good source for understanding the properties of sandwich structure. Reference book [3] by *T.Bitzer* gives an input on measurement of properties of honeycomb cell structures by mechanical laboratory tests. Material design and understanding on a general sense can be understood from *M.Ashby* in reference [2]. Another source for composite materials is by *I.Daniel* in reference [4].

The actual study on the concept of shell landers like the cushion model and exploring small bodies is addressed by *C.Grimm* in reference[6]. It gives an overview of the results recorded during the pendulum laboratory tests conducted at DLR Laboratory. FEA models are to be setup in correspondence to these laboratory test conditions for correlation of the laboratory test results. Another paper by *S.Schroeder* in reference [18] gives the details about the initial concepts on the cushion models of the lander.

The trade off's on the material of the face sheet is outlined in reference [17] by *B.Reinhardt*. It also gives a way for determining the shape of the cushion and estimates a minimum height for the cushion. A mass optimized shape of cushion is then considered for the laboratory test conditions.

Development on this study is further carried out in reference [9] by *V.Knappe* in her thesis. This work highlights mechanical laboratory test procedure of measuring the properties of the core through compression and shear laboratory tests and suggests the material models for FEA setup- *MAT_ keyword for the core and face sheet. It is also suggested to use solid element formulation over shell or beam elements for core in the FEA models in LS Dyna . The core properties used on simulation level is same as that mechanically laboratory tested. Face sheet used in this work is Kevlar of $0.2mm$ thick. The works of *V.Knappe*, is a good start to understand the procedure of measuring the properties of the core through physical laboratory tests and to apply these measured property values into the FEA material models. The values measured are dependent on the size and material of the honeycomb cells. As a result the property values of the core analysed in reference [9] cannot be used directly to the current models as the core cells are of different sizes which thus varies the strength properties.

F.Meyer further developed on the FEA simulation setup in reference [14]. He gives an input on the *CONTACT parameter that defines the contact type between each

part of the FEA setup. On continuation of developments of work, *B.Reinhardt* in her master thesis in reference [16] has studied the element formulation and the control parameters of the element behaviour such as the *HOURGLASS. Hourglass energy defines the non physical energy that occurs due to the deformation of mesh elements in the FEA model. It is a way to define the type of integration of mesh element in a finite element analysis. A refined mesh decreases the hourglass energy.[10]. *B.Reinhardt* has carried out laboratory test conditions and FEA model setup for spherical geometry of the cushion. The core properties is same as that been mechanically laboratory tested in [9]. Face sheet suggested in is Dyneema, and the laboratory tests are performed with four layers of Dyneema with a total thickness of $1.41mm$.

The manuals from Livermore Software Technology Corporation (LSTC), on LS- Dyna manuals *Volume-II*, *Material Model*, and *Volume-I*, *Keywords* in reference [12] and [10] gives details about the material models on LS Dyna and helps in the formulation of simulation setup. The theory manual in reference [11] facilitates in understanding and optimising the material models of the FEA setup.

Further references provides guidance on sandwich and core properties and setting up of simulation models are by *A.Petras* in reference [15], by *M.Stanczak* in reference [19] and *A.S.M.A.Ashab* in reference [1].

2.2 Limitations of Previous Work

Setting up of simulation model on LS Dyna involves interrelated parameter definitions and each of the values has to be defined as per our requirements. Physical laboratory test results from [9] serves as input values on material keyword which further requires the stress strain behaviour of the core as a curve plot which are recorded during laboratory testing in *MAT_126 material model. Since honeycomb core are anisotropic material, the mechanical properties vary accordingly and hence material card properties are to be defined in accordance, to account for the anisotropy of the honeycomb core.

As seen in the literature survey the properties of the core used in demonstrator level and simulation level in [16] is same as the core in [9]. Hence the mechanical properties for the core on *MAT_126 is the same in both the works which are obtained by mechanical laboratory tests. In the current condition the cell size of the honeycomb is different from that of previous works. Cell sizes vary the mechanical properties relatively. Hence *MAT_126 values cannot be used directly from the previous works. Table 1 shows a comparison of properties of core and face sheet being used in previous works and that used in current thesis.

The face sheet material model *MAT_054 on LS Dyna is setup with properties of Kevlar with $0.2mm$ thickness in [9]. Although Dyneema face sheet is suggested in [16] and is used at demonstrator level, properties of Kevlar face sheet as setup in [9] is used in the FEA set up, by only changing the density of Kevlar to density of

Table 1: Difference in properties of core and face sheet from previous works to current work

Part	Nomenclature / Properties of Previous works	Nomenclature / Properties of current work
Core	**3/16-Al5056**-0.0007-1.0	**3/8-Al5052**-0.0007-1.0
Face sheet	Kevlar [[9]] t=0.2mm- 2x, Dyneema [[16]] t=1.41mm-4x	Dyneema t=0.45mm 1x, 2x

Dyneema in [16]. The change in thickness and change in properties associated with tensile strength and compressive strength for Dyneema that develops depending on the arrangement of composite face sheets are not included on the FEA material model. Hence *MAT_054 has to be setup based on the current requirements. These difference from [16] are to be taken into account in the FEA model setup for the current work.

The current work is further developed from the works mentioned above. Current model and laboratory test conditions are considered and simulation setup is completed with tasks of meshing the cushion and other lander parts, material definition, application of loads which in our condition is free fall due to gravity and lastly analysing the results. Even though most of the inter related parameters are adopted from previous works, the properties have to be set up with right parametric values on *MAT_126 and *MAT_054, that affects the behaviour of core and face sheet, so as to see the relevance in results. The finite element model set up for correlation with laboratory test conditions of model 1 and a prediction of results for model 2 are discussed in the next sections.

PART I

3 Simulation Setup for FE Analysis

"Somewhere something incredible is waiting to be known."
— Carl Sagan

This section has a theoretical approach in understanding the behaviour of the cushion. In a FEA analysis, appropriate meshing of components is one of the important aspect in pre-processing. FEA mesh models becomes well defined with material selection and with the input of right parametric values of mechanical properties. In general these values can be obtained either by the data sheet or by performing laboratory tests or by analytical calculation. If the components are more complex, analytical solutions are prone to an increase in errors. Since the property values defining the core and face sheet behaviour are unknown, it is approximated by theoretical approach while understanding the variation of the values and approximating it to the closest available values.

The component manufacturers adopt standard laboratory testing methods to predict the values of mechanical properties. These values are primary properties that defines the performance of a component and can be obtained as a data sheet by the manufacturers.These values could be taken as direct input to the material model. There are certain secondary mechanical properties which are not measured and are not given in the data sheet. Theses values are approximated accordingly. The material model on LS Dyna requires values of both primary and secondary properties to be define. For measuring the properties of composite face sheet there are software available that gives the values when certain parameters are given as input.

This thesis is not directly associated with optimizing the honeycomb structure or the sandwich cushion itself and hence only the macro mechanics of the core and the face sheet are considered in the next sections. The deformation mechanics of the core and the face sheet individually and together as a sandwich structure serve as a guide in selection of parametric values for the material model *MAT_ in LS Dyna and to understand the deformation behaviour.

3.1 Deformation Mechanics of Sandwich Structure

Sandwich panels are known for being stiff and light weight. A sandwich panel is a hybrid material that has a core and faces glued on top and bottom of the core. The core and faces offer certain mechanical advantages individually which will be discussed in section 3.1.1 and section 3.1.2. These properties are utilized when designing a sandwich structure. The mechanical properties of both core and faces characterizes the mechanical behaviour of the sandwich panel. The core creates a distance between the faces. This increases the section modulus Z_s or in other words offers flexural resistance. The separation also offers good resistance to bending as it contributes to an increase in second moment of inertia I_s of the sandwich structure. Hence sandwich

structures provides good resistance against buckling and bending loads.[5], that makes it a good energy absorber. This shows that the efficiency of the sandwich panel as an energy absorber depends on the relative density of aluminum honeycomb core which also depends on geometry.

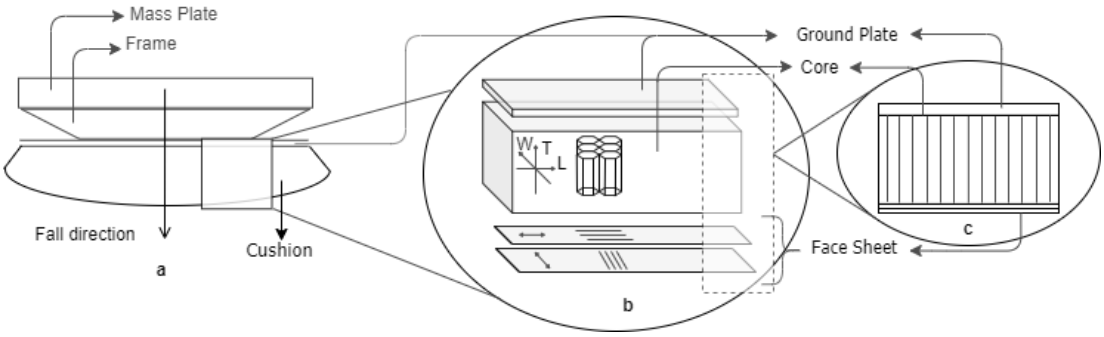

Figure 10: a.Components of the lander system highlighting the b.macro segments of the sandwich structure of the cushion. c. Sectional view of the cushion as an assembled sandwich structure.

Figure 10 highlights the cushion structure as a sandwich assembly. It highlights the macro mechanical segments of the cushion which is composed of core and faces. Here the faces are the ground plate and Dyneema face sheet. The central core is an anisotropic structure of honeycomb cells. Material directions $T - L - W$ represents the axes of the core. The bottom face of the sandwich is the Dyneema face sheet. It is a woven-fibre reinforced composite. The fibres are considered to be orthogonally woven. For our analysis, it is assumed that the face sheet is glued uniformly over the core.[3].*(As explained in chapter 'Sandwich Design' in [3])*. In depth discussion about the honeycomb core and face sheet is done in the next section.

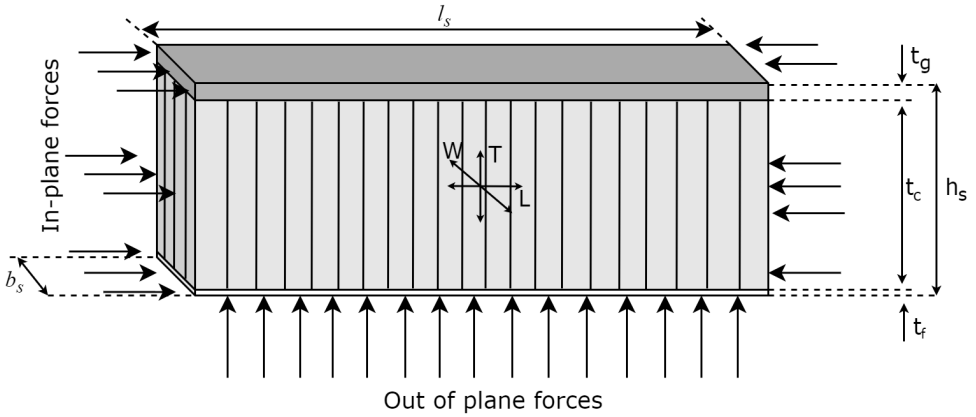

Figure 11: A sandwich structure of length l_s and width b_s described with the major axis (T) and minor axis (L and W). The forces acting in *In-plane* (L-W) and *Out of plane* (T) directions are described.

The stress distribution analysis over the cross sections of the sandwich panel will give

a better understanding with the failure modes of the cushion.

The description of a sandwich structure of length l_s and width b_s is seen in figure 11. The honeycomb core has a height t_c which is the transverse thickness of the core. The thickness of face sheet is given as t_f and the thickness of ground plate as t_g. Over all thickness of sandwich is taken as h_s. The subscript s refers to the sandwich panel, subscript c refers to the core, f refers to the face sheet and g refers to the ground plate. The sandwich panel have faces of different thickness and it is assumed that the resistance against bending offered by core is negligible.[3].*(As explained in chapter 'Sandwich Design' in [3])*.

$$h_{\mathsf{s}} = t_{\mathsf{f}} + t_{\mathsf{c}} + t_{\mathsf{g}} \tag{1}$$

Loading in axial direction $(L - W)$ is referred as in-plane loading and transverse loading in$T$ direction is referred as out-of-plane loading. Although only uni-axial forces along the out-of-plane direction is considered for analysis, bi-axial forces in in-plane and out-of-plane are shown in the figure11.

The FEA models are considered for a free fall and central impact and hence deformation of sandwich structure discussed here is considered only for transverse loading. Therefore when sandwich structures are loaded in out-of-plane direction, normal stresses and shear stresses are generated within the cushion. On impact, the face sheet takes up the in-plane *compressive stress* up to its compressive yield strength. The core provides *shear resistance* along the thickness of the core t_c there by taking out-of-plane shear loads τ^*_c. Depending on the efficiency of the sandwich design as an energy absorber, the forces gets transmitted to the second face that is the ground plate. The ground plate again takes up the in-plane *tensile stress* up to its tensile yield strength. The stress distribution within the faces is assumed to be uniform.[3]. *(As explained in chapter 'Sandwich Design' in [3])*. Failure occurs if the loading is larger than the yield strengths of the faces.

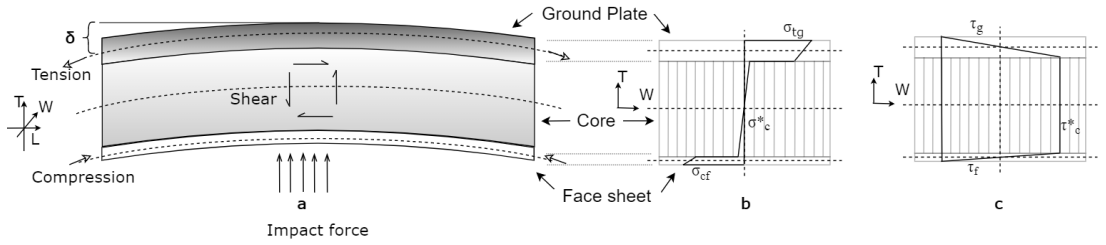

Figure 12: a.Deflection of the sandwich cushion b, Normal stress distribution c. shear stress distribution across the thickness of the core and faces. (Based on [3])

In figure 12 normal stress distribution and shear stress distribution across a sandwich panel is depicted.[3] . Figure 12a shows the bending load distribution in compression and tension taken up by face sheet and ground plate respectively. The shear stress

is taken up by the core, based on the concept of sandwich panels. Figure 12b shows the normal stress σ distribution through the cross section of the cushion. It can be seen that the normal stress σ^*_c within the core is very low or approaches zero. This concludes that the resistance to bending offered by the core is almost zero. The normal stress distribution across the thickness of the face sheet σ_{cf} is due to compressive stress, here subscript c refers to compression. Stresses in face sheet are assumed to be uniform although it is not uniform for a composite material. The normal stress distribution σ_{tg} across the thickness of ground plate is due to tensile stresses, here subscript t refers to tensile forces. Tension in the ground plate are approximated to be uniformly distributed.[5] This implies that almost all of the in-plane bending stress are taken up by the faces. Figure 12c shows the shear stress distribution across the cross section of cushion and it can be seen that most of the shear loads are taken up by the core and are approximated to be constant through out the thickness.[5] Since the thickness of the faces are very thin compared to the thickness of the core, the shear resistance of the faces is almost insignificant.

Total deflection δ_s of the sandwich panel is the sum of deflections that occurs due to both bending and shear. The deflection that occurs due to shear depends mostly on shear modulus G^*_c of the core, impact forces and length l_s of the cushion. The deflection occurring in the cushion can be better understood knowing the distribution of stresses. Some of the common failure modes of sandwich structures are face wrinkling and dimpling, face indentation, face yielding - occurs when face behaves like a brittle material, bond failure and core failure.[3]. Such failures are noticed in the laboratory test conditions. Some of these failures are favourable for the current laboratory testing conditions since energy absorption capacity of the cushion is defined by the deformation of core and face sheet.

Sandwich panels are considered good energy absorbers as the impact forces are dissipated in the form of deformation of the core and the faces. The core takes up the out-of-plane shear stress and face sheet takes up the in-plane tensile and compression stress and therefore making the sandwich assembly a good energy absorber. Impact forces are converted into either fracture or buckling or into elastic plastic deformations of core and faces. The energy absorption efficiency of a sandwich panel can be measured by knowing the deformation of the cells or in other words its volumetric strain for the amount of work done in deforming the cells.[5]. Hence designing an efficient cushion depends on the total deflection of the cushion which in turn depends on the energy dissipation of the impact forces i.e the deformation of the core and face sheet.

3.1.1 Deformation Mechanics of Honeycomb Core

Material Axes:
The core of the sandwich cushion is made of regular hexagonal cell structure. Multiple layers of aluminium foils of thickness t are bonded with strong adhesives. Adhesives are smeared for a length h. Non-adhesive spaces are left alternately for every adhesive length at equal distance. It is repeated on alternate foils. It is then expanded in W

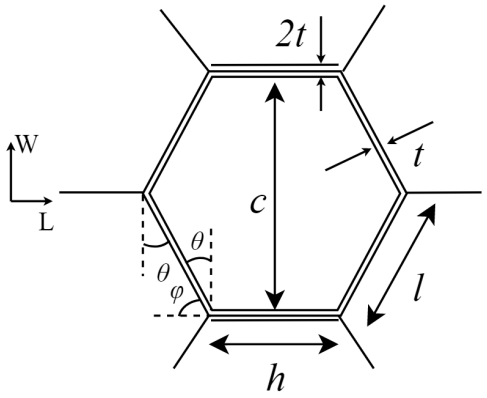

Figure 13: Honeycomb cell nomenclature along the L-W plane.(Based on [3])

direction to create honeycomb core by expansion method. These regions of bonded aluminum foil has double thickness $2t$. Figure 13 shows the nomenclature of each cell. The plane orthogonal to the plane of expansion $(L - W)$ is the out-of-plane axis T. The length of the foil along T is the core thickness t_c. The properties along each of these axes is different and hence honeycombs cores are anisotropic material. Table 2 gives the description of the nomenclature hexagonal cell.

Table 2: Honeycomb cell nomenclature description

Geometry	Nomenclature
c	Cell size
t	Foil thickness
l	Cell length
h	Cell height
θ	Cell angle

The material is stiffer in the T direction in contrast to other direction. This is considered as the major axis. The compressive properties measured along the T axis is one of the primary properties of the core which defines the crush strength of the core. It is further discussed in section 3.2. The crush strength defines the energy absorption capacity of the cushion. The direction in which the foils are expanded is considered to be the weakest axis of the core W. The lateral direction to that of expansion is the L direction offers lower stiffness to that in T and hence is considered as minor axis. The core is assumed to be isotropic in the in-plane direction $L - W$. This makes the core to be regarded as transversely isotropic.

Elastic Constants:
For an orthotropic material nine elastic constants E, G, ν in each of the three axes are required to define the properties, but since it is considered to be transversely isotropic five properties are sufficient to define a honeycomb core. One of the two independent elastic properties is the Young's moduli E^* in each axis E^*_T, E^*_L. Here superscript

* refers to core and subscript T and L refers to the major and minor axis in consideration. The other independent elastic constant is the shear modulus G^* in the two major planes L-T and W-T, G^*_{LT} and G^*_{WT}. The last constant is the Poisson's ratio $\nu*$. These properties form the basic input values for EAAU, EBBU, ECCU, GABU, GBCU on the material card *MAT_126 to define the core. This is further discussed in section 3.2.1.

For a given cell size c and foil thickness t, the length l of the cells is calculated with equation 2. Relative density of the honeycomb core $\rho*/\rho_s$ varies linearly with t/l as in equation 4. In-plane properties such as the Young's modulus in the minor axis E^*_L and E^*_W varies with t/l as a cubic power. This means that an increase in l will decrease E in cubic root values as in equation 6. The out-of-plane Young's modulus E^*_T and strain at densification ε_D vary linearly with relative density as in equation 7 and equation 8.

For a given *t* and *c* of the cells from the manufacturers, and considering regular hexagonal cells that is $h = l$ and θ=30°

Cell size c:

$$c = 2l\cos\theta \tag{2}$$

Core Density ρ^*:

$$\rho^* = \frac{2(h+l) * t * \rho_s}{h + (l * cos\theta)} \tag{3}$$

where θ is taken in radians

Relative density:

$$\frac{\rho^*}{\rho_s} \propto \frac{t}{l} \tag{4}$$

$$\frac{\rho^*}{\rho_s} \sim (\frac{2}{\sqrt{3}} * \frac{t}{l}) \tag{5}$$

Relative density approximation for hexagonal closed cells (Based on eq 4.Ib from [5])

Young's Modulus in minor axis E_L and E_W:

$$\frac{E^*_L}{E_s} = \frac{E^*_W}{E_s} \propto (\frac{t}{l})^3 \tag{6}$$

Young's Modulus in major axis E_T:

$$\frac{E^*_T}{E_s} \propto (\frac{t}{l}) \tag{7}$$

Densification strain ϵ_D:

$$\epsilon_D \propto (\frac{1}{\frac{\rho^*}{\rho_s}}) \tag{8}$$

$$\epsilon_D = (1 - (1.4 * (\frac{\rho^*}{\rho_s}))) \tag{9}$$

[5](all equations based on Table 4D.I *Properties of honeycomb with double thickness vertical wall*, Chapter4 *'The mechanics of honeycombs'*)

The above discussed elastic properties are associated with relative density ρ^*/ρ_s of the core where $\rho*$ is the density of the core and ρ_s is the density of the solid material with which it is made of. The core properties of the previous work has different relative density to that of the current core since core densities vary with t, l, h of the cell size. The variation of the properties depending on cell size and its adaptation on the material model is discussed in section 3.2.

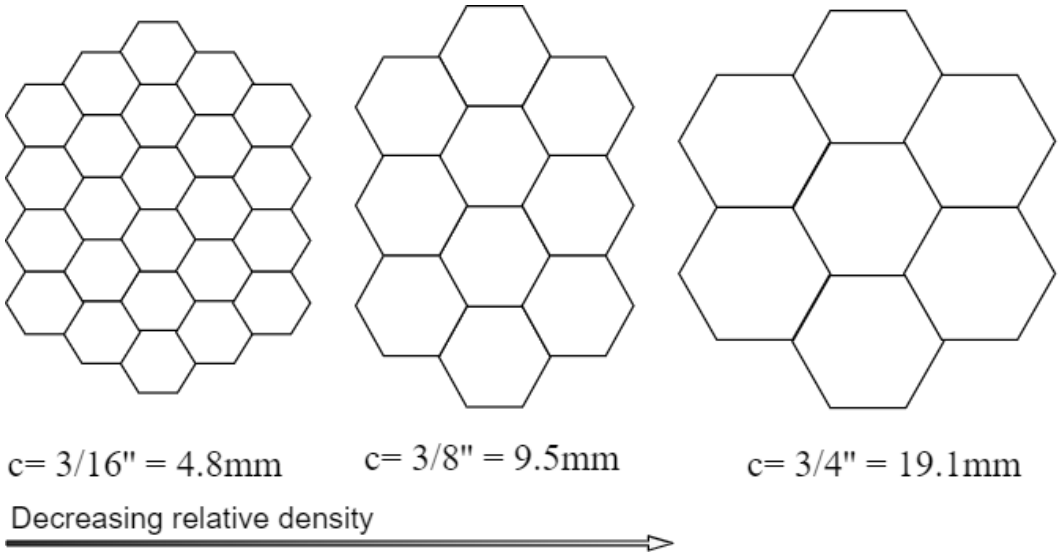

Figure 14: Comparison of hexagonal cells of different cell size with same foil thickness describing the decrease in relative density.

Figure 14 shows the hexagonal cells of different sizes. It is to be noted that the figure is not to exact dimension but only for comparison. The first cell size $3/16''$ was the core cell size used in [16] and [9]. The second cell size $3/8''$ are the ones being correlated in the current work. The comparison is considered for cells of same foil thickness t and of different cell side length l, which has been the condition from previous work to current work.

In relation with table 3, observation on variation of relative density with cell size can be made. As the cell size c that is related to length l increase for the same thickness of foil t, relative density decreases there by decreases the E modulus. Although the

Table 3: A comparison of properties of honeycomb core of different cell sizes and relative density that further defines the core behaviour

Cell Size	**Cell size** c	**Cell wall thickness** t		**Cell wall length** l	t/l	ρ^*	**Relative Density**	E_T/E_s	E_L/E_s
(in)	(mm)	(in)	(mm)	(mm)	(10^{-2})	kg/m^3	(10^{-3})	(10^{-3})	(10^{-7})
3/16	4.8	0.0007	0.01778	2.76	6.4	37.30	7.4	7.40	3.06
3/8	9.5	0.0007	0.01778	5.48	3.2	18.80	3.7	3.70	0.39
3/4	19.1	0.0007	0.01778	10.97	1.6	9.40	1.8	1.80	0.049

calculations carried here is for solid aluminum 5052 of density ρ_s of $2.71g/cm^3$ and the aluminum used in the previous work is Al5056, the solid density ρ_s is approximately same. Relation between the elastic constants and relative density is concluded with equations 2-9. If a comparison on properties with different foil thickness t of same cell size ($c = f(l)$) is made it is seen that the relative density increases for increase in foil thickness. This decreases densification strain and therefore the plateau regime (explained in the next paragraph *'Stress-Strain Curve'*) is decreased. Young's modulus at beginning of compression increases and increase in crush strength can also be anticipated. Although these variations could be small, core behaviour with change in t, l, h of the cells can be better understood when approximation of values are to be made. Therefore increase in cell size for same foil thickness t decreases E_T^* that implies lower a crush strength.

Stress-Strain Curve:
In the material model of the core on the simulation set up it is required to define stress-strain curve of the core in the major axis and minor axis and also its variation with an off axis loading. These curve are plotted on the material card LCA, LCB, LCC of the material model *MAT_126 which is further adapted in section 3.2.1. Hence it is essential to understand the curves before defining on the material model.

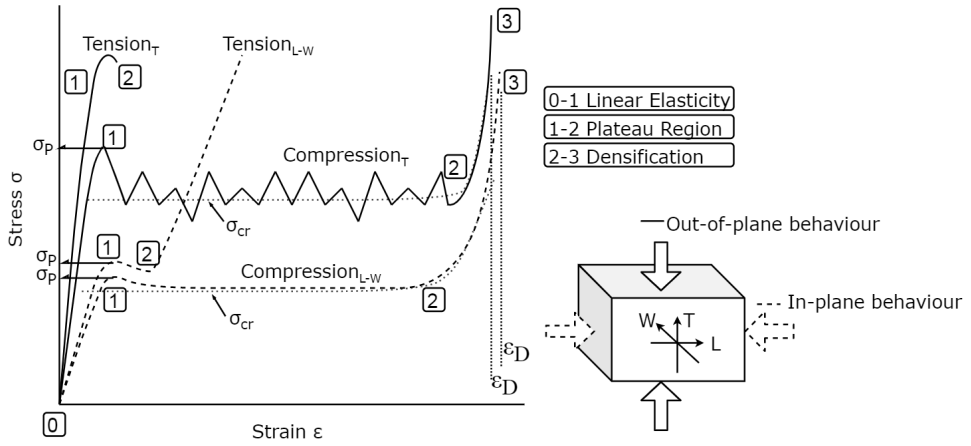

Figure 15: Typical stress-strain curve of an orthotropic honeycomb celled core describing the basic regimes of elasticity(0-1), plateau region(1-2) and densification(2-3).(Based on [5])

Based on the solid foil material used in manufacturing the honeycomb cells, a honeycomb core can behave either (a) elastically for an elastomeric honeycomb, or (b) elasto-plastically for a plastic honeycomb or (c) elastic-brittle for a brittle honeycomb.[5]. Considering these variations in the material behaviour a generalised discussion is given here with reference to figure 15. If the material type of honeycomb is known before hand and if the core is not mechanically laboratory tested for the variation in its stress-strain, an approximation can be possibly made. An approximation with stress-strain curve can be made more closely when the yield stress at peak, densification and fracture are known.

Figure 15 shows stress strain curve for honeycomb structure. Each curve in the figure shows three regimes 0-1, 1-2, 2-3. The first regime 0-1 is referred as the linear elasticity, second regime 1-2 is referred as the plateau region and third regime 2-3 is referred as the densification. It is to be noted that the curve representation is a general depiction of stress strain curves for different loading condition in different axes and different material types. It is not based on any measured values.

In compression for an (a) elastomeric material and (b) plastic material the curves are rather smooth with constant plateau region. The behaviour in compression for both the material types shows stress-strain curve similar except with the peak stress which would be elastic yield point and plastic yield point respectively. This curve variation can be observed in the smooth dotted curve in $Compression_{L\text{-}W}$. When the core is made of a (c) brittle material, the curve is with multiple fracture points and the plateau region are more like the one depicted for $Compression_T$. In tension for material type (a) and (c) the failure is rather abrupt like the curve depicting for $Tension_T$ only with a variation of fracture points, being elastomeric fracture or brittle fracture point respectively. In tension, for material type (b) the plateau region are very small and densification occurs quicker as depicted in the curve with $Tension_{L\text{-}W}$.

With the discussion until now, the axis of loading was not given attention rather only to the type of core material. The loading axis varies in the deformation mechanics of the cells and the stress-strain plots would differ accordingly. The stress-strain curve when loaded in the in-plane i.e in the minor axis are represented by dotted lines and in the out-of plane i.e the major axis direction are represented by solid lines are different since the strengths are different. The loading conditions on the cells considered here are tension and compression.

Out-of-Plane Loading:
When honeycomb is loaded in the out-of plane direction the mechanism of deformation in the initial stage of loading is linear until peak stress are reached. Stress strain curve shows linear elastic behaviour in the first regime 0-1. The E moduli is much greater in T direction. Large amount of stress is taken for small deformation. Once the peak stress is reached buckling for material type (a) and (b) or brittle crushing for material type (c) of the cell walls is much more prominent shown in regime 1-2. The buckling of the cells is shown in figure 16. Based on the type of material and stiffness the

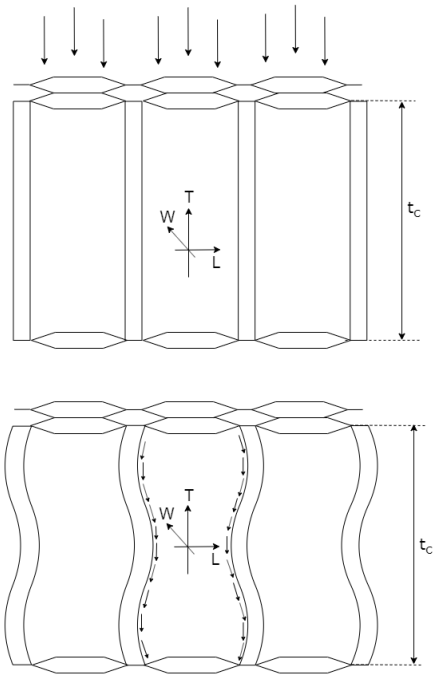

Figure 16: Buckling of honey comb cells seen as a behaviour in the plateau region of the stress-strain curve, when loaded in the out of plane (T) direction.

strength during collapsing varies. For material type (c), which is 12 times stronger in compression than in tension [5], cells collapses and fractures there by taking up the load. Stress at this point is the crush strength σ_{cr} of the core. The buckling of the cells continues until the cells are folded or fractured completely providing stiffness to the structure and starts *densifing* [5]. This increases the crush strength and the stress-strain curve steeps rapidly at densification strain ϵ_D. The compressive strain varies linearly with relative density and hence for a larger cell size i.e with smaller relative density, compressive strains are smaller that is the plateau region tends to be smaller. This curve definition helps in defining the curve LCA and LCB on the material model for core. This is further discussed in section 3.2.1.

In-Plane Loading:

When honeycomb is loaded in the in-plane direction, mechanism of deformation of the cells is seen on figure 17. The cells that are initially influenced by impact starts to bend in the direction of loading and the cells stretches out orthogonal to loading direction. A linear elastic deformation behaviour is seen this is depicted for the regimes 0-1. This behaviour is due to the geometry of the structure. The voids in a hexagonal cell distorts the cell wall, similar to that like a spring.[5]. The collapsing of cells starts once peak stress is reached. The collapse behaviour of the cell depends on the type of foil material which can be either elastomeric buckling or brittle fracture or plastic yielding. This variation is illustrated for regime 1-2 defining the plateau stresses. For material type (b) elasto-plastic material, the plateau is almost a straight line at constant yielding. The crushing continues until the cells touch the adjacent cell walls.

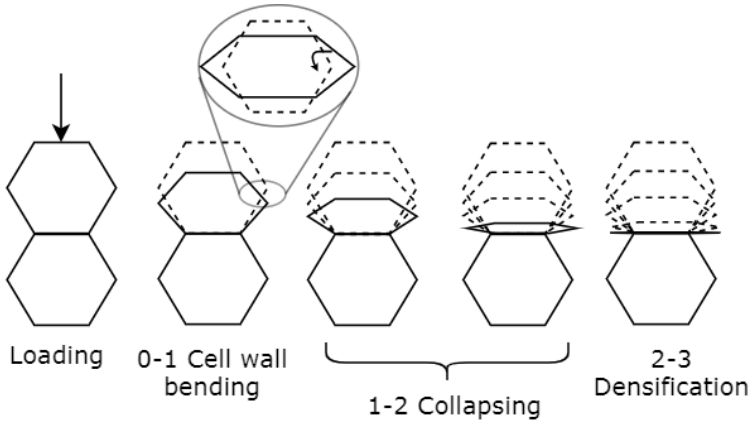

Figure 17: Collapsing of honey comb cells seen as a behaviour in the plateau region of the stress-strain curve, when loaded in the in-plane (L-W) direction. Cell behaviour in the elastic region and densification is also described.(Based on [5])

Once all the cell walls are crushed, the core begins to stiffen. This is the onset of *densification*. The stress at densification increases steeply due to the strength offered by the crushed cells. At this stage strain is referred as densification strain. This curve helps in defining the curve definition of LCC on the material model.

A honeycomb has various deformation mechanism, only a general overview is given to understand the selection of parameters for the chosen type of foil material when exact values of the elastic constants are unknown. Based on these understanding the material property of the core *MAT_126 is adapted with given primary values for elastic constants by the data sheet from the manufacturers. Based on the discussion until now, the values of secondary property are approximated accordingly. This adaptation into *MAT_126 is discussed in section 3.2.1.

3.1.2 Deformation Mechanics of Composite Face Sheet

A composite material is constructed by mixing fibres and matrix in certain volumetric ratio. Fibres are reinforced either as individual fibres or as a woven fabric. Resin matrix are injected over layers of fibre and are infused together during manufacturing of a composite. The resin matrix binds the fibre layers together. When a composite is loaded, matrix transfers stresses between each layer.[4]. In a fabric reinforced composite, fibre fabrics are woven in a certain weaving pattern. These weaving pattern also contributes to the behaviour of a composite material. Tensile strength of fibres along the direction of fibre are much larger than in its orthogonal direction. The tensile properties of the fibres are taken advantage and are woven in the direction where high strengths are required.

Figure 18 shows a typical stress-strain curve for fibres, matrix and together as a composite material that behaves based on fibres and matrix behaviour. Properties of com-

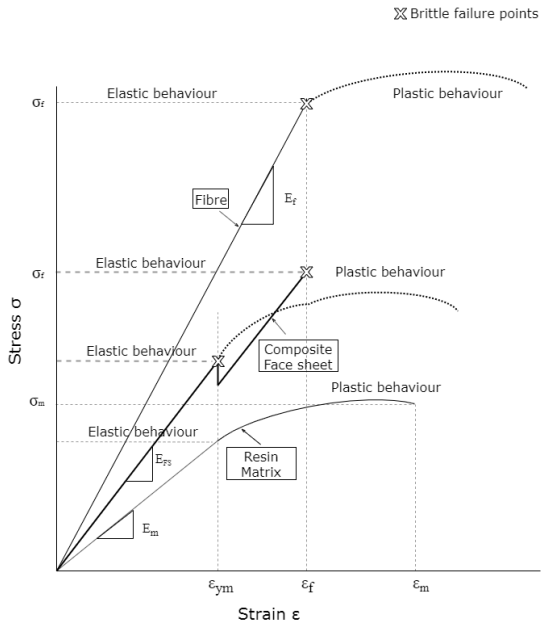

Figure 18: Stress-strain curve for a typical composite material made of fibres and resin matrix.(Based on [2])

posite like the Young's modulus E_FS varies in combination of the two constituents. A linear variation of stress and strain is seen for elastic materials until yield stress is reached. The drop seen for the composite curve is due to the failure of layers of the composite. The rise seen again is due to the strength offered by the under lying layers. If the fibres are brittle, the composite material would have brittle fracture of layers.

Fibre and Woven-Fibre Fabric:
Woven-fibre fabric has properties different from that of the individual fibre based on its weaving pattern. These properties can be measured through standard tensile and compression laboratory tests. Property definitions like thickness t_L and areal weight σ_A can be obtained by the manufacturers. At times volume fraction V_f of a woven-fibre can also be obtained by the data sheet. For the current work, Dyneema fibres are used as a woven fabric. It is mixed with Epoxy resin to create the composite face sheet. Dyneema fabric used in the laboratory tests has a special weave pattern. Currently these fabrics are not explicitly laboratory tested for mechanical properties. Hence laminate theory is applied considering unidirectional fibre layers in 0°and 90°as one layer of fabric. More on this and the determination of property values are discussed in section 3.2.2.

Figure 19 outlines the properties that defines a composite material. The fibres as an individual strand has density ρ_{f}, Young's elastic modulus E_{f}. Properties measured in fibre direction is subscripted with x and in its orthogonal direction as y. G_{xyf} refers to shear elastic modulus and ν_{xyf} is referred to Poisson's ratio of the fibre. These mechanical properties can be obtained by data sheet of the fibre. Normal stress σ_{xt}, σ_{yt} due to tension load are subscripted t and when measured along fibre direction is

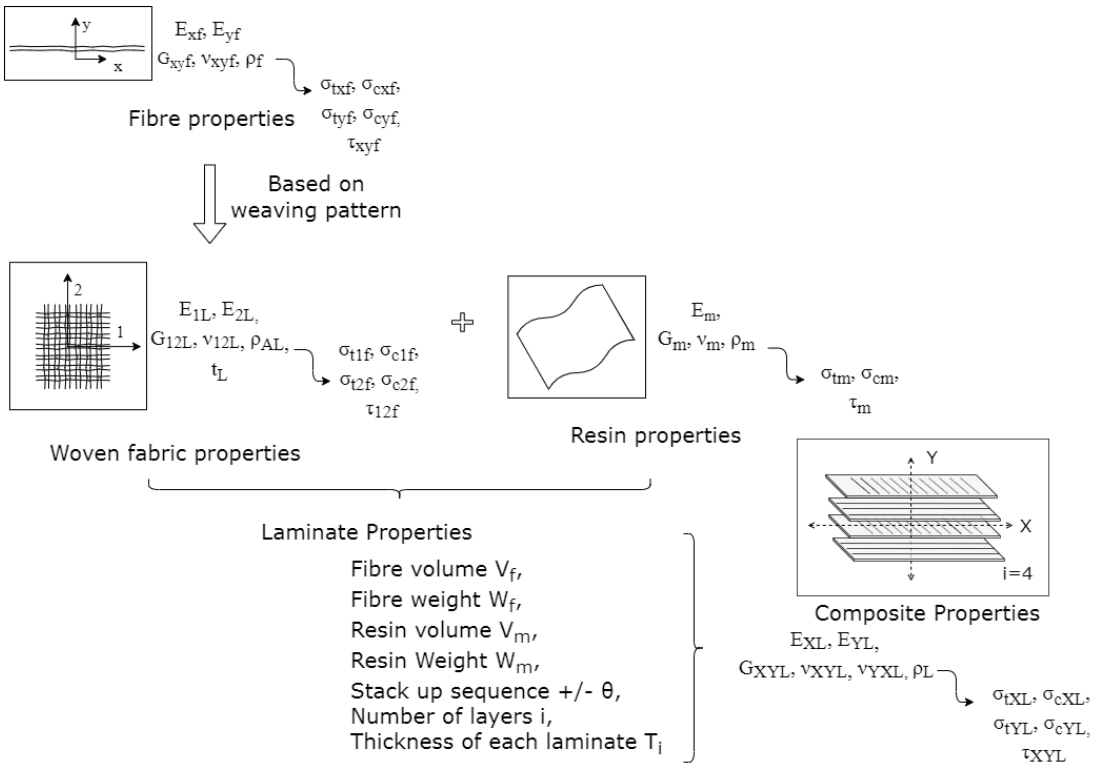

Figure 19: Fibre properties and resin properties describes the micro-properties of a composite laminate which when stacked up in a sequence defines the composite material.

subscripted with x. Normal stress σ_{xc}, σ_{yc} due to compression load are subscripted c and when measured orthogonal to fibre direction is subscripted with y. Shear stress of the fibre is given as τ_{xyf}. Analogous to fibre properties with subscript f measurement, matrix properties are subscripted with m. And since matrix is isotropic properties are not direction dependent.

When woven fabric layers are reinforced into matrix, each layer referred as *ply* or *lamina* of the composite adds to the performance of the composite structure. *Laminate theory* can be applied for analysis on each laminate of the composite. The micromechanics of a composite would depend on the geometry and arrangements of each fibre strand in relation with the volume fraction. Analysis on a level of micromechanics deals with stress distribution through each lamina. Although the stress strain distribution across each laminate varies for a composite material, corresponding calculations are out of scope of this thesis and only global variations of the face sheet is considered. Therefore, in the current analysis conditions only the macro mechanics of the face sheet are discussed. Hence values of failure points of composite face sheet is not considered.

Composite Laminate: Woven Fabric + Resin:
Depending on the orientation and distribution of fabric, composites may be balanced or unbalanced, symmetric or asymmetric. When the fibres are oriented at angles symmetric about a reference mid-plane of the composite and are of equal thickness, it is

referred as *symmetric layup*, for example [-45/0/-45]$_s$ where subscript s is for symmetric layups. For a balanced lay up, the orientation of the fibres are mirrored about the reference plane, for example [-45/+45/0/+45/-45] = [$\pm$45/$\bar{0}$]$_s$ which is both balanced and symmetric. A balanced laminate composite need not always be symmetric.[4]

When the fibre are equally distributed in all direction and the properties of the composite is same in all direction, it is referred as *quasi isotropic composite*. A quasi isotropic composite can be considered to have symmetric and balanced laminate arrangement. A quasi isotropic laminate has elastic constants are identical in all directions.[4]. One condition of quasi isotropic composite are [0/+45/-45/90]$_s$= [0/+45/-45/90/90/-45/+45/0]. In the current analysis a one layer of face sheet is considered to be oriented in [0/90] and two layers of face sheet in [0/90/+45/-45]. This two layer arrangement is neither balanced or symmetric and hence we see difference in values with elastic constants that are explained in section 3.2.2.

Volume fraction:

$$V_f = \frac{\rho_{comp} - \rho_m}{\rho_f - \rho_m} \tag{10}$$

or

$$V_f = \frac{(\frac{W_f}{\rho_f})}{(\frac{W_{comp}}{\rho_{comp}})} \tag{11}$$

Equation 11 is obtained based on [4]. To know volume fraction of the fibre, it is necessary to know the fibre weight fraction weight W_f, weight of composite face sheet W_{comp} and density of the composite face sheet ρ_{comp} . But these quantities are unknown. In equation 10 [7], density of fibres and matrix is known but density of composite face sheet ρ_{comp} is not known. Therefore volume fraction of the composite can not be calculated without knowing its distribution fraction. Hence volume fraction of fibre is assumed to be 60% [13] which is usually the condition for closely woven fabric and void percentage is assumed to be 0%. This helps in calculation of the ρ_{comp}, laminate thickness T_i, which is necessary for the application of Laminate theory.

In laminate theory, stack up sequence θ of the uni-directional fibre layers and thickness of each composite laminate T_i are important factors that defines the overall properties of a composite. Apart from these, fibre volume fraction V_f or resin volume fraction V_m, percentage of void in the mixture, composite density in ρ_{comp} is necessary to defines the composite. When analysing a composite, laminate thickness T_i and fibre orientations θ and volume fraction V_f of the fibres are of higher importance. Although the stress-strain distribution in each composite layer is different, it is assumed to be uniform in the current condition, since only macro mechanics of the face sheet are in concern.

An efficient composite can be obtained with right formulation of stack up sequence θ with an increase or decrease in the number of layers for the same over all thickness

of the laminate by varying the laminate thickness T_i. [4]. Therefore the face sheet properties are calculated considering one layer or two layers with the arrangement of uni-directional fibres and these values are adapted on to material model *MAT_054 as explained in section 3.2.2.

3.2 Material Formulation of the Core and Face Sheet

3.2.1 MAT_126

Material model *MAT_126 - *MAT_Modified_Honeycomb on LSDyna is used for defining aluminum honeycomb core properties. This material card has the provision of including primary and secondary properties that define the behaviour of the anisotropic honeycomb core. As discussed in section 3.1.1 about the primary properties i.e the elastic constants E_T, G_{WT} and G_{LT} which defines the core behaviour, it can be obtained by mechanical laboratory testing. Apart from which yield stress limits at peak, at crushing and at densification is necessary to be input on to the material card as load curves. Obtaining these values are easier when the mechanical standard laboratory testing is carried out. Figure 20 shows a generalised summary of laboratory testing methods to obtain the primary and secondary properties to define the material model. Compression laboratory test properties and shear laboratory test properties are sufficient for obtaining the parametric values. laboratory testing methods depicted in reference to (1a), (2b), (2c) in figure 20 provides primary property values and (1b) provides secondary values.

In figure 20 mechanical laboratory testing conditions (1a) refers to laboratory testing in out-of-plane loading or compression in T direction, (2b) refers to laboratory testing in in-plane LT shear laboratory tests and (2c) refers to laboratory testing in in-plane WT shear laboratory test. Mechanical laboratory test condition (1b) is a laboratory testing process that is not usually conducted and hence the measurement values from this laboratory test is referred as secondary properties. Subscripts c refers to compression laboratory testing condition.

The elastic constants measured through laboratory testing method (1a) are Young's modulus E_T that is input as EAAU and crush strength σ_T which is interpolated for off axis loading to input for the load curve LCA. This laboratory test also provides the point at which densification starts. The stress measured at this point σ_T and strain ϵ_D at densifiction will provide a base in defining the curve for LCB and LCC as explained further. The elastic constants measured through laboratory testing method (1b) is with reference to compression in the weak axis i.e L direction which provides E_L input as EBBU on the material card and the yield stress σ_L input for curve LCC as discussed again further. Simple shear laboratory test (2b) and (2c) gives values for G_{WT} input as GABU and G_{LT} input as GBCU, along with which Shear yield limit τ_{LT} is obtained that is input as ECCU.

The variables involved with the material card *MAT_126 and the values that can be

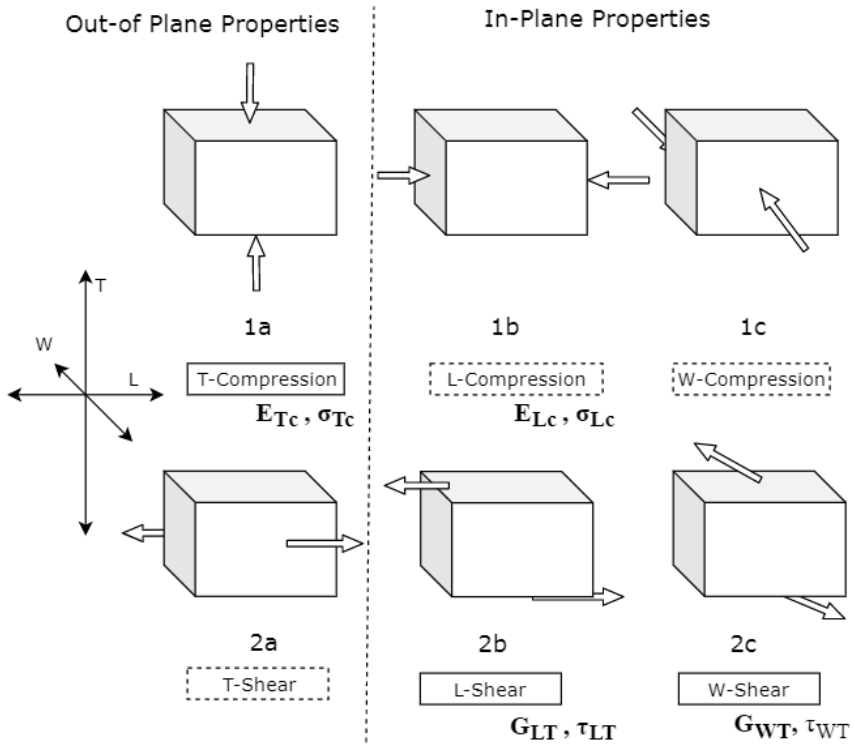

Figure 20: Simplified version of the mechanical laboratory tests required for obtaining the exact values for defining the properties of a honeycomb core. 1a, 1b, 1c refers to compression laboratory tests and 2a, 2b, 2c refers to shear laboratory tests. The highlighted laboratory tests 1a, 2b, 2c are of higher importance.

measured through laboratory tests and the description of the variables is summarised in table 4. The importance of each variable is also given. The core considered here are not defined with values that predicts a fracture of the cell but rather only the crush capability. A fracture limit can be defined at TSEF and SSEF variables. Variables E, SIGY on the material card is for the state when the core has reached densification and has completely stiffened. The variable E refers to the Young's modulus when core is fully compacted that is the slope that can be measured at regime 2-3 (refer section 3.1.1) with reference to the stress-strain curve of the aluminum honeycomb core. SIGY refers to the yield stress measured at the end the densification regime 2-3. Hence for the current condition SIGY is approximated for solid aluminum material.

In the current condition the laboratory tested values for the properties of core is not available and cannot be directly taken from previous work as discussed in section 2.2. For these reasons an approximation to the properties defining the core behaviour is taken from the data sheet available from Hexcel honeycomb manufacturers. The data sheet for Al5052 alloy is considered. Since the units maintained on LS Dyna input are SI units the values from the data sheet are converted for SI Units.

The data sheet in figure 21 is obtained by honeycomb manufacturers Hexcel Corporations. These laboratory test data from the data sheet are obtained for laboratory

Table 4: Definition of parameters on the material card- *MAT_126. (Based on [12])

MATERIAL CARD FOR *MAT_126			
Card Variable	**Importance of defined values**	**Mechnical Properties**	**Definition of variables**
RO	++	ρ^*	Material density
E	++	E_s	Young's modulus of completely compacted honeycomb material
PR	+	ν	Poisson's ratio of completely compacted honeycomb material
SIGY	++	σ_s	Yield stress of completely compacted honeycomb material
VF	+		Relative volume at which honeycomb is completely compacted
MU	+		Material viscosity coefficient
BULK			Bulk viscosity flag
LCA	++	Crush strength	Load curve for yield stress vs. angle with the strong material axis
LCB	++	σ_T vs ϵ	Load curve for stiffening stress in direction of the strong axis vs. Volumetric strain
LCC	++	σ_L vs ϵ	Load curve for stiffening stress in direction of the weak axis vs. Volumetric strain
LCS	++	Strain rate	Strain rate
LCAB			To be defined when damage is desired
LCBC			To be defined when damage is desired
LCCA			To be defined when damage is desired
LCSR			Optional strain rate curve
EAAU	++	E_T	Elastic modulus in a-direction in uncompacted configuration
EBBU	++	E_L	Elastic modulus in b-direction in uncompacted configuration
ECCU	++	τ_{LT}	Yield stress in simple shear
GABU	++	G_{LT}	Shear modulus in ab-plane in uncompacted configuration
GBCU	++	G_{WT}	Shear modulus in bc-plane in uncompacted configuration
GCAU			Yield stress in hydrostatic compression
AOPT	+		Material axes option which defines type of coordinate system
MACF			Material axes change flag
XP,YP,ZP			Coordinates of point p for the global coordinate system X,Y,Z
A1 A2 A3	+		Component of vector a for the element coordinate system
D1 D2 D3	+		Component of vector d for the element coordinate system
TSEF			Tensile strain at element failure (element will erode).
SSEF			Shear strain at element failure (element will erode).
VREF			Optional Parameter
TREF			Optional Parameter
SHDFLG	+		Damage flag for LCA

testing with samples of 0.625" thickness as mentioned from the manufacturers on the data sheet. As highlighted in figure 21 RO, EAAU, ECCU, GABU, GBCU are taken as direct input from data sheet to the material card and the values for E and EBBU for the material card is approximated. Curve definition for LCA is the crush strength interpolated for off axis loading as done in the previous studies. The crush strength for the core is obtained by the data sheet.

For the LCB curve plot which is basically the plot of regime 2-3. Since the stiffening stress at the onset of densification is unknown, it is approximated as the maximum strength value in the T direction. This forms the ordinate of LCB curve plot. Similarly stiffening stress at the onset of densification in L compression is taken with the lowest strength value obtainable from the data sheet since L is a weaker direction. Although in reality it could be even lower than the approximated value. This forms the ordinate of LCC curve plot. The abscissa for LCB curve plots is approximated to 80% densification strain and for LCC curve plots to 60% densification strain . For variables needed in fully compact conditions E is approximated to Young's modulus EAAU measured in T compression assuming it to be of almost same slope, that is the slope of regime 1-2 and 2-3 to be the same. The other variable SIGY is approximated to yield strength of aluminum as a solid material since it is the yield strength definition at full compaction of the core.

Figure 22 shows the entry values of the material model *MAT_126 for the FEA model.

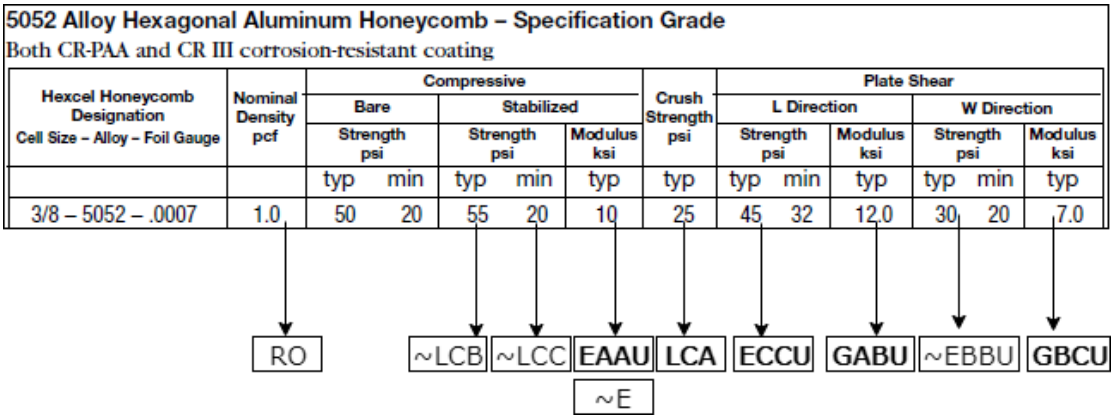

5052 Alloy Hexagonal Aluminum Honeycomb – Specification Grade

Both CR-PAA and CR III corrosion-resistant coating

Hexcel Honeycomb Designation Cell Size – Alloy – Foil Gauge	Nominal Density pcf	Compressive					Crush Strength psi	Plate Shear					
		Bare		Stabilized				L Direction			W Direction		
		Strength psi		Strength psi		Modulus ksi		Strength psi		Modulus ksi	Strength psi		Modulus ksi
		typ	min	typ	min	typ	typ	typ	min	typ	typ	min	typ
3/8 – 5052 – .0007	1.0	50	20	55	20	10	25	45	32	12.0	30	20	7.0

Figure 21: Hexcel datasheet for core- 3/8-1.0-5052-0.0007 from *Honeycomb Attributes and Properties*[8]. The values in relation to the material card parameters are also defined. ∼ approximated values.

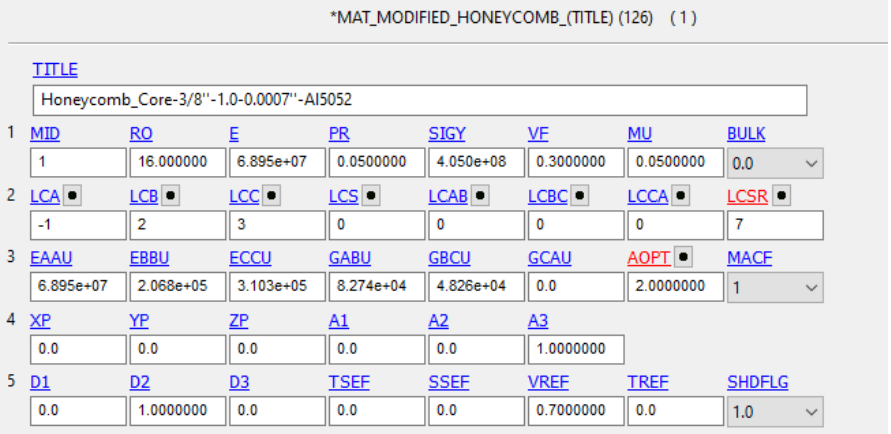

*MAT_MODIFIED_HONEYCOMB_(TITLE) (126) (1)

TITLE

Honeycomb_Core-3/8"-1.0-0.0007"-Al5052

1	MID	RO	E	PR	SIGY	VF	MU	BULK
	1	16.000000	6.895e+07	0.0500000	4.050e+08	0.3000000	0.0500000	0.0
2	LCA	LCB	LCC	LCS	LCAB	LCBC	LCCA	LCSR
	-1	2	3	0	0	0	0	7
3	EAAU	EBBU	ECCU	GABU	GBCU	GCAU	AOPT	MACF
	6.895e+07	2.068e+05	3.103e+05	8.274e+04	4.826e+04	0.0	2.0000000	1
4	XP	YP	ZP	A1	A2	A3		
	0.0	0.0	0.0	0.0	0.0	1.0000000		
5	D1	D2	D3	TSEF	SSEF	VREF	TREF	SHDFLG
	0.0	1.0000000	0.0	0.0	0.0	0.7000000	0.0	1.0

Figure 22: Parametric values defined on *MAT_126 for aluminum honeycomb core required for the current FEA analysis of the cushion.

In general, the material model requires three yield surface definition. First is the SIGY that is the yield at densification, second yield surface is flagged by the ID for load curve LCA that is yield stress at crushing. This curve LCA, plots curves for off axis loading when the ID value is less than 0. The third yield surface definition is defined in ECCU which defines initial yield limit in simple shear.[12]. The curve plot for LCSR is taken from previous works.

3.2.2 MAT_054

The material model for face sheet chosen by previous works *MAT_054 is to be defined for one layer of face sheet and two layers of face sheet since the model are correlated with a variation with the number of layers of face sheet. Correlation of variation with number of face sheet layers is discussed in section 4.3. The method adopted in defining the face sheet properties on LS Dyna with this material model is along with the variation of *SECTION_SHELL keyword. As discussed in section

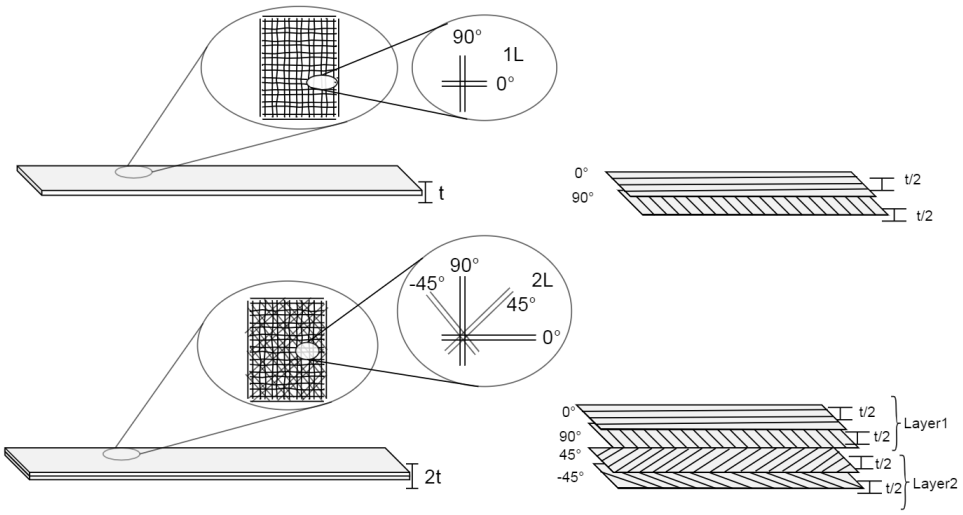

Figure 23: Formulation of woven fabric of the Dyneema face sheet as a uni-directional composite layers. One layer of woven fabric is defined by 0/90 lay up of the uni-directional fibres. Two layers of woven fabric is defined by 0/90/45/-45 layup of uni-directional fibres

3.1.2, the properties of composite layer or laminate is different from that of individual fibres. Hence care has been taken in defining the laminate properties on the material model and based on the number of layers *SECTION_SHELL keyword is adapted.

Table 5: Properties of Epoxy resin taken as the matrix of the composite material used for defining on *The Laminator*

Resin		
Properties	**Units**	**Data sheet values**
Em	GPa	4.237
Gm	GPa	1.027
$\nu_m{}^+$		0.33
Xtm	GPa	0.046
Xcm$^+$	GPa	0.046
Sm$^+$	GPa	0.046
Dm	g/cm^3	1.12

Figure 23 shows the variation in arrangement of the fibre layers for the considered unidirectional laminates of the face sheet. A single laminate of the face sheet is considered to have orthogonal unidirectional fibres and hence a single layer of face sheet is formulated as two unidirectional laminates for FEA model. The thickness of actual one fabric of face sheet is $0.45mm$, for the above mentioned reason the thickness of each uni directional layer is approximated to be half. For the arrangement of two layers of face sheet, four unidirectional laminates are considered to be arranged in 0° and 90° for one layer and 45° and -45° for the second layer of arrangement. This configuration of laminate stack up is considered in formulating the composite face sheet in the current conditions.

Table 6: Thickness and areal weight of each specially woven fabric of Dyneema, obtained from data sheet

Fabric Properties	Units	Dyneema Special Weave
Thickness	mm	0.45
Areal weight	g/m2	245

Table 7: Properties of individual Dyneema fibre of the composite material used for defining on *The Laminator*

Fiber		
Properties	**Units**	**Dyneema data sheet**
E_{xf}	GPa	116
E_{yf}	GPa	3
G_{xyf}	GPa	77.14
ν_{xyf}		0.33
σ_{txf}	GPa	3.6
σ_{cxf}	GPa	0.1
σ_{tyf}	GPa	0.03
σ_{cyf}	GPa	0.1
${\tau_f}^+$	GPa	1.8
ρ_f	g/cm^3	0.97

Calculation of composite properties is done through a software called *'The Laminator'* by Micheal Lindell. It is a composite laminate analysis software that gives results of ply stress and strain based on classical laminate theory. Based on the laminate theory the assumption considered is that the third dimension composite, that is the length, is infinitely large when compared to the thickness of the laminate. Hence a three dimensional composite is simplified to a two dimensional layer with the consideration of only in-plane loads acting upon the laminate. Here in the software, the properties of resin and woven fabric can be given as input with the definition of stack up sequence θ and thickness of each laminate T_i as discussed in section 3.1.2. Since only the thickness of woven fabric is known through data sheet which does not include the change in thickness offered by the addition of resin an approximation to each laminate thickness is made which is discussed further for each layer.

Table 5 gives the values of resin matrix input on *'The Laminator'*. Property value E_m, G_m is the Young's modulus and shear modulus of the matrix which is obtained from the data sheet of the resin. ν_m refers to Poisons ratio of epoxy resin. Superscript $+$ refers to values that are approximated. X_{cm} is the compression strength of matrix. This is assumed to be equal to tensile strength X_{tm}. Property value D_m is the density of the resin. S_m refers to the shear strength of the resin matrix which is assumed to be same as tensile strength since it is assumed to be equally distributed and resin failure is not taken into consideration.

Table 8: Properties of laminates of Dyneema-Epoxy composite calculated for 60% fibre volume.

Laminate Properties		
Property	**Units**	**Dyneema and Epoxy resin**
Composite density	g/cm3	1.03
Fibre Vol Vf	%	60
Fibre weight	%	56.5
Fibre Den	g/cm3	0.97
Resin Vol	%	40
Resin Weight	%	43.5
Resin Density	g/cm3	1.12

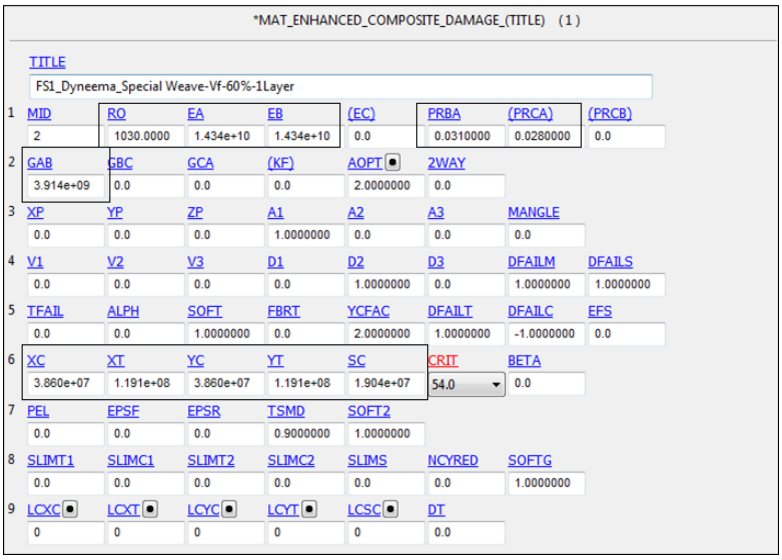

Figure 24: Parametric values defined on *MAT_054 for Dyneema face sheet of one layer required for the current FEA analysis of the cushion.

Fibre properties can be obtained from data sheet. These properties are of individual fibres and not of woven fabric properties. The only data obtained for woven fabric are the areal weight and thickness as shown in table 6. Hence the assumption with each layer in uni-directional arrangement is taken for the composite face sheet with a defined stack up sequence θ. Within the software there is provision for the input of properties of individual fibre strands which can be obtained from the manufacturers of Dyneema.

In the current condition the values for Dyneema fibres are taken from a *DSM Brand* data sheet. These properties are summarised in table 7. Subscript x and y refers to the x and y direction of the fibre. Property values E_{xf} and E_{yf} refers to young's modulus of the each fibre strand in fibre direction and in its transverse or y direction. G_{xyf} refers to the rigidity modulus. ν_{xyf} refers to Poisons ratio as explained in section 3.1.2. The value for shear strength τ_f is assumed to be half of tensile yield strength in fibre direction. This approximation is based on Von-mises failure criteria. Density of each fibre is given by ρ_f. These values are input for fibre properties on *'The Laminator'*.

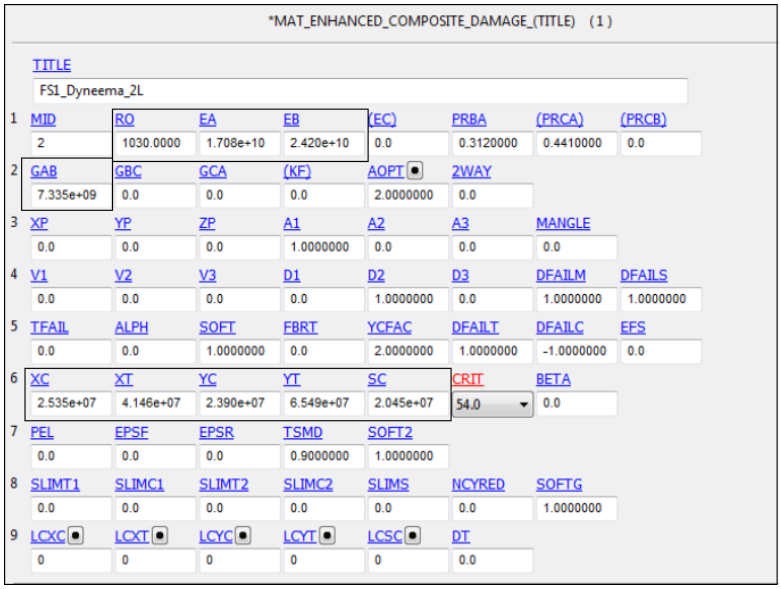

Figure 25: Parametric values defined on *MAT_054 for Dyneema face sheet of two layer required for the current FEA analysis of the cushion.

Along with the properties of resin and individual fibre strands, the stack up sequence θ and the thickness of each laminate layer T_i is to be input on *'The Laminator'* which then calculates the values for composite as a whole. It also calculates values for tensile strength XT, YT and compressive strength XC, YC in each direction of the composite. SC is the shear strength. GAB is the shear modulus, EA is the elastic modulus in x direction and EB is the elastic modulus in y direction. For different layers of face sheet, these values are obtained as output from the composite calculator. It is entered on the material card *MAT_054. Density of composite as a whole is not known. With the input of fibre density, resin density and volume fraction of fibres, composite density, resin volume fraction, fibre weight and resin weight can be calculated with online calculators. One such calculator available is from the Hexcel Corporation. These values are necessary to obtain composite density. The composite density is defined as RO parameter for the material model *MAT_054. A summarization of values is given in the table 8. Volume fraction is assumed to be 60% as discussed in section 3.1.2.

Figure 24 shows the values of the material model for one layer of face sheet i.e with two uni-directional arrangement of fibres in the composite face sheet. With reference to figure 73 in the appendix is the keyword *SECTION_SHELL that defines the face sheet thickness on LS Dyna. The value entered for T1 is the thickness of the composite face sheet. It is approximated to be $0.5mm$ since woven fabric is of $0.45mm$ and on addition of resin the composite thickness is approximated for an increase of $0.05mm$. The definition of uni-directional fibre can be given with two integration point at NIP with angle definition in Bi. Bi is defined as 0 and 90 for each integration point. It is to be noted that the values entered on both material and section keyword are in SI units.

Figure 25 shows the material model with values entered for face sheet when two layers are used. The input of property values of resin and fibres is same as discussed above only varying the stack yp sequence θ and thickness of each laminate T_i. The composite property values can be calculated with uni-directional fibre stacked up in 0°, 90°, 45° and -45°. The change in angle at each integration points are updated on values of Bi. The thickness of each laminate is defined with the consideration of resin addition. The values obtained for the composite of two layer i.e four unidirectional laminate are entered on the material model. Young's modulus in each direction, rigidity modulus tensile and shear strengths of the composite laminate is obtained for two layer stack up. The integration points for the definition of co-rotational properties on LS dyna is defined on *SECTION_SHELL keyword as seen on figure73 in the appendix for two layer of face sheet. The thickness of composite for the two layer is measure to $1.8mm$ by a sample which is updated at T1 on the *SECTION_SHELL keyword for two layer face sheet condition.

4 Test Correlation

'One of the basic rule of Universe is that nothing is perfect. Perfection simply doesn't exist, Without imperfection neither you nor I would exist.
— Stephan Hawking

Correlation between FEA models and laboratory test models is the main requirement of the current work. As discussed so far, the correlation of cushion model is carried out for the cushion geometry model 1. The laboratory testing of the cushion with the pendulum system has adopted variation with the type of core, the number of face sheet layers being used and the type of target. As discussed in the section 1.1, for the current correlation two types of surface on which the cushion impacts is chosen. One is the obstacle or penetrator type and the other is the flat surface type of target. Each component of the cushion in the laboratory test condition is modelled and meshed appropriately to perform the finite element analysis (FEA). In relation with sections 1.3 and 1.4, correlation of the laboratory test condition is performed by modelling of *Core, Face sheet, Target, Ground plate* and *Mass plate*. Pendulum system is not modelled rather boundary conditions are given such that the model is under free fall.

Figure 26 shows an over view of all the FEA model setup considered for laboratory test correlation and laboratory test prediction. The FEA model with the cushion model1 with one layer of face sheet under free fall with a velocity of 4m/s on a penetrator target is taken as a base setup which is discussed in section 4.1. First variation considered is with the type of target surface. Since base model is with penetrator target, model set up with flat plate target is considered for correlation and is discussed in section 4.2. As the force distribution for penetrator target and flat surface target gives more information about the behaviour of core and face sheet, these model correlation would also validate the formulation of core and face sheet in the FEA models.

The second variation of model setup considered, is with the change in number of layers of the composite face sheet used. Since the base model is considered with one layer of face sheet, correlation for laboratory test condition with two layer of face sheet is considered as one of the other model, which is discussed in section 4.3. This would provide more information on formulation of composite face sheet for FEA. Correlation of displacement, velocity, acceleration and force as recorded during the pendulum laboratory tests condition is carried out for all the FEA models.

The material properties for core and face sheet as discussed in section 3.2 are given as input for the material models *MAT_126 and *MAT_054. As discussed in section 3.2.1 and 3.2.2, the values of core properties and face sheet properties are approximated. The property values of core are approximated from the data sheet. Hence as discussed in Chapter 3 the variation with the values of properties are regarded and an error of $\pm 20\%$ or more can be expected in the simulation results. Also to be considered is the overall system mass of the laboratory test condition is $15kg$ where as FEA model is about $10.5kg$.

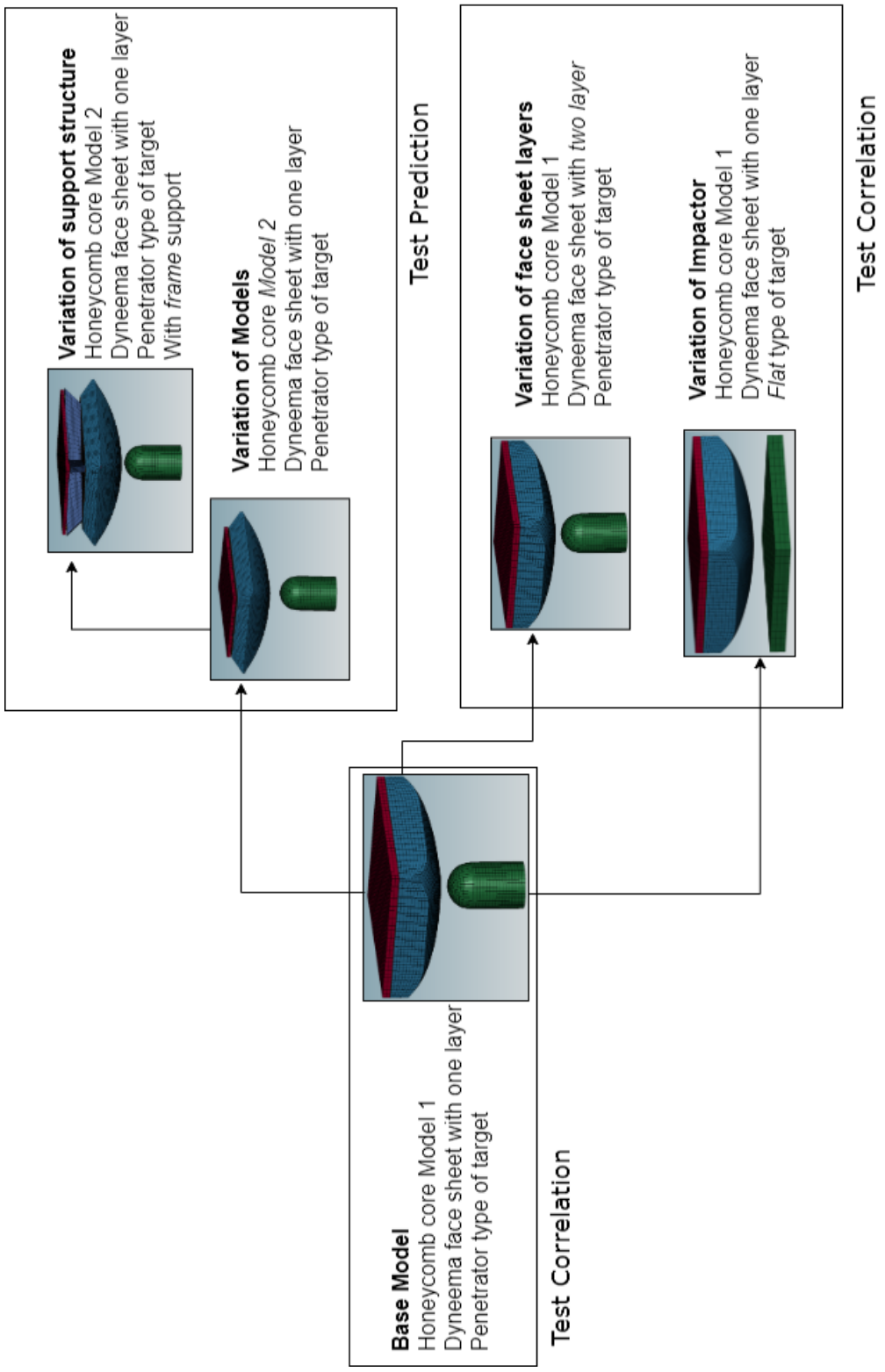

Figure 26: Different conditions of FEA model setup of the cushion model.

4.1 Model1 with Penetrator target

The model setup for correlating the cushion with aluminum honeycomb core and Dyneema face sheet is carried out by considering a base FEA model. The Dyneema face sheet is considered with one layer of $0/90$ woven fabric. Penetrator target is considered as the surface on which the cushion impacts. The mass plate is formulated to be of approximately $10kg$ as per the requirement. Table 9 compares the FEA model setup to laboratory test condition set up. The thickness of Dyneema fabric is $0.45mm$ from the data sheet before infusing with resin. Hence FEA model of face sheet is formulated for $0.5mm$ thickness to account for the thickness offered when fibre is infused together with resin.

4.1.1 FEA model Setup

Figure 27 shows the simulation set up with the type of material models used and the mass of corresponding part with the colour codes of each part. Mesh elements of core, target, ground plate and mass plate are defined as solid elements. Face sheet mesh elements are defined as shell elements with an over all thickness of $0.5mm$. In relation with table 9, the mass and the dimensions of each part can be considered for comparison. The source of each part as a mesh model for the FEA model is also tabulated. CAD model of the cushion geometry is imported on the preprocessor and meshed accordingly. Face sheet elements are created as a copy of core elements to match with the nodal attachments between the core elements and face sheet elements. Penetrator target is also imported as a simple CAD model with corresponding dimensions and meshed accordingly. The mesh of the target is created with *Block Mesher* option, with a CAD model of cylinder of radius 45mm corresponding to the target used in the laboratory test conditions. Ground plate and Mass plate are created by simple box solid mesh. The mass of the Mass plate is formulated to an approximate of $10kg$ as per the requirement. Mass of core and face sheet of the laboratory test model was calculated by interpolation. The mass of core and face sheet together in the FEA model is about $284g$ and that of the laboratory test model is $270g$. The overall system mass of the laboratory test condition is $15kg$ where as the overall system mass of the FEA model is about $10.5kg$.

Name	Type	Id	Color	PlotMode	MatId	MatName	Thickness	Mass
Assembly 1		1						
1 Honeycomb Core	Solid	1		Shade	1	Mat_126_Modified_Honeycomb	0	0.114359
2 Dyneema face sheet - Vf~60%	Shell	2		Shade	2	Mat_054_Enhanced_Composite_Damage	0.0005	0.168974
3 Impactor- Penetrator	Solid	3		Shade	3	Mat_020_Rigid	0	6.39802
5 Aluminum Ground plate	Solid	5		Shade	5	Mat_024_Piecewise_Linear_Plasticity	0	0.24164
6 Mass plate	Solid	6		Shade	6	Mat_024_Piecewise_Linear_Plasticity	0	9.99701

Figure 27: FEA model setup of cushion system with corresponding colour codes of each part. The material cards used for each part definition and the mass of each mesh part formulated for FE analysis is shown.

Meshing of core is carried out using *Block Mesher* option by selecting the edges of the core and projecting it to the corresponding curvatures of surface. Face sheet is created

by generating elements corresponding to the solid face of the core with *Element Generation* option. Boundary condition of free fall is given as *Intial* condition to all nodes under free fall with *Entity* option. The free fall is formulated as initial velocity in the negative Z direction with 4 m/s. The model under gravity condition taking $9.8m/s^2$ is given as pre-loading with *Dynamic Relaxation*. Pre-loading with dynamic relaxation is adapted from the previous works.

Table 9: Comparison of dimensions and mass of the FEA model to laboratory test model. The source for each mesh part for the FEA model is also tabulate.

		FEA Model			Laboratory test Model	
Part	**Part reference**	**Part Source**	**Dimension (mm)**	**Mass (g)**	**Dimension (mm)**	**Mass (g)**
Core	1	CAD model of the cushion	300 * 300 * 100	114	300 * 300 * 100	170
Face sheet	2	Element generation	Thickness with resin = 0.5mm	170	Thickness = 0.45mm	100
Ground plate	5	Shape Mesher_Box solid	300 * 300 * 1	241	300 * 300 * 1	230
Mass plate	6	Shape Mesher_Box solid	300 * 300 * 14	9997	Dummy Lander	14500

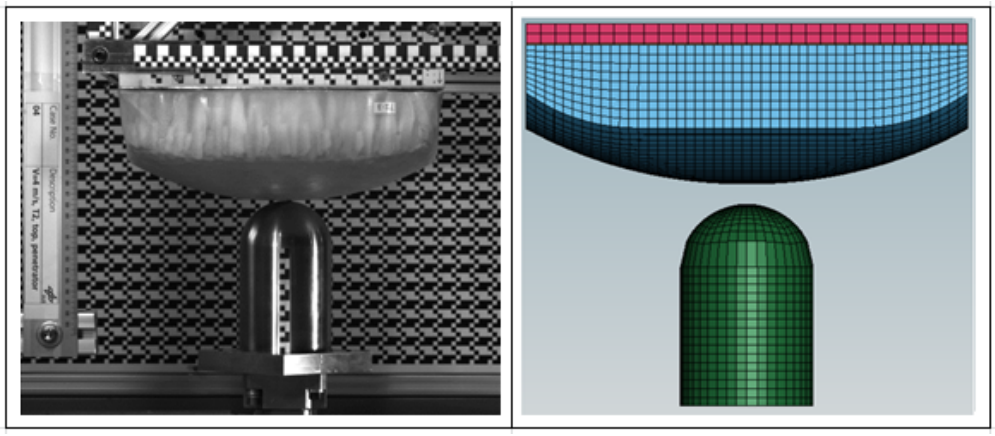

Figure 28: Comparison of laboratory test conditions of the cushion with laboratory setup on the left and FEA model setup on the right showing base model of the cushion model 1 with one layer of face sheet impacting on a penetrator target.

Figure 28 shows the laboratory setup in comparison to the FEA model of the crash impact laboratory tests. The FEA model is not restricted in motion in any direction that is it has all six degrees of freedom of motion, three translational and three rotational. Velocity of fall is given in one of the translational motion that is in Z direction. Acceleration due to gravity is also a preloading condition given. It is taken for Earth's acceleration that is $9.8m/s^2$. It is to be noted that the core is covered by face sheet in the images of the FEA models since it is an integral part. As mentioned above the dimensions of each part are formulated as per the laboratory test conditions.

The instantaneous time step animation of the free fall of the cushion beginning at $0s$ to end of simulation at $0.1s$ is shown as series of images in figure 29. At $time = 0$ shows the start of the free fall. At about $time = 0.003s$ the first contact with the penetrator takes place. The face sheet takes up the initial in-plane loads and the reaction

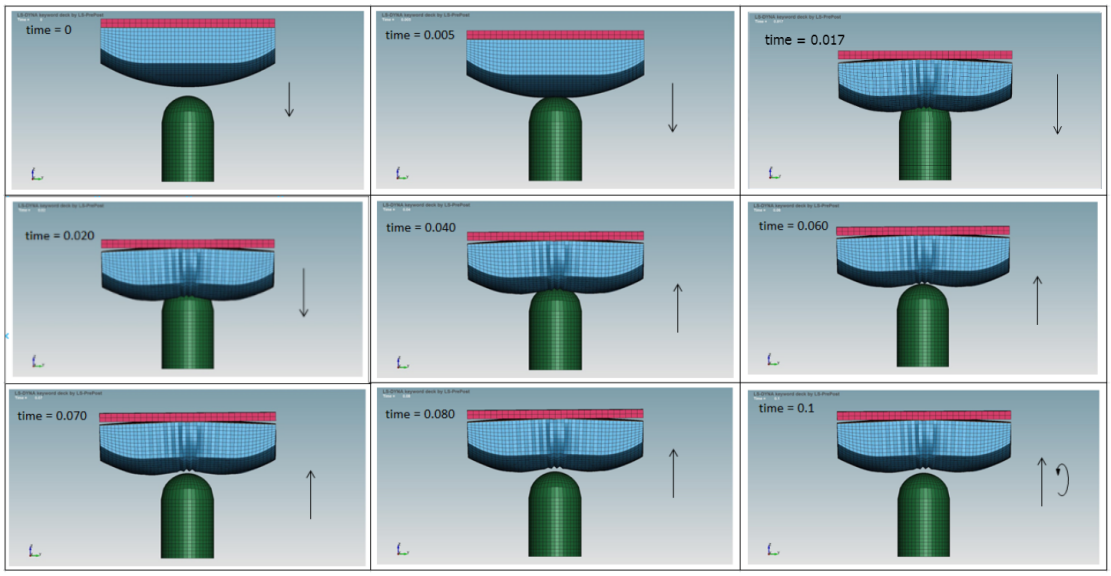

Figure 29: Simulation run of FEA model of the cushion under free fall at different time instances for cushion model 1 with one layer of face sheet impacting on a penetrator target

is seen as wrinkling of the face sheet. And the core takes the shear load by buckling or crunching of the cells. Energy is absorbed by the cushion until its $time = 0.020s$. The cushion reaction to impact results in bending. Once the impact energy is absorbed and converted into deformation of the cushion, the cushion is seen to bounce off of the target surface. At about $time = 0.060s$, the cushion is out of contact with the target surface. Plastically deformed cushion retains its deflection. At the end of the simulation run $time = 0.1s$ the model is also seen to topple about its central axis. The total deformation of the cushion is taking place between the time intervals of about $0.003s$ to $0.020s$. Indentation depth, velocity variation and energy absorption takes place at this stage. These are discussed in section 4.1.2.

The cushion models in FEA in comparison with laboratory test model is depicted in figure 30. The laboratory condition cushion is shown on the left while the FEA model of the cushion before impact is shown on the right. In relation to this, the figure 31 shows the cushion model of the laboratory test condition and the FEA model after the impact. The impact pattern can be compared between the models. The wrinkling of the face sheet observed in both the models are very similar. It takes place along the fibre direction that gives higher strength to the face sheet. The failures of the components of the sandwich panel observed due to impact are *Core indentation* and *Face wrinkle*. Core indentation is a core failure and face wrinkle is face sheet failure conditions. Core indentation occurs depending on its crush strength in compression. Face wrinkling occurs depending on the relative strength of core in compression. [3]. These failure conditions acts favourable to this study since the energy absorption occurs through the deformation of core and face sheet as discussed in section 3.1.

Figure 32 shows the deflection of the cushion seen as bending, as a result of impact. It

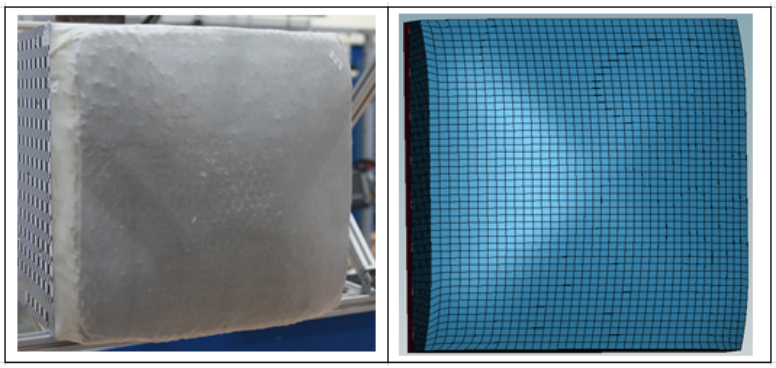

Figure 30: Comparison of the cushion with laboratory model on the left and FEA model on the right showing before impact of the base model of the cushion model 1 with one layer of face sheet.

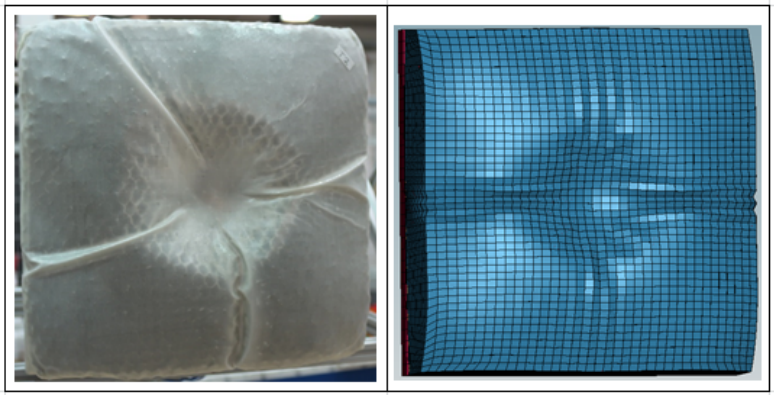

Figure 31: Comparison of the cushion with laboratory model on the left and FEA model on the right showing after impact of the base model of the cushion model 1 with one layer of face sheet.

shows the comparison between the deflection seen in the laboratory test condition to the FEA condition. In this study the deflection of the cushion is not measured in both the conditions. Nevertheless the pattern of deflection observed are synchronous. As discussed in section 3.1 total deflection of the cushion or a sandwich structure is due to bending loads and shear load distributed between the core and face sheet. Hence these observation and comparison on the pattern of impact and deflection are in close agreement.

4.1.2 Correlation of Results

Indentation Depth:
The correlation between values of the stroke or displacement of the pendulum system in the laboratory test condition and the global displacement of the cushion in the FEA model is shown in figure 33. The laboratory test condition measures the displacement of the whole pendulum system with laser measurement and reflector as discussed in section 1.3. The red curve shows the change in displacement of the cushion, measured by the displacement sensor L1 with reference to figure 5. The green curve shows the

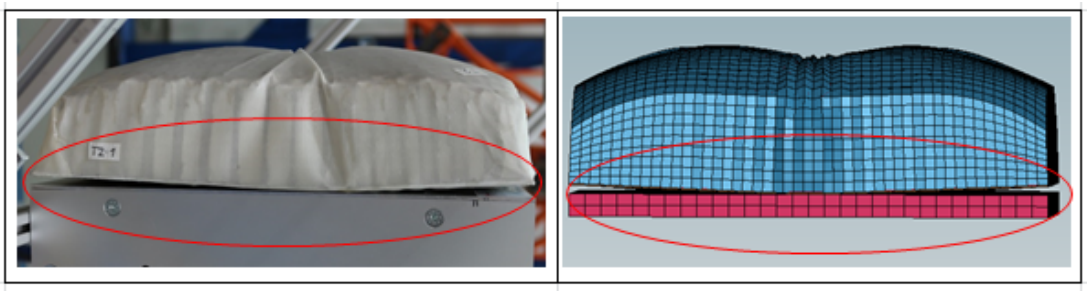

Figure 32: Deflection of the sandwich cushion seen during the laboratory test on the left as opposed to the similar deflection or bending seen in FEA on the right.

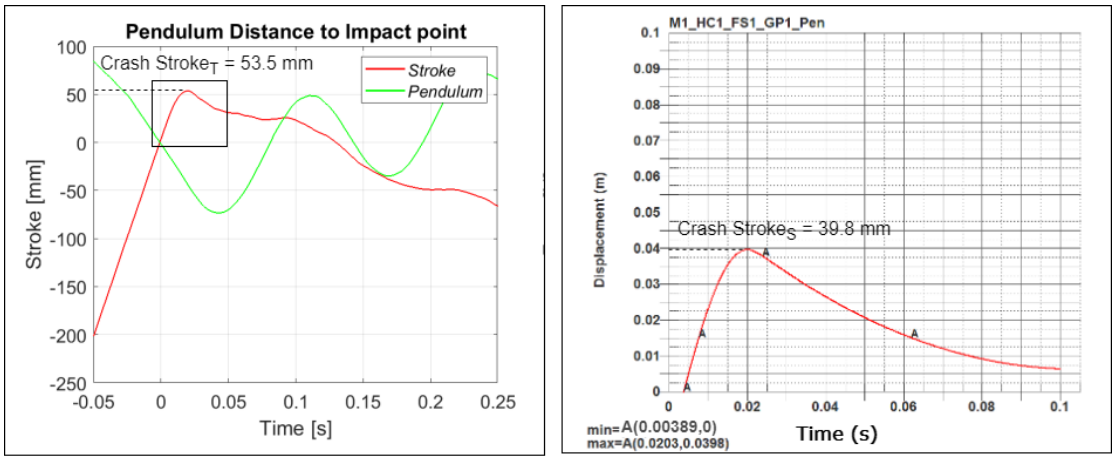

Figure 33: Correlation of indentation depth of the cushion with one layer face sheet impacting on a penetrator target between laboratory test condition on the left to FEA simulation on the right. Maximum indentation measured in each condition is highlighted.

change in distance of the arms of the pendulum measured by L2 displacement sensor. The sinusoidal variation of the curves is due to the oscillation of the pendulum. The zero reference in the laboratory test graph is the point of first contact between cushion and target. The change in measured distance from the point of zero reference that is at the crossing over of the two laser measurement and the maximum displacement is found to be $54mm$ in the laboratory test results.

In the FEA model the resultant displacement of the system is given from the beginning of the simulation, but here the graph is taken from the first point of contact. The zero reference for the FEA model is taken at time $t = 0.003s$ on the abscissa, which is the first point of contact and the ordinate gives the displacement. In the FEA model at time $t = 0s$, the cushion displaces $0.015m$ which is the fall height of the cushion above the target. This part of the displacement covering the fall height is not taken in the graph. The actual curve of displacement in the FEA model is negative because of the downward or fall motion of the cushion. However, it is inverted and a positive displacement curve is taken to have an easier correlation with the laboratory

Table 10: Tabulation of correlation results for indentation depth of the cushion with one layer face sheet impacting on a penetrator target

M1_HC1_FS1_1L_GP1- Pen				
Impact Point	Laboratory test		FEA	
	Time	Stroke (mm)	Time	Stroke (mm)
First contact	0	0	0.004	0
Deepest	0.025	54	0.020	40

test condition.

At time $t = 0.02s$, when the cushion has absorbed energy upto its capacity, the maximum displacement measured is $40mm$. In correspondence to the laboratory test condition value, a difference of -26% is seen. This is because the laboratory test system has an overall mass of $15kg$ and the FEA model is formulated with a $10kg$ mass plate and the over all system is about $10.5kg$. This accounts for the total energy of the system based on mass load distribution over the cushion that influences the impact depth. This deviation in values can be expected. Also taken into consideration is the property values of the core and face sheet of the FEA model which is approximated as discussed in section 3.2.1 and 3.2.2. The summary of the indentation at different instances is tabulated in table 10.

Velocity:

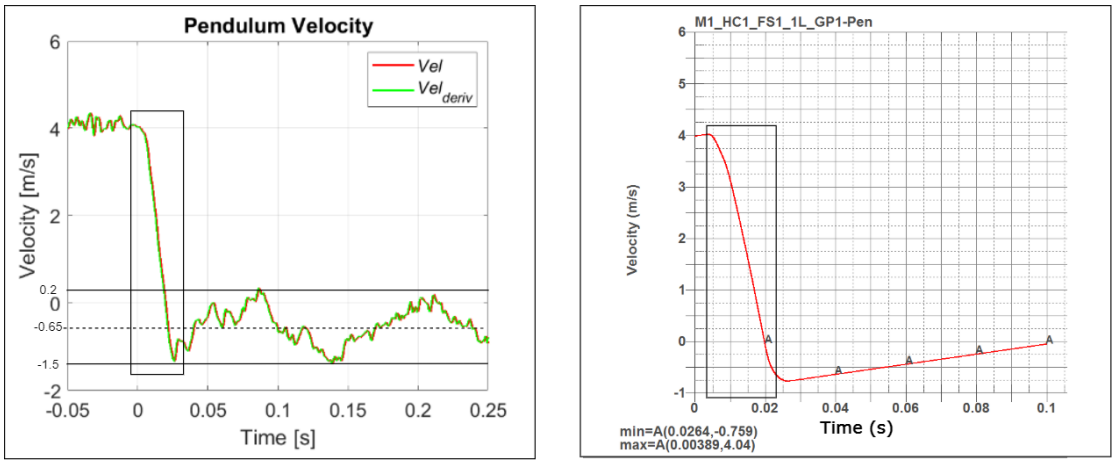

Figure 34: Correlation of velocity reached by the cushion with one layer face sheet impacting on a penetrator target between laboratory test condition on the left to FEA simulation on the right. Bounce off velocity measured in each condition is highlighted.

The velocity measured in the laboratory test condition is an interpolation of the displacement of the cushion measured by laser-reflector plate displacement sensor L1. The drop velocity in the laboratory test model was set at a $4m/s$ at time $t = 0s$. The path taken by the laboratory test model is an arc motion of the pendulum system.

The pendulum system starts decelerating from $4m/s$ until impact. At impact, the velocity is reduced to $0m/s$. After impact the pendulum system is pushed backwards, this velocity is measured as negative velocity that is seen on the graph. The rest of the curve is due to the impact induced oscillation of the pendulum system. After bounce off, the velocity reached by the system is the mean of the sinusoidal curve which corresponds to an approximate of $0.65m/s$ in the opposite direction.

In the velocity graph of the FEA model, at time $t = 0s$ the drop of the cushion toward the target begins. There is a slight increase in the velocity from the beginning until impact. This maximum velocity is measured to be $4.04m/s$. This increase is because of the additional acceleration due to gravity given as a necessary pre-loading condition to the FEA model. At around time $t = 0.003s$ the cushion comes in first contact with the target. The velocity starts decreasing until time $t = 0.02s$. The cushion absorbs the energy by deformation and the velocity is reduced to $0m/s$. After impact the cushion bounces off of the target with a decreased speed in upward direction. This is measured as a negative velocity of the system and it reaches $0.76m/s$ until time $t = 0.026s$. The cushion starts slowing down to come to an halt and this is seen as a positive slope from time $t = 0.026s$ until end of simulation. The cushion falls back again to the surface after bouncing off, due to acceleration due to gravity. The mass of the system in the FEA model is lower than the laboratory models and hence the FEA model bounces off with a higher velocity after impact than that of the laboratory model.

Table 11: Tabulation of correlation results for velocity reached by the cushion with one layer face sheet impacting on a penetrator target

M1_HC1_FS1_1L_GP1- Pen				
Impact Point	Laboratory test		FEA	
	Time	Velocity (m/s)	Time	Velocity (m/s)
First contact	0	4.02	0.004	4.04
Bounce off	0.025	0.65	0.026	0.76

A summary of the observation made on the measure of velocity between laboratory test and FEA is given in table 11. Velocity of the system at the beginning of the fall and the bounce off velocity reached by the system is tabulated. The bounce off velocity reached by the cushion in the FEA model is $0.76m/s$ which is higher than the laboratory model of $0.65m/s$ due to difference in the overall mass of the systems. A system with lower mass has dissipated lower energy and hence has higher residual energy to bounce off. There is a difference in the FEA value of 17% from that of laboratory model. However, for a mass difference of 30%, it is still in the range of expected deviation of results. Hence it can be concluded that these are values are in close agreement with each other.

Acceleration: In the laboratory test condition, acceleration is measured using accelerometers. Figure 35 shows the correlation between acceleration measured during

the laboratory test condition on the left and FEA model values on the right. The sharp strokes seen on the curves in the graphs of laboratory test condition is due to wrinkling of face sheet and crushing of the honeycomb cells of the core. The acceleration for correlation is compared for the values only along the fall direction that is in Z direction. The measurement of acceleration in the laboratory test condition is started when the system reaches a load corresponding to $20N$. The acceleration measured at this point is seen as a constant horizontal curve at around time $t = 0s$.

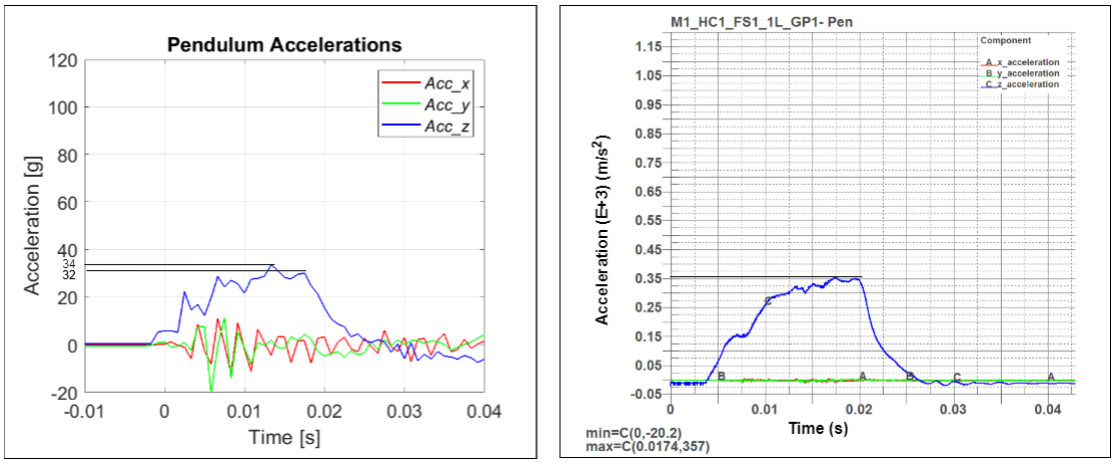

Figure 35: Correlation of acceleration of the cushion with one layer face sheet impacting on a penetrator target between laboratory test condition on the left to FEA simulation on the right. Maximum acceleration measured in each condition is highlighted.

The figure 35 can be studied and is summarised in table 12. Correlation between measured values of the laboratory test condition on left to the FEA measured values on right are shown as graphs in the figure. The first contact in FEA occurs at time $t = 0.003s$. The acceleration measured at the first contact is $2g$ in magnitude in both the conditions. At impact the maximum acceleration reached by the system is $34g$ in laboratory tests and $36g$ in FEA. The maximum acceleration seen at the peak is due to complete absorption of energy. It then drops while bouncing off of the surface after impact. Once the crushing of cells are complete, the system accelerates in the opposite direction as a reaction to the impact with some residual energy.

The very first peak stroke seen at about $20g$ in the laboratory test condition and at $15g$ seen in the FEA graph observed here might be because of the curvature of the cushion being deformed. The curved surface of the cushion comes in contact with the impactor at first contact. From the first contact to the point where the bulged curvature of the cushion absorbs energy which is seen as the first peak. During the flattening of the curvature of the cushion, the elements of core as wide as the surface area of the target buckles while the face sheet wrinkles along the fibre directions. Once the curvature flattens out, distribution of the load among the adjoining elements begins and this is seen as the curve rising back to absorb the rest of the load until peak acceleration is reached. The other instances of first contact, maximum acceleration

Table 12: Tabulation of correlation results for acceleration of the cushion with one layer face sheet impacting on a penetrator target

M1_HC1_FS1_1L_GP1- Pen				
Instant	**Laboratory test**		**FEA**	
	Time	**Acceleration (g)**	**Time**	**Acceleration (g)**
First contact	0	2	0.003	-2.02
Max. acceleration point	0.015	34	0.017	36
Loss of contact and return	0.018	32	0.020	35

point and the point of loss of contact is also tabulated in table 12 . A difference in value measured for peak acceleration is

Force: The force measurement for the system is recorded by the force sensor placed behind the target in the laboratory test condition. In the FEA force is measured by multiplying the acceleration measured with the mass of the system. Although there might be ways on the simulation setup to measure the force directly using interrelated keywords, currently these keywords are not studied under this work.

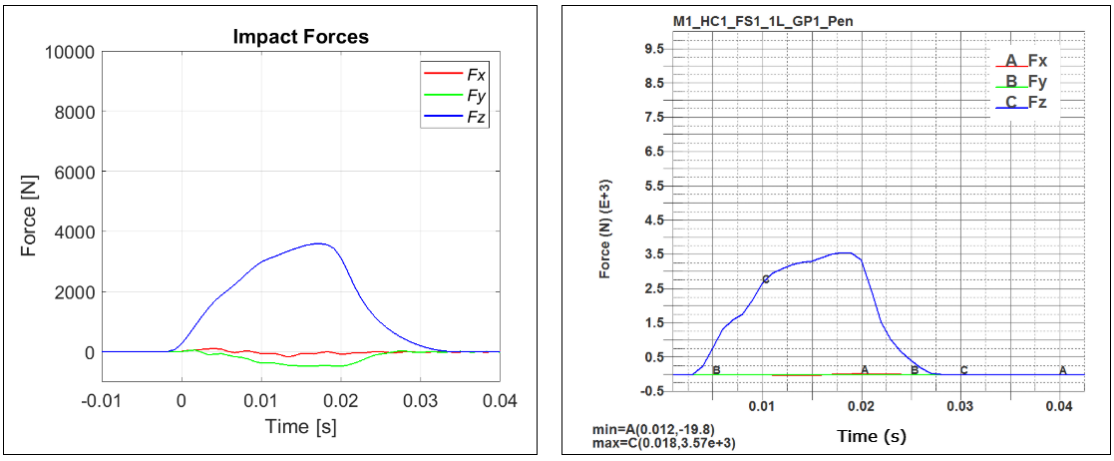

Figure 36: Correlation of force acting on the cushion with one layer face sheet impacting on a penetrator target between laboratory test condition on the left to FEA simulation on the right. Maximum force acting on the system is highlighted.

Figure 36 shows the graphs plotted for force measured by the laboratory test condition on the left and FEA simulations on the right. The maximum force acting on the system can be measured by the end of impact. After which the system starts to accelerate in the opposite direction with a residual energy after impact energy is absorbed. The maximum force acted on the system is when the energy with which the system falls is absorbed completely and the residual energy makes the system to bounce off of the surface. The maximum force measured in the laboratory test condition is $3588N$ in contrast to FEA is $3570N$ at time $t = 0.018s$. The maximum force absorbed in the FEA model is lower because of the overall system energy being lower. These results are summarised in the table 13.

Table 13: Tabulation of correlation results for force acting on the cushion with one layer face sheet impacting on a penetrator target

M1_HC1_FS1_1L_GP1- Pen				
Impact Point	Laboratory test		FEA	
	Time	Force (N)	Time	Force (N)
Max.Force	0.015	3588	0.018	3570

Correlation of Indentation depth, velocity, acceleration and force between the laboratory model and FEA has given close results. The deviation with the values that is seen are due to the difference in the overall system mass and also due to the approximations considered and discussed in the earlier sections. The difference in the values of indentation with 24% lower, velocity with 17% higher, acceleration with 5% higher and force with 0.5% lower are either negligible or still within the range of expected deviation of results. The results discussed until here has been for the penetrator target. A better understanding can be obtained for validating the FEA set up by considering and correlating few other conditions.

4.2 Model 1 with Flat Plate target

The next laboratory test condition considered is the cushion model 1 with one layer of face sheet as in the previous condition but with a flat plate target. Since the penetrator target can show how efficient the core is, varying the target for our studies will give us the understanding of the face sheet formulation.

4.2.1 FEA model Setup

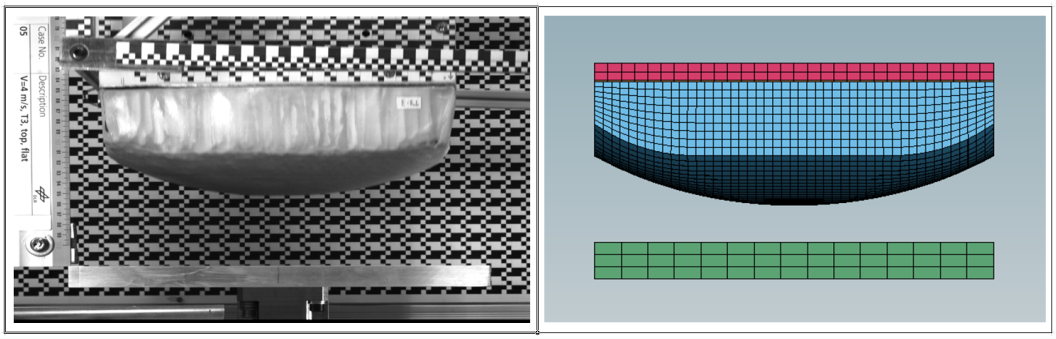

Figure 37: Comparison of laboratory test conditions of the cushion with laboratory setup on the left and FEA model setup on the right. The cushion model 1 with one layer of face sheet impacting on flat target is shown.

The FEA model setup for the cushion model 1 with one layer face sheet is set up similar to the previous condition. The impact condition considered here is the flat

plate target. The flat plate is generated using Box solid mesh option with properties similar to that of the penetrator target. When cushion falls on a flat surface the area of cushion that comes in contact with the flat target is more than that when it falls on the penetrator target. The increased area distributes the load in the in plane direction. As discussed in the earlier sections, the cushion model consists of core and face sheet which is modelled the same way as the previous. The choice of material cards on LSDyna for core and face sheet is the same as discussed in section 3.2. Flat surface for impact is modelled as a rigid body similar to that of penetrator target. FEA simulation is carried out for a velocity of 4 m/s in the negative Z direction or the downward fall direction.

Figure 37 shows the FEA set up of the cushion in comparison with laboratory set up. The target is a flat plate. The core is not visible since the face sheet is modelled as an outer layer over the cushion. Mass plate is modelled for $10kg$ weight, same as in the previous condition. The wide area of the cushion that comes in contact at impact can be observed in the images.

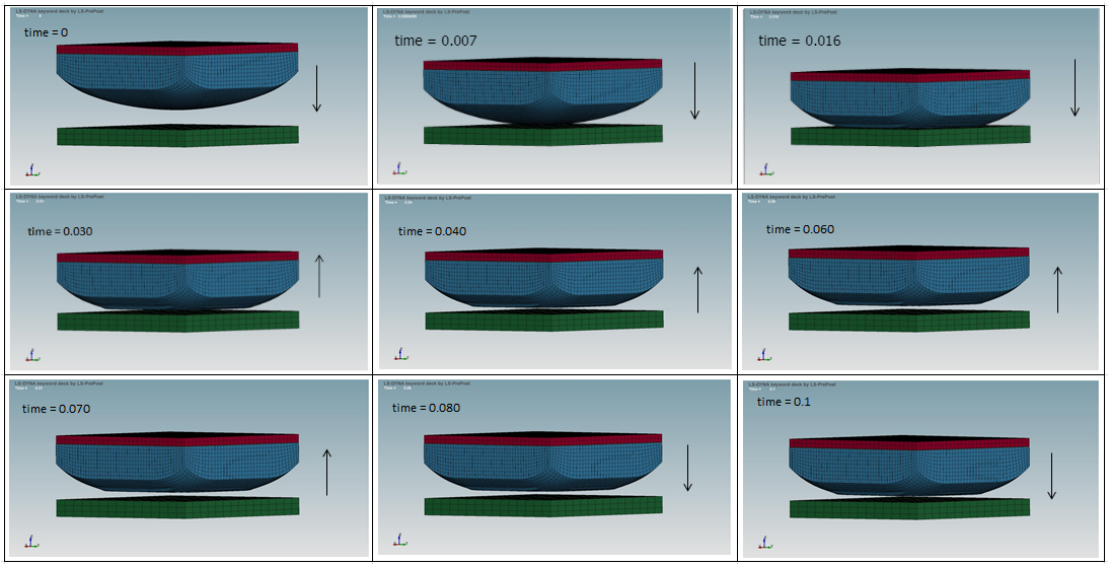

Figure 38: Simulation run of FEA model of the cushion under free fall at different time instances for cushion model 1 with one layer of face sheet impacting on a flat target

Figure 38 depicts the stage wise animation of the free fall scenario of the cushion. At $time = 0$ shows the start of the free fall. At about $time = 0.007s$ the first contact with the flat target takes place. The face sheet takes up the initial in-plane loads and the reaction is seen in wrinkling of the face sheet. Energy is absorbed by the cushion until its $time = 0.016s$. The cushion reaction to impact results in face sheet wrinkling. Once the impact energy is absorbed and converted into deformation of the cushion (as discussed in section 3.1), the cushion is seen to bounce off of the surface. At about $time = 0.016s$, the cushion is out of contact with the target surface. The total deformation of the cushion is taking place between the time intervals of about

$0.007s$ to $0.016s$ in contrast to the time duration of contact when cushion falls on penetrator target between $0.003s$ to $0.020s$ as seen in the previous condition which is longer. Indentation depth, velocity, acceleration, force distribution are discussed in the following subsections.

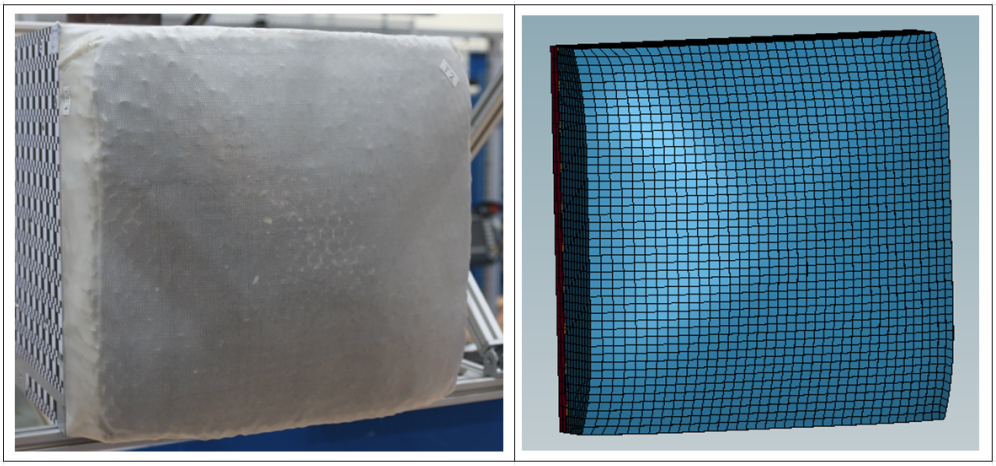

Figure 39: Comparison of the cushion with laboratory model on the left and FEA model on the right showing before impact of the cushion model 1 with one layer of face sheet impacting a flat target.

Figure 39 shows the set up of the of the cushion in the laboratory testing condition in comparison to the FEA setup before impact. In relation to this figure, the figure 40 shows the same comparison of the cushion after impact. The area that has come under impact and reacted with the in-plane distribution of load can be noticed. The face sheet wrinkling is noticed.

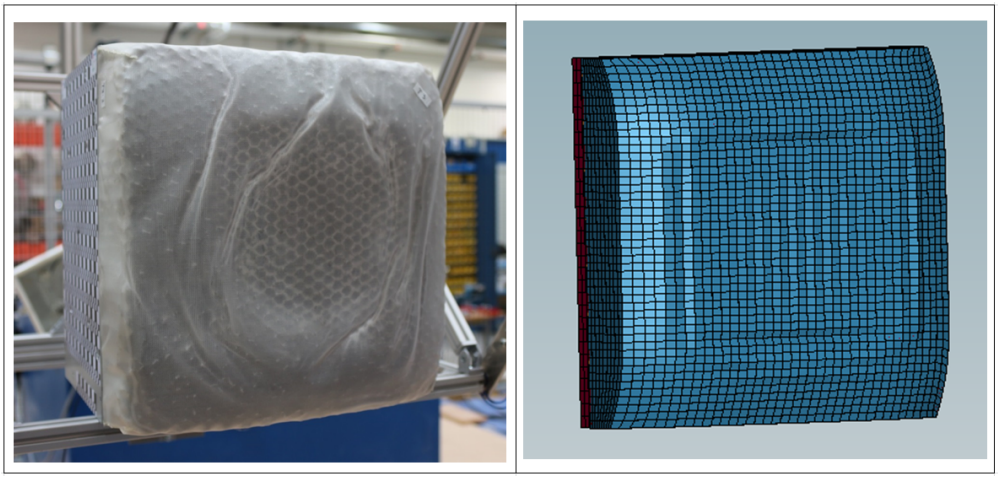

Figure 40: Comparison of the cushion with laboratory model on the left and FEA model on the right showing after impact of the cushion model 1 with one layer of face sheet impacting a flat target.

Since FEA is an ideal condition, the in-plane distribution of load is seen until it gets equally distributed throughout the surface area of the cushion in contact with flat target. In the laboratory condition, the distribution is not as equally distributed as in the FEA condition. One reason might be for the method adopted for gluing the face sheet over the core in the laboratory testing. The other possible reason might be because of the circular inertia of the pendulum system in the laboratory testing. Although the laboratory testing is in linear motion for that millisecond instant of impact, the system still has the circular inertia and the load seems to be distributed slightly more towards the topside than the bottom. Hence there exist a change in deformation of face sheet. Since the energy transfer due to impact is dissipated as core and face sheet deformation, it can be seen that most of the in-plane load is taken up by the faces. Face sheet *wrinkling* and *dimpling* is seen as a pattern of dip and rise of the surface as a reaction due to impact.

4.2.2 Correlation of Results

Indentation:

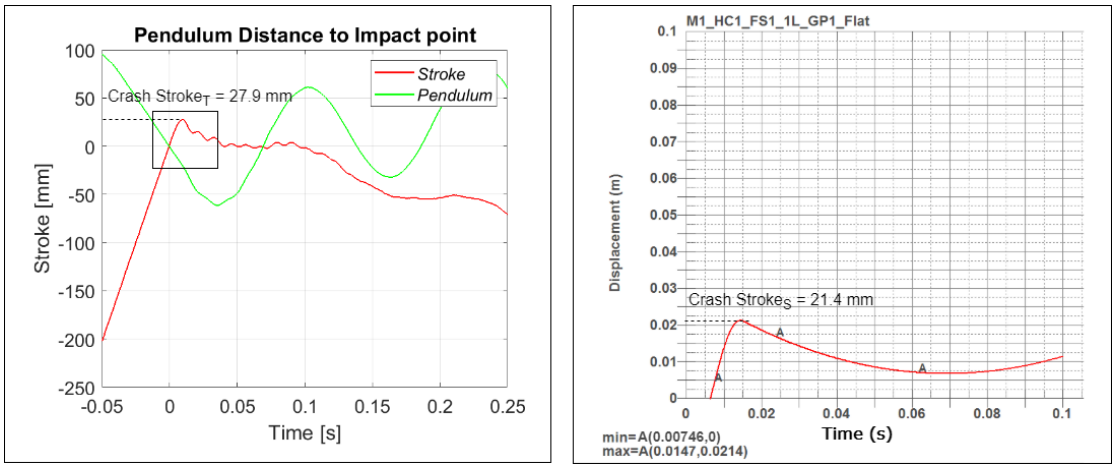

Figure 41: Correlation of indentation depth of the cushion impacting on a flat target between laboratory test condition on the left to FEA simulation on the right. Maximum indentation measured in each condition is highlighted.

Figure 41 shows the correlation of indentation depth measured for the condition of the cushion impacting on a flat target. The abscissa records time in seconds and the ordinate measures the stroke or distance of motion of the cushion system. The graph on the left is the measurement obtained in laboratory test condition and the graph on the right is of the FEA condition. The red and green curves on the graphs of laboratory testing is measured in the same way as described for the penetrator target condition. In the FEA simulations, the time interval between the first contact and the end of contact is from time $t = 0.007s$ to $t = 0.016s$. The maximum indentation of the cushion seen through laboratory testing is $27.9mm$ depth. As observed in the FEA simulation, the maximum indentation of $21.4mm$ occurs at time $t = 0.015s$, but the end of contact is observed at time $t = 0.016s$. Which mean that between $0.007s$ and $0.015s$ the in-plane distribution of the load occurs which results in dimpling and

wrinkling of the face sheet and out-of-plane load distribution as core indentation. After which the model bounces off relaxing until $t = 0.016s$. Since the area of distribution of the impact force on the cushion is larger for a fall on a flat target, indentation of the cushion is smaller in depth but wider in area within a short duration of time.

Table 14: Tabulation of correlation results for indentation depth of the cushion with one layer face sheet impacting on a flat target

M1_HC1_FS1_1L_GP1- Flat				
Impact Point	Laboratory test		FEA	
	Time	Stroke (mm)	Time	Stroke (mm)
First contact	0	0	0.007	0
Deepest	0.011	27.9	0.015	21.4

Table 14 shows the summary of results of maximum indentation measured in laboratory condition and FEA simulation. These recorded results are for cushion model 1 with one layer of face sheet impacting on the flat target. The indentation depth is measured from the first point of contact until the deepest depth of the cushion is reached. A value of $27.9mm$ is measured in the laboratory condition as opposed to $21.4mm$ in the FEA simulation. The difference in the values is because the mass plate setup in FEA is about $10kg$ where as the system mass in the laboratory condition is $15kg$. A higher energy exist in the system in the laboratory condition than that of the FEA simulation and hence cushion model goes deeper in laboratory test.

Velocity:

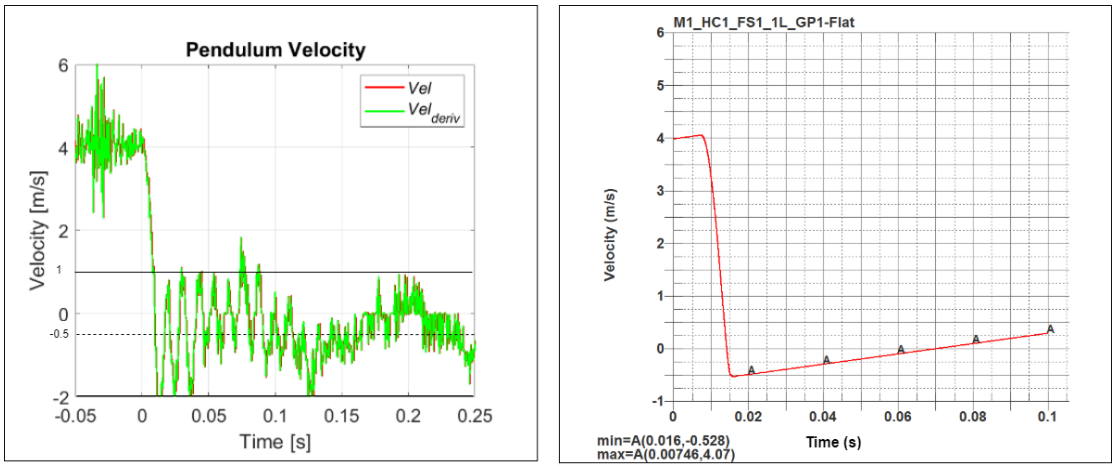

Figure 42: Correlation of velocity reached by the cushion impacting on a flat target between laboratory test condition on the left to FEA simulation on the right. Bounce off velocity reached by the system is highlighted.

The figure 42 shows the graph correlating velocity measurement for cushion model 1 with one layer face sheet impacting on flat target. The graph on the left is the measurement taken for the cushion during the laboratory testing condition. The graph

on the right is obtained for the cushion through FEA simulation. The graph for the laboratory condition is measured as explained in subsection 4.1.2. The maximum velocity recorded is $4.05m/s$ in the laboratory condition as opposed to $4.07m/s$ in the FEA simulation condition. The bounce off velocity in the system is reached when the energy of system is absorbed by the cushion there by reducing the velocity of fall. The bounce off velocity measured in the laboratory condition is the mean of the sinusoidal curves seen on the left due to the pendulum system as explained in the penetrator target condition. It is measured to be about $0.5m/s$ in magnitude in the laboratory test condition. The FEA results have shown the bounce off velocity reached by the system is about $0.53m/s$ at time $t = 0.016s$ which is at the point of loss of contact of cushion and the target. These values of bounce off velocity is in close agreement. Hence the energy absorption of the cushion can be correlated with each other.

Table 15: Tabulation of correlation results for the velocity reached by the cushion with one layer face sheet impacting on a flat target

M1_HC1_FS1_1L_GP1- Flat				
Impact Point	Laboratory test		FEA	
	Time	Velocity (m/s)	Time	Velocity (m/s)
First contact	0	4.05	0.007	4.07
Bounce off point	0.016	0.50	0.016	0.53

The table 15 is a summary of the recorded values of velocity in laboratory test condition to and FEA simulations. Until the first point of contact the velocity increases during the fall, as additional acceleration due to gravity acts on the system. The velocity at the first contact is $4.05m/s$in the laboratory condition as opposed to $4.07m/s$ in the FEA simulation. The bounce off velocity reached by the system in laboratory condition is $0.5m/s$ in magnitude as opposed to $0.53m/s$ in the FEA simulation. The value in the FEA simulation is measured to be higher than laboratory test because of the mass of the system in FEA is lower. For a difference 30%, in the over all mass values of the system, the difference in values measured as bounce off velocity is negligible with an error of 6%. Hence the approximations considered for defining the properties are not too off from the actual model properties. The bounce off velocity measured is for the amount of residual energy the system has after impact. A system with higher mass with less stiffer core has higher dissipation of impact forces and hence lower residual energy. This makes the system bounce off with lower velocity.

Acceleration:
The figure 43 is the correlation of acceleration. Each graphs gives the measured value for acceleration at each instant of time. Acceleration measured in the laboratory testing condition is on the left and FEA simulation on right. The values on the ordinate is the acceleration and abscissa is the the relative time. The ordinate value on the graph of laboratory test condition is measured in gs which corresponds to a factor of $9.81\ m/s^2$, but for simplicity, it can be approximated to 10 times of m/s^2. As studied above, the impact duration in FEA simulation is between time $t = 0.007s$

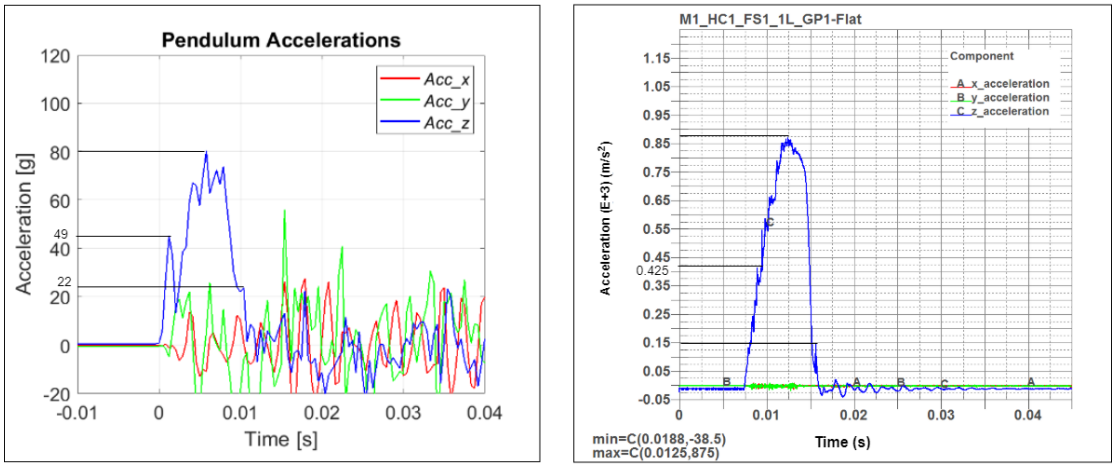

Figure 43: Correlation of acceleration of the cushion impacting on a flat target between laboratory test condition on the left to FEA simulation on the right. Maximum acceleration measured at each noticeable instant is highlighted.

and $t = 0.016s$, the maximum acceleration measured during this interval is considered as the amount of energy being absorbed for the load acted upon the system. Hence decreasing the momentum in the system and preventing the transfer of impact. This measurement defines the deceleration experienced by the system which the instruments measure the acceleration of the system. The maximum acceleration measured in the laboratory testing condition is $80g$ or approximately $800m/s^2$. Correspondingly the maximum acceleration measured through FEA is $87.5g$ or approximately $875m/s^2$. The flat impact condition in the FEA shows wider indentation pattern because of wider distribution of force therefore decelerates higher than the laboratory test value.

Table 16: Tabulation of correlation results for acceleration of the cushion with one layer face sheet impacting on a flat target

M1_HC1_FS1_1L_GP1- Flat				
Instant	**Laboratory test**		**FEA**	
	Time	**Acceleration (g)**	**Time**	**Acceleration (g)**
First contact	0	2	0.007	-3.85
Max. acceleration point	0.005	80	0.012	87.50
Loss of contact and return	0.016	22	0.016	15.00

The table 16 is the summary of the acceleration measured at each instant of time. The acceleration measured at first contact is the instant at which the cushion touches the flat target. The first peak value tabulated for the sharp dip seen on the graph for the acceleration in laboratory test value might be because of the curvature of the cushion surface. Although the number of tests discussed in this work is not sufficient enough to confirm this. It could also be a local material failure. From the first point of contact to the point till the curvature of the cushion flattens, there is a sharp absorption of energy. This peak acceleration is at $49g$ in the laboratory testing. The distribution of

load because of curvature is rather gradual in the FEA condition observed at around $42g$. On further impact the maximum acceleration measured is reached and tabulated up to the instant where the cushion losses its contact with the target. Another observation made on the small raise in the curve at the point of loss of contact and return is that, it is due to the wrinkling and dimpling of the face sheet.

When the values at each instant between laboratory test and FEA is compared, the values in relation has an error of 9% for the maximum acceleration measured. This means that the system in FEA condition is being decelerated more than the laboratory condition because the overall system mass is lower.The other reason might be because of the overlooked lower shear value given for the core in FEA which is given in GABU and GBCU in the material card. Lower shear value helps in in-plane distribution of load through the face sheet.

Force:

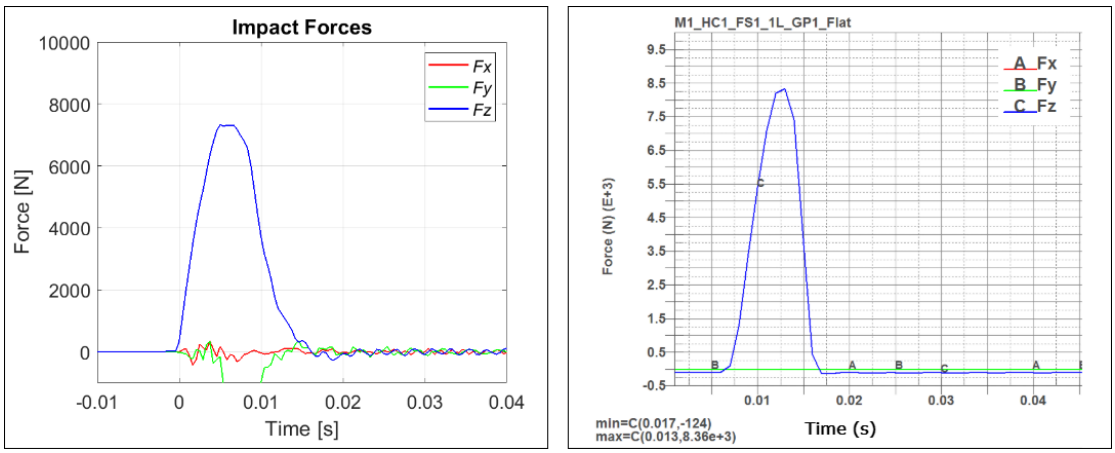

Figure 44: Correlation of force of impact on the cushion impacting on a flat target between laboratory test condition on the left to FEA simulation on the right. Maximum force experienced by the system can be seen.

The force in the laboratory condition is measured through the force sensors placed behind the target in the laboratory testing. The figure 44 is a correlation of force measurements between the laboratory test and FEA simulation. Force is measured in newtons along the ordinate vs time in seconds on abscissa. Force measured along only in z direction or fall direction is considered for the correlation. The graph on the left is the measurement taken through the laboratory testing with the pendulum system. The graph on the right is the measurement obtained through FEA simulation. The small flat plateau seen at the peak of the curve is the constant force distribution across the surface area of the cushion. The maximum force measured, is distributed in a short interval of time between $0s$ and $0.016s$ through wider surface area in the laboratory testing and between $0.007s$ and $0.016s$ in FEA.

The summary of the maximum values of force measured by the laboratory testing and FEA is tabulated in table 17. The maximum force acting on the system in the

Table 17: Tabulation of correlation results for force acting on the cushion with one layer face sheet impacting on a flat target

M1_HC1_FS1_1L_GP1- Flat				
Impact Point	Laboratory test		FEA	
	Time	Force (N)	Time	Force (N)
Max.Force	0.005	7331	0.013	8360

laboratory test is $7331N$ whereas the maximum force measured in the FEA simulation is $8360N$. A difference of 14% in the values are seen which is within the range of expected deviation of results. Although the over all system load of $15kg$ in the laboratory condition is larger than the FEA, the FEA results show higher value of force being absorbed and distributed. One of the reason is the distribution of force in FEA is throughout the surface area of the the curvature of the cushion until it is flattened. This is seen in the impact pattern showing wider distribution in the FEA. Based on the analysis made so far, another observation is that the core in the FEA is weaker in shearing plane because of the overlooked conversion of the value into SI unit in the material card. This could also mean that the the absorbed amount of force and distribution of force in the in-plane direction can be more in the FEA simulation.

4.3 Model 1 with Two Layers of Face Sheet

Based on the correlations and results seen with the condition of the cushion model 1 with one layer face sheet with flat target. Further analysis on the core and face sheet formulation can be made with the correlation of another laboratory testing condition.

4.3.1 FEA model setup

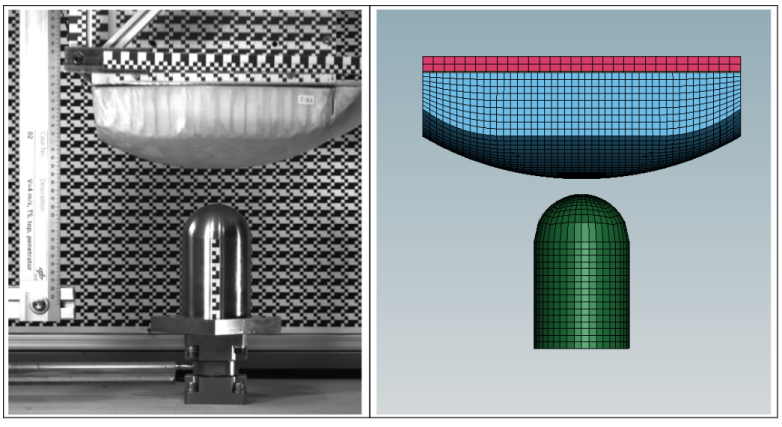

Figure 45: Comparison of laboratory test conditions of the cushion with laboratory setup on the left and FEA model setup on the right. The cushion model 1 with two layer of face sheet impacting on penetrator target is shown.

The condition considered here is the cushion model 1 with two layers of Dyneema face sheet glued over the core with a penetrator target. The cushion model 1 is meshed as discussed in the earlier sections. The formulation of core, ground plate, mass plate and penetrator is as it is discussed in the section 4.1. The face sheet formulation for two layer is only varied in the values on the material card. The meshing for the face sheet is done similarly as for the previous conditions. The cushion model in the laboratory condition is attached with one of the corner cushion pieces along with the main cushion. This is not seen in the FEA model since only the main cushion model is considered for analysis. The figure 45 shows the comparison of the laboratory testing conditions in the laboratory condition to that of the FEA simulation. The over all system mass of the laboratory condition is 15kg and the over all system mass in the FEA is $10.5kg$ similar to earlier conditions.

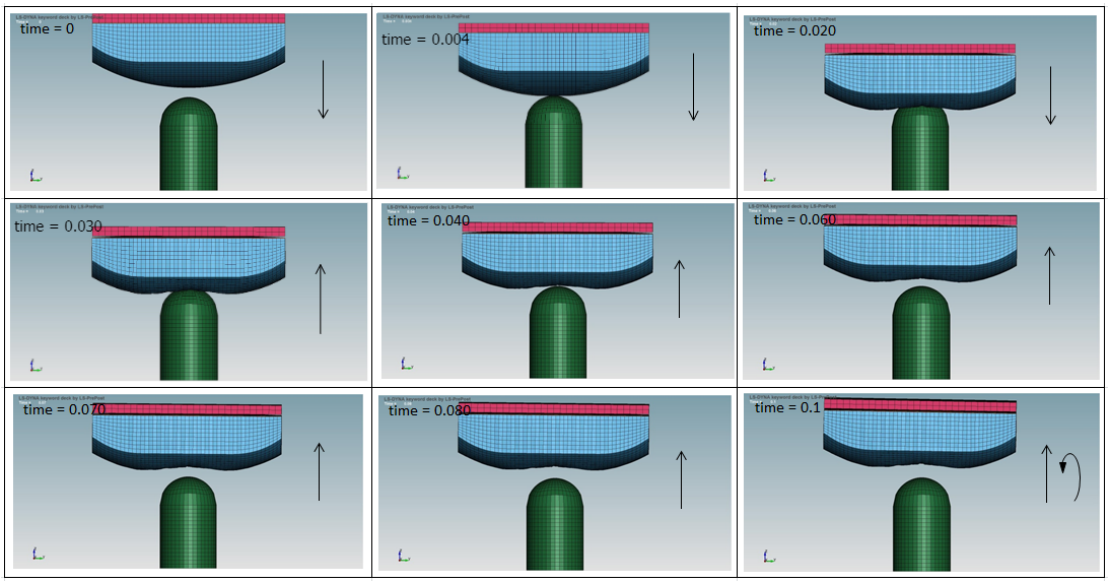

Figure 46: Simulation run of FEA model of the cushion under free fall at different time instances for cushion model 1 with two layers of face sheet impacting on a penetrator target

The figure 46 depicts the stage wise animation of the free fall scenario of the cushion. At $time = 0$ shows the start of the free fall. At about $time = 0.004s$ the first contact with the penetrator takes place. The face sheet takes up the initial in-plane loads and the reaction is seen in wrinkling of the face sheet. Energy is absorbed by the cushion until its $time = 0.016s$. Once the impact energy is absorbed and converted to deformation of the cushion, the cushion is seen to bounce off of the surface. At $time = 0.020s$, the cushion is out of contact from the target surface. At the end of the simulation run $time = 0.1s$ the model is also seen to topple about its central axis. The total deformation of the cushion is taking place between the time intervals of about $0.004s$ to $0.016s$. Indentation depth, velocity variation and energy absorption takes place at this stage. These are discussed in the following.

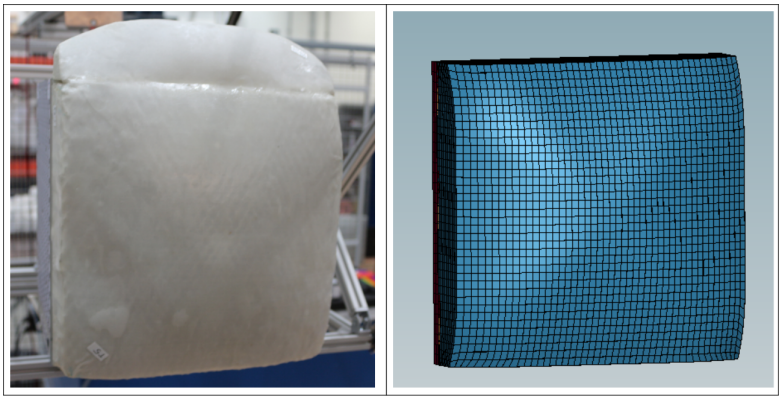

Figure 47: Comparison of the cushion with laboratory model on the left and FEA model on the right showing before impact of the cushion model 1 with two layers of face sheet impacting a penetrator target.

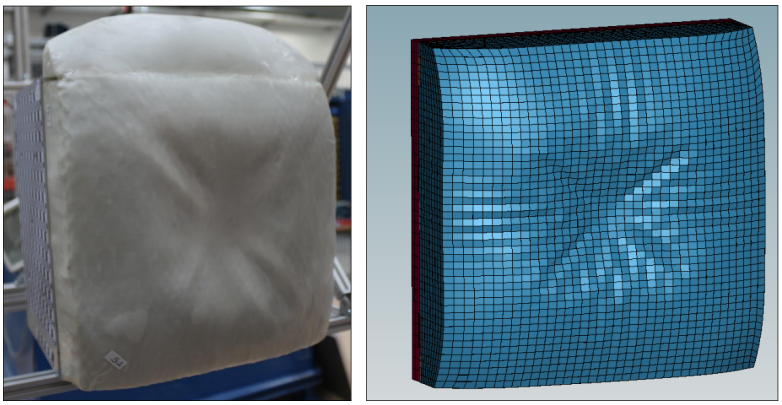

Figure 48: Comparison of the cushion with laboratory model on the left and FEA model on the right showing after impact of the cushion model 1 with two layers of face sheet impacting a penetrator target.

The figure 47 compares the cushion model in the laboratory testing condition to the FEA simulation model before impact. Some bubbles can be noticed in the face sheet in the laboratory model which is due to the glueing process. In relation to that, figure 48 compares the cushion models after impact. The image on the left is the impact pattern observed in the laboratory condition and the one on right is the pattern observed in FEA models. The wrinkling of the face sheet occurs at the first contact along the fibre directions. Since this is a condition with two layers of face sheet, it helps in further distribution of the load in the in-plane direction. This is seen as the diagonal wrinkling pattern because of distribution of load. In the FEA simulation, the wrinkling of the face sheet is seen as the very first reaction to impact. This is the due to the distribution of load along the fibre directions. As the face sheet is relatively thicker in this condition further distribution of the load is seen along the diagonals of the face sheet. Although the load and fall condition is similar to the condition seen in 4.1, the thicker but still elastic face sheet takes up the in-plane load. As discussed in section 3.1, faces takes up the bending load and hence the thicker face sheet in this condition prevents the bending of the cushion. The cushion does not show prominent bending

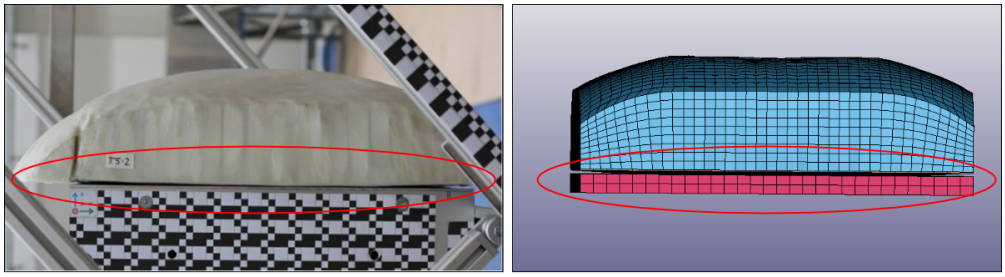

Figure 49: Deflection of the sandwich cushion seen during the laboratory test on the left as opposed to the similar deflection or bending seen in FEA on the right.

or shows very little bending in this condition. Figure 49 shows the deflection of the cushion as a result of impact. It shows the comparison between the deflection seen in the laboratory test condition to the FEA condition. As discussed in section 3.1 total deflection of the cushion or a sandwich structure is due to bending and shear load distribution between core and face sheet.

4.3.2 Correlation of results

Indentation:

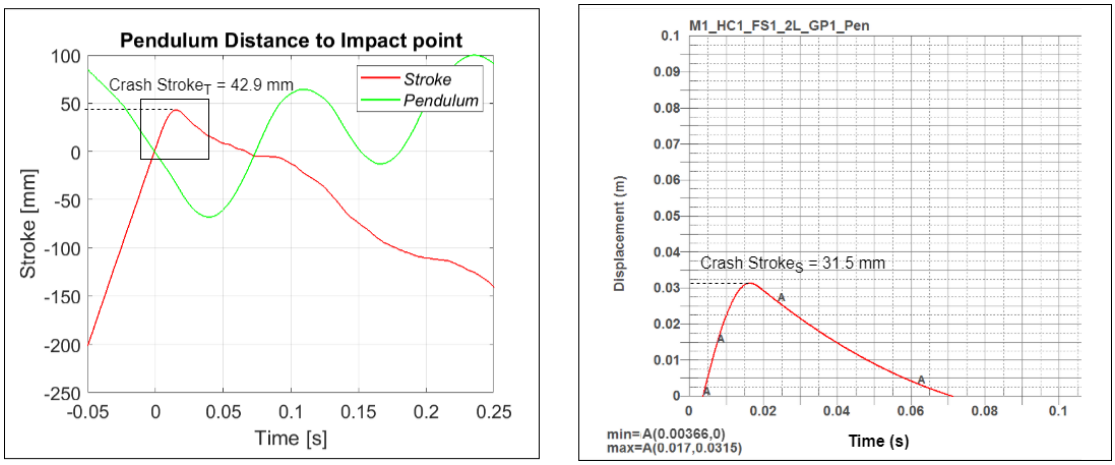

Figure 50: Correlation of indentation depth of the cushion with two layer face sheet impacting on a penetrator target between laboratory test condition on the left to FEA simulation on the right. Maximum indentation measured in each condition is highlighted.

The figure 50 shows the graphs recorded to measure the global indentation depth of the cushion. The displacement sensors records the distance of the cushion from its reference point while in motion. These reading can be read for the depth up to which the cushion gets impacted when hit on the target. The graph on the left is from the laboratory test values. The graph on the right is from FEA simulation. The depth of indentation is measured from the first point of contact until the cushion is completely out of contact from the target. The depth measured by the laboratory test is $42.9mm$

as opposed to FEA value to be $31.5mm$. As in the earlier conditions, this deviation in values is because of the difference in overall energy within the system.

Table 18: Tabulation of correlation results for indentation depth of the cushion with two layer face sheet impacting on a penetrator target

M1_HC1_FS1_2L_GP1- Pen				
Impact Point	Laboratory test		FEA	
	Time	Stroke (mm)	Time	Stroke (mm)
First contact	0	0	0.004	0
Deepest	0.02	42.9	0.016	31.5

The table 18 gives the summary of the values measure to the values recorded by the laboratory test conditions. The instant of first point of contact between the cushion and target and the deepest point of contact is tabulated. A difference of 26% decrease can be noticed in the values of indentation depth measured. For a difference in overall system mass of 30% between laboratory model and FEA model, this difference in the indentation measured is still within the expected range of deviation of results.

Velocity:

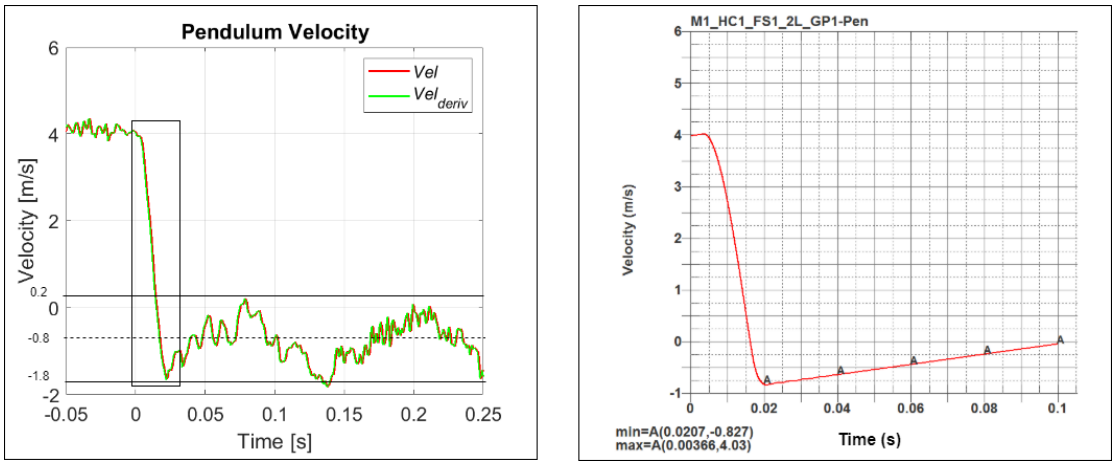

Figure 51: Correlation of velocity reached by the cushion with two layer face sheet impacting on a penetrator target between laboratory test condition on the left to FEA simulation on the right. Bounce off velocity measured in each condition is highlighted.

Similar to observations made on earlier conditions, the velocity measured for the cushion model 1 with two layers of face sheet impacting on a penetrator target is recoded in figure 51. The graph on the left is recorded for laboratory test conditions and the graph on the right are the values obtained through FEA. The bounce off velocity reached by the system on impacting with the initial velocity of $4m/s$ is $0.8m/s$ in the laboratory condition in contrast to the FEA system reaching a velocity of $0.83m/s$. A difference of 3.7% is seen in the values measured for the bounce off velocity. Since the

bounce off velocity is mainly due to the material characteristics of the cushion, being able to absorb the impact energy and the bounce of velocity is due to the residual energy, the approximations of properties done for core and face sheet can be now be concluded to be in better correlation with the model. The previous conditions has also shown close agreement with the bounce off velocity on correlation. The values recorded for the velocity reached by the system in each condition of laboratory and FEA is tabulated in table 19. The time of first contact and the time instant at which the system reaches the bounce off velocity is tabulated.

Table 19: Tabulation of correlation results for velocity reached by the cushion with two layer face sheet impacting on a penetrator target

M1_HC1_FS1_2L_GP1- Pen				
Impact Point	**Laboratory test**		**FEA**	
	Time	**Velocity (m/s)**	**Time**	**Velocity (m/s)**
First contact	0	4.01	0.004	4.03
Bounce off point	0.02	0.80	0.020	0.83

Acceleration:

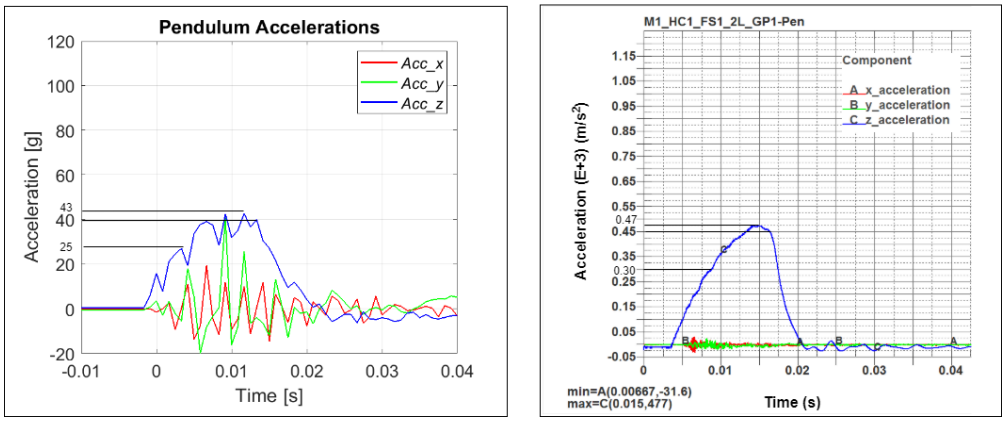

Figure 52: Correlation of acceleration of the cushion with two layer face sheet impacting on a penetrator target between laboratory test condition on the left to FEA simulation on the right. Maximum acceleration measured in each condition is highlighted.

The figure 52 is the correlation of acceleration. Acceleration measured in the laboratory testing condition is on the left and FEA simulation on right. The values on the ordinate is the acceleration and abscissa is the the relative time. The ordinate value on the graph of laboratory test condition is measured in gs as discussed in other above conditions. The maximum acceleration measured during the interval of first contact and loss of contact is considered as the amount of energy being absorbed for the load acted upon the system, thereby decreasing the momentum in the system and preventing the transfer of impact. The maximum acceleration measured in the laboratory testing condition is $43g$. Correspondingly the maximum acceleration measured

through FEA is $47.7g$. The difference in the values measured for the acceleration measured at impact has 11% difference. This higher value in the FEA model is because of the lower overall mass of the system.

Table 20: Tabulation of correlation results for acceleration of the cushion with two layer face sheet impacting on a penetrator target

M1_HC1_FS1_2L_GP1- Pen				
Instant	**Laboratory test**		**FEA**	
	Time	**Acceleration (g)**	**Time**	**Acceleration (g)**
First contact	0	2	0.004	-3.16
Max. acceleration point	0.011	43	0.015	47.70
Loss of contact and return	0.015	40	0.020	45.00

The table 20 is the tabulation of the acceleration measured at different instant of time. The acceleration measured at first contact is the instant at which the cushion touches the penetrator target. On further impact the maximum acceleration measured is tabulated up to the instant where the cushion losses its contact with the target. As compared to the earlier condition of one layer face sheet the curvature of the cushion absorbs the initial impact load and since this condition has two layers of face sheet, the load gets distributed in the in-plane direction. This in-plane distribution is also seen in the impact pattern with the axial and diagonal wrinkling of the face sheet. The first rise observed in the graph of one layer condition is rather gradual in two layer condition which shows the in-plane distribution of load through two layers of face sheet. Hence the distribution of load and the peak acceleration point reached, is gradual and smooth.

Force:

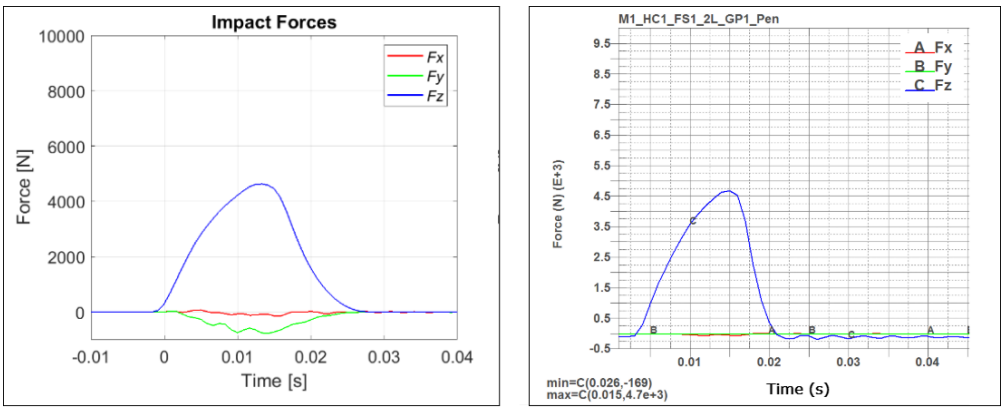

Figure 53: Correlation of force acting on the cushion with two layer face sheet impacting on a penetrator target between laboratory test condition on the left to FEA simulation on the right. Maximum force acting on the system is highlighted.

The figure 53 is a correlation of force measurements between the laboratory test and FEA simulation. As discussed in other conditions, the force measured is through the

force sensors placed behind the target in the laboratory testing. Force is measured in newtons along the ordinate vs time in seconds on abscissa. The force measured only along z direction is considered for correlation. The graph on the left is the measurement taken through the laboratory testing with the pendulum system. The graph on the right is the measurement obtained through FEA simulation. A maximum force is measured between the time interval of $0s$ and $0.012s$ in the laboratory testing and $0.003s$ to $0.016s$ in the FEA simulation.

Table 21: Tabulation of correlation results for force acting on the cushion with two layer face sheet impacting on a penetrator target

M1_HC1_FS1_2L_GP1- Pen				
Impact Point	**Laboratory test**		**FEA**	
	Time	**Force (N)**	**Time**	**Force (N)**
Max.Force	0.012	4627	0.015	4700

The summary of the maximum values of force measured by the laboratory testing and FEA is tabulated in table 21. The maximum force acting on the system in the laboratory test is $4627N$ whereas the maximum force measured in the FEA simulation is $4700N$. Even though the overall system mass is lower in the FEA model, the value measured for absorbed impact force in the FEA is higher than the laboratory value. This is because of higher distribution of force in the face sheet seen as wrinkling in the fibre directions and diagonal directions. In comparison to that for one layer condition which shows lower absorption of impact force. A difference in values of 1.5% is seen between the force measured which is well within the range of expected deviation of results.

In all the above FEA conditions the overall system energy that is the mass of the cushion system is the same with mass plate mass formulated at $10kg$. The laboratory models has an overall system mass corresponding to $15kg$ while that of FEA model is $10.5kg$. During the development of the simulation setup of the FE models, the core and face sheet weight was not anticipated until the final formulation. During this process the mass plate mass was formulated for $10kg$ trials in the FEA, since a cushion model with low mass impact is of higher interest. Considering the priorities with the tasks within the frame of this thesis work, the mass plate adaptation and simulation runs with approximate $15kg$ overall mass could not be performed within the stipulated time. Hence it can be taken up as one of the future works to adapt the models to an over all mass of $15kg$. With the results seen through the discussed conditions, the formulation of the core and face sheet gives close agreement with the values and hence a similar process can be adapted for future immediate studies.

PART II

5 Evaluation of Frame and Test Prediction

5.1 Evaluation of Frame

The cushion model 1 was discussed until here. The correlation of the results for cushion model 1 was done since the earlier laboratory testings was conducted for that model. After correlating the results and having got reliable formulation of core and face sheet, the same is applied to cushion model 2. As discussed in the beginning of this work in section 1.4, model 2 is a development of design from cushion model 1. The second task concerning the current thesis is the design of a frame support and the evaluation of design of the frame. To have a better evaluation scale, cushion model 2 with one layer of face sheet is formulated without a frame at first. The frame is then assembled to the cushion model 2 and the changes in the reactions can be compared.

Model 2 Setup Without Frame
In the FEA simulation for evaluating the frame design, the cushion model 2 is considered since the future laboratory tests will be conducted with this model. CAD model of the cushion geometry *Model 2* is imported as a step file into LS Dyna and meshed using *Block mesher* similar to the process carried out for *Model1*. Face sheet mesh elements is also created using *Element Generation* similar to model 1 as discussed in section 4.1. Ground plate, mass plate and penetrator target of $45mm$ radius is created similar to earlier conditions. An additional part considered for these condition is the assembly of ground plate and mass plate with standoffs. Standoffs act as a holder for the housing so that housing is not directly in contact with the cushion. A standoff with material properties of aluminum 5052 is created using *Block Mesh* option with a diameter of $12.7mm$ and a height of $3mm$. Standoffs are fixed at four corners over the ground plate. These standoffs are created such that mass plate is fixed at only these four corner on the standoffs allowing room between the ground plate and mass plate.

The figure 54 shows the cushion model 2 setup with one layer face sheet, ground plate, standoffs and mass plate falling on a penetrator target. A comparison with before impact on the left and after impact on the right can be made. The cushion model 2 is of the dimensions $300mm$ x $200mm$ x $100mm$, ground plate and mass plate are created accordingly to match with the cushion. Since standoffs are place between ground plate and mass plate the deflection or the bending of the cushion is more apparent in the figure on the right. The stage wise animation run for the impact of the cushion is the appendix in figure74. The time duration from first point of contact to loss of contact is between time $t = 0.008s$ to $t = 0.03s$.

Based on the results seen through laboratory testing and studying the outcomes, a frame is decided to be designed and placed over the ground plate. The design of the frame in discussed in the next section.

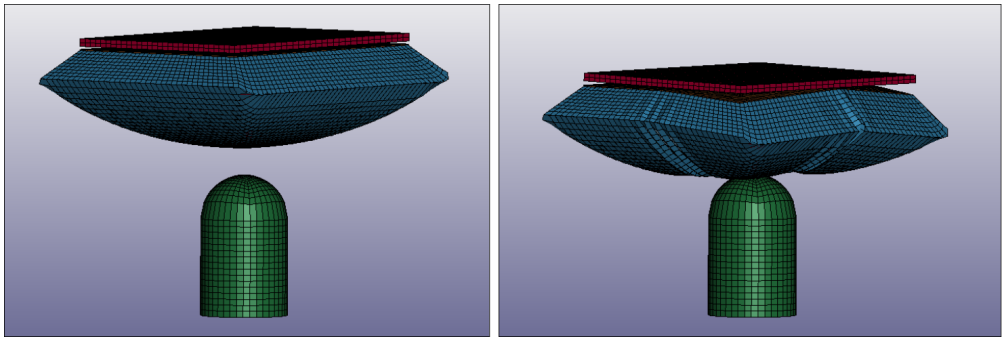

Figure 54: Isometric view of the model setup with cushion model 2 with one layer of Dyneema face sheet. A comparison of the cushion before impact on the left and after impact on the right is seen.

5.1.1 Frame Requirements and Design

Once the force and energy distribution is studied through laboratory testing of the cushion, the next task considered within the scope of this thesis is to design and evaluate a frame interface between the housing and the cushion so as to prevent the transfer of impact energy.The frame is required to be designed such that it provides support across the diagonals of the cushion over the ground plate. With this requirement, an *X* shaped interface frame is to be designed. For the ease of manufacturing, the *X frame* is to be an assembly of two beam components.

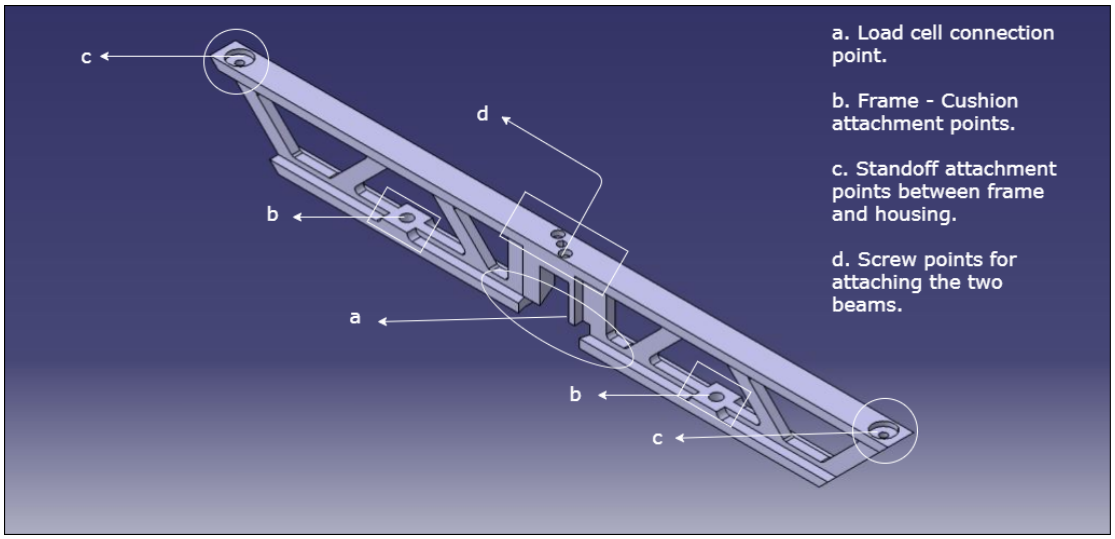

Figure 55: Beam A of the frame assembly highlighting the attachment features. In an assembled frame, in relation to this view, the cushion will be fixed on the bottom side and housing on the top.

The beam components are referred as beam A and beam B for explanation. The cross section of the both the beams is an I-section beam. As for the I-section, the flanges on top and bottom takes the bending load of the beam and the web takes up the

shear load as per the general behaviour of an I section beam. The I section is doubly symmetric with thickness of flanges and web to be $5mm$. The height of the web is designed to be $30mm$. These values of the cross section of the beam is obtained by simple calculations by applying bending beam theory. As per the theory, the allowable stress are defined to be below the critical stress that occurs due to impact force, and the minimum dimension of the I section required to withstand the critical stress are taken into consideration while defining the allowable stress. The 2D computer aided drawing of the beam elements are attached in the appendix in figure 71 and figure 72.

The figure 55 shows the design of beam A, one of the beam component of the frame assembly. The requirement for the frame to accommodate a load cell to measure the force of impact is considered. The load cell placement is highlighted at *a*. The highlighted feature at *b* is the screwing point of the frame to the ground plate with the provision of a flat surface for the resting of screw head. Standoffs are place on the top edges of the beam highlighted at *c*. These standoffs form the one of the diagonal support to the housing. The feature at *d* shows three holes of which the outer two holes at the edges are for screwing in order to fix beam A over beam B. The central hole is for the a screw connecting the load cell at the bottom with the Ejector Release Mechanism (ERM) on the top, through the beam. The ERM is used to separate the cushion element from the lander after impact, in order to not interfere with normal surface operation (uprighting or jumping). Symmetrical pockets are created across the web for reducing the over all weight since most of the load is taken up by the flanges.

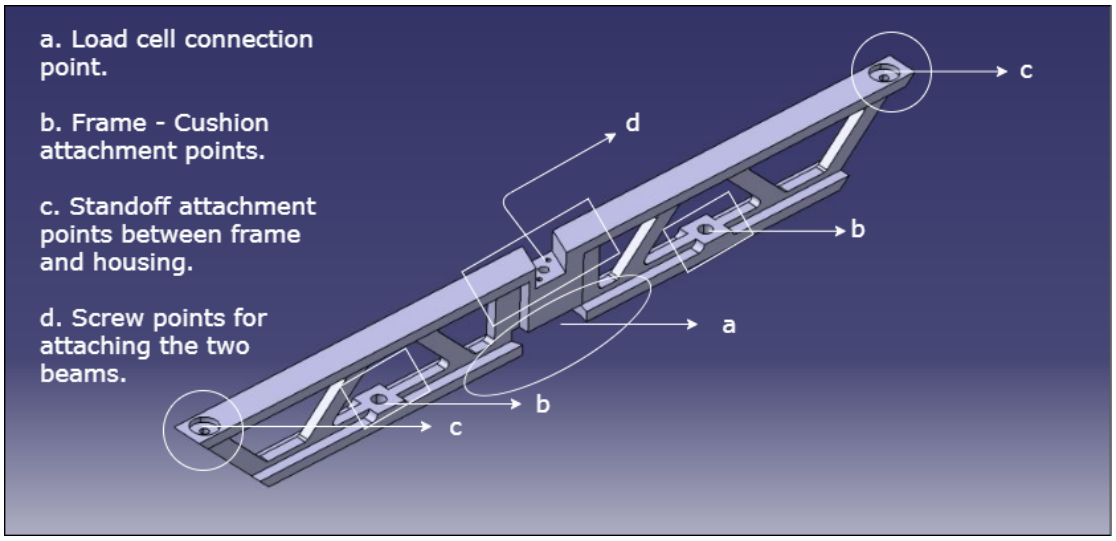

Figure 56: Beam B of the frame assembly highlighting the attachment features. In an assembled frame, in relation to this view, the cushion will be fixed on the bottom side and housing on the top.

Similar to beam A, beam B is designed with the same requirements. The frame shall accommodate a load cell and shall provide a connecting point between load cell and the Ejector Release Mechanism (ERM). The frame shall have a simple design with an ease of manufacturing and shall be of low weight. The figure 56 shows the design

of beam B, one of the other beam component of the frame assembly. The load cell placement is highlighted at *a*. The highlighted feature at *b* is the screwing point of the frame to the ground plate with the provision of a flat surface for the resting of screw head. Standoffs are place on the top edges of the beam highlighted at *c*. These standoffs form the one of the other diagonal support to the housing. The feature at *d* shows three holes of which the outer two holes at the edges are for screwing for assembling the two beams. The central hole is for the a screw connecting the load cell and ERM. Symmetrical pockets are created across the web for reducing the over all weight since most of the load is taken up by the flanges.

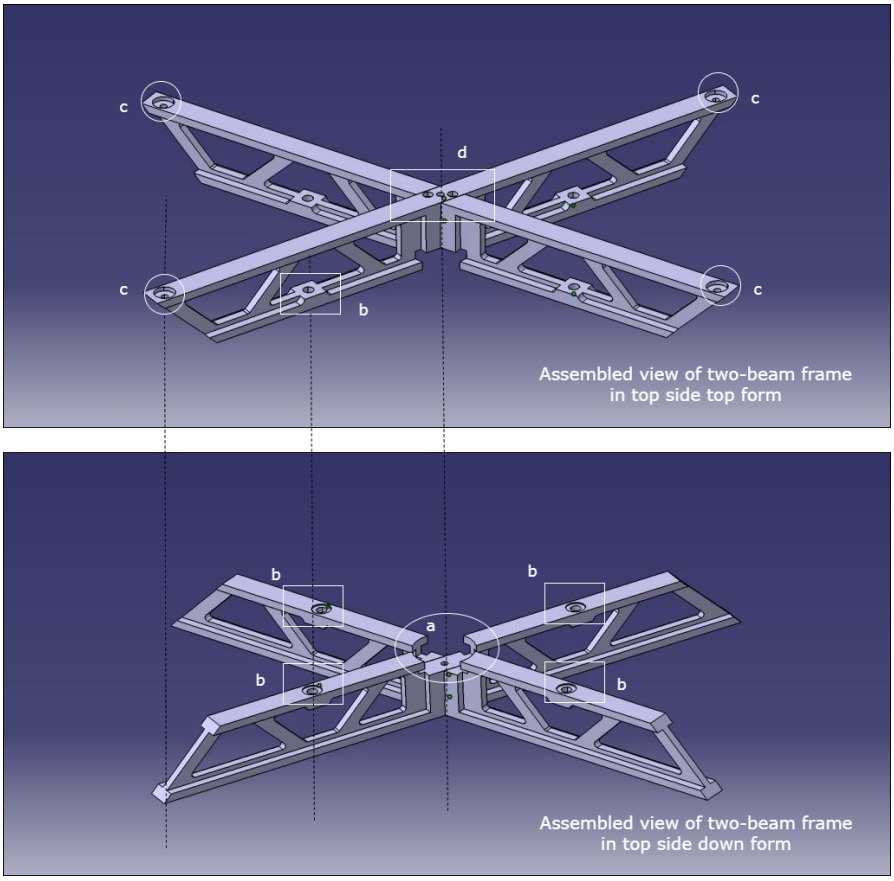

Figure 57: Isometric view of the assembled beams of the interface frame. The image on the top shows the top-down view of the frame where cushion is fixed on the bottom of the frame. The image in the bottom shows the upside down view of the frame.

The figure 57 shows the assembled frame with beam A and beam B. The top figure is the assembled frame on top of which the housing is fixed and cushion at the bottom. The bottom figure shows the upside down view of the assembled fame to highlight the feature *a* which is the load cell connecting and placement point. The bottom figure of the assembled frame shows clearly the circular socket of diameter $38.4mm$ made for load cell. Feature *b* highlights the screwing point of the frame to the ground plate of the cushion. The feature at *c* forms the four legged support to the housing by

the standoffs. The feature *d* shows the same attributes as of the individual beam for the assembled frame. The dotted lines highlights the axis of the through holes. The material in the central region of the assembled beam provides the central support for the cushion to prevent it from bending.

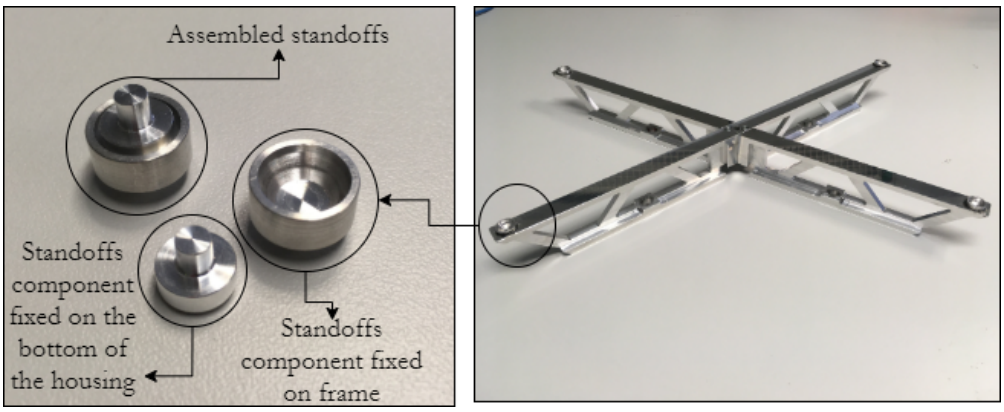

Figure 58: Actual standoff components on the left and a manufactured frame on the right for the assembly with model 2 cushion.

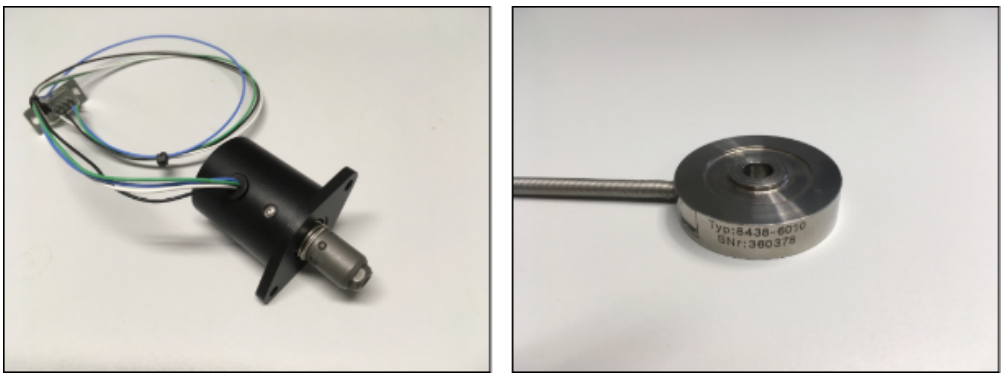

Figure 59: The actual Ejector release mechanism is shown on the left and the load cell is shown on the right.

The figure 58 shows the actual standoff components on the left and a manufactured frame on the right. The standoffs are a two component assembly with one fixed on the frame and the other fixed to the housing. The figure 59 shows the actual ERM used for the assembly on the left and the load cell on the right. These components are assembled with cushion model 2 for the future test. The figure 60 shows the complete assembly of the housing, frame and cushion. The housing is of similar size as that of MASCOT. The standoffs are between the housing and the frame. The standoffs are basically a two piece set. One piece is glued to the housing and the other piece are glued on the frame at feature points *c*. The frame assembly forms the interface support across the diagonals of the housing. Based on the requirements and design, the frame can accommodate the load cell and a connect with ERM. The connection of load cell with ERM is through the central hole at the feature point *d*. The frame

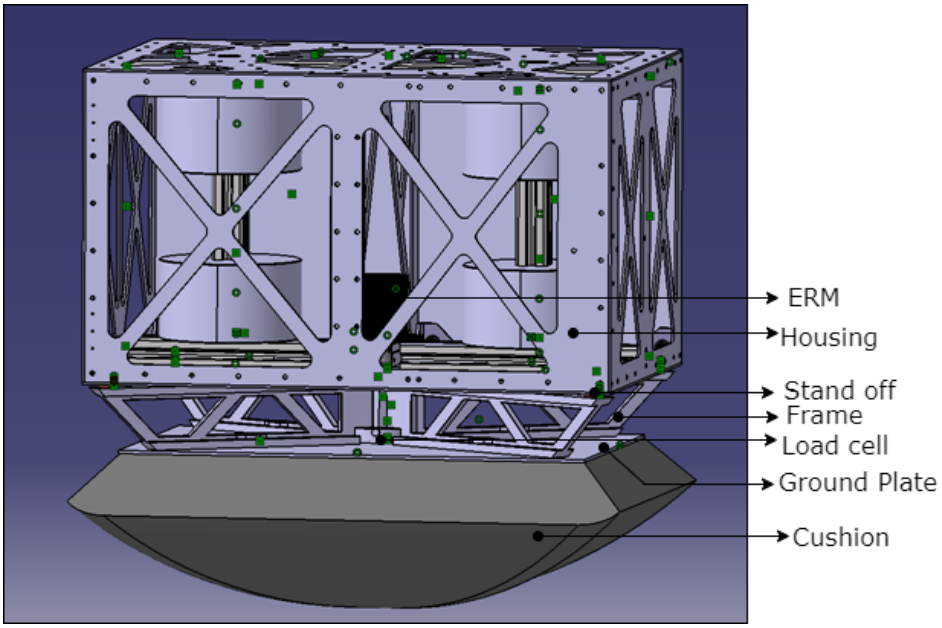

Figure 60: CAD assembly of frame with the housing on the top and the cushion at the bottom along with standoffs placed between the frame and the housing. The attachment of load cell with ERM is also seen.

is then fixed to the ground plate of the cushion through screws. This arrangement is considered for the future laboratory testing.

Model 2 Setup With Frame

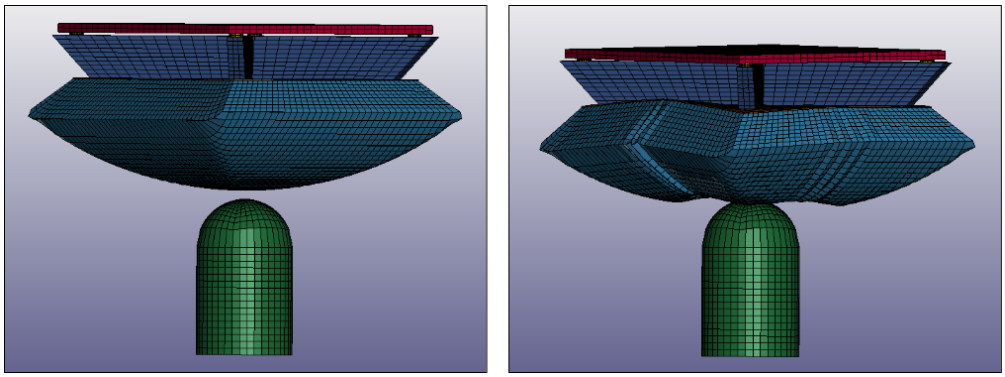

Figure 61: Isometric view of the model setup with cushion model 2 with one layer of Dyneema face sheet with frame. A comparison of the cushion before impact on the left and after impact on the right is seen.

The model 2 geometry of the cushion is meshed as explained earlier for the condition without frame. The only addition to the condition of model 2 of cushion without frame is the addition of the frame in this condition. The actual frame is not being implemented in the analysis since the meshing of the frame involves process that did not fall within the time duration of this work. Hence a simple X frame without cut outs

and pockets but a solid frame is designed. The CAD of the simple frame is imported and meshed using *Block Mesher* option. The frame is fixed through node contact with ground plate surface. Standoffs are fixed on top of the frame at the corners over which mass plate is created again being attached only at nodes of standoffs. Both standoffs and frame is setup with material card *MAT_024. The frame properties is taken for aluminum 7075. The property values are taken from an online source. The setup definition for the models is attached in the appendix.

The figure 61 shows the cushion model 2 setup with one layer face sheet, ground plate, standoffs and mass plate falling on a penetrator target. A comparison with before impact on the left and after impact on the right can be made. The cushion model 2 is of the dimensions $300mm$ x $200mm$ x $100mm$, ground plate and mass plate are created accordingly to match with the cushion. Standoffs are place between mass plate and frame, there is no deflection of the frame or the impingement of the frame towards the housing as seen in the figure on the right. The bending of the cushion towards the mass plate is effectively reduced. However, the cushion itself still bends, since due to the X-cross pattern of the frame not being given as a support to the entire base of the cushion. The stage wise animation run for the impact of the cushion is the appendix in figure75. The time duration from first point of contact to loss of contact is between time $t = 0.002s$ to $t = 0.028s$.

5.2 Test Prediction

The prediction of values for model considered here is done for values similar to the results correlated in Chapter 4. As for the correlation of results for the cushion model 1, there were results from the laboratory test conditions which was then correlated for values recorded through FEA . Here similar prediction of the results for the cushion model 2 can be made. Since the laboratory test for cushion model 2 will be done in the future, a prediction of the values is given here. As discussed in section 5.1, evaluation of the frame can be made with the predicted results. The two models in comparison is the one cushion without frame and the other cushion with frame. These results for the model setup without frame and with frame is discussed further. The same parameters of results as for correlation is considered for prediction. These values are the values of indentation depth, velocity, acceleration and force.

Indentation depth:
The figure 62 shows the comparison of values for the maximum indentation depth reached by the cushion system when impacted on a penetrator target. The graph on the left is for the cushion model 2 with one layer face sheet when considered without a frame. The time duration to be considered for this condition is between $0.007s$ and $0.025s$. The instantaneous time of impact through FEA is seen in figure 74 in appendix. The depth measured between this duration is $0.021m$. The graph on the right is for the condition of the cushion considered with frame. The time duration to be considered for this condition is between $0.002s$ to $0.022s$. The zero on both the graphs is from the beginning of the simulation run. Hence the time between zero

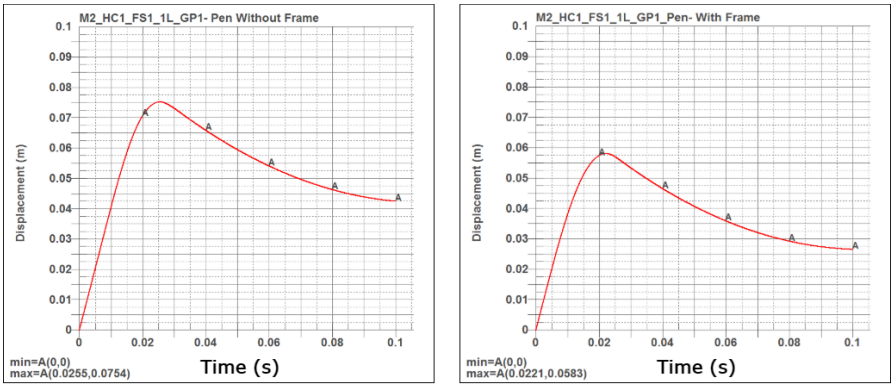

Figure 62: Comparison of maximum indentation depth reached by the system on impact. The system setup when considered without frame is on the left and with frame is on the right.

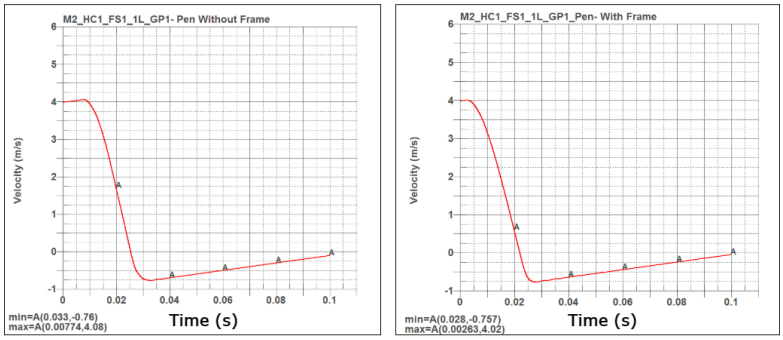

Figure 63: Comparison of velocity reached by the system on impact. The system setup when considered without frame is on the left and with frame is on the right.

to the first contact is the motion of the cushion downwards towards the target until the first contact. The depth measured between first contact to the last contact with the target is $0.060m$ and $0.043m$ for the condition of without frame and with frame respectively. As in the test correlation the indentation depth graphs were adapted for the zero reference being at the first contact. Here the graphs seen are for the total depth of motion of the model from the start of the simulation run. Hence here the zero time is from the start of simulation. The maximum peak motion of the model seen when the cushion bounces off without a frame is $75mm$ as opposed to $58mm$ in the condition when the total stroke is measured for the cushion with frame. The initial fall height of the model has to be subtracted for measuring the indentation depth.

Velocity:

The model in both conditions in comparison are the same. The mass of the system with frame is higher than that of the system without a frame. The figure 63 shows the comparison velocity reached by the system when the cushion impacts the penetrator target. The graph on the left is for the cushion model 2 without frame and on the right is for the cushion system with frame. The bounce off velocity reached without

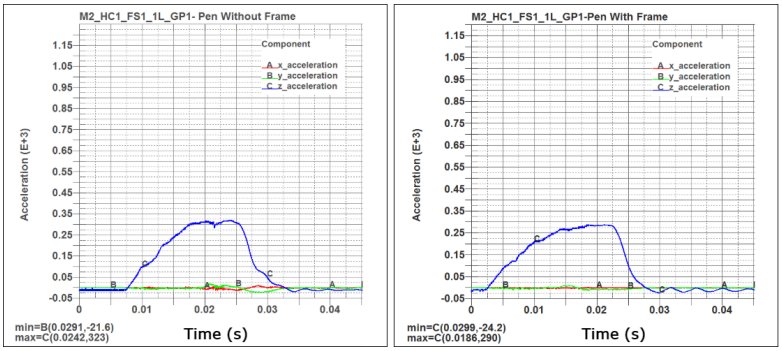

Figure 64: Comparison of maximum acceleration reached by the system on impact. The system setup when considered without frame is on the left and with frame is on the right.

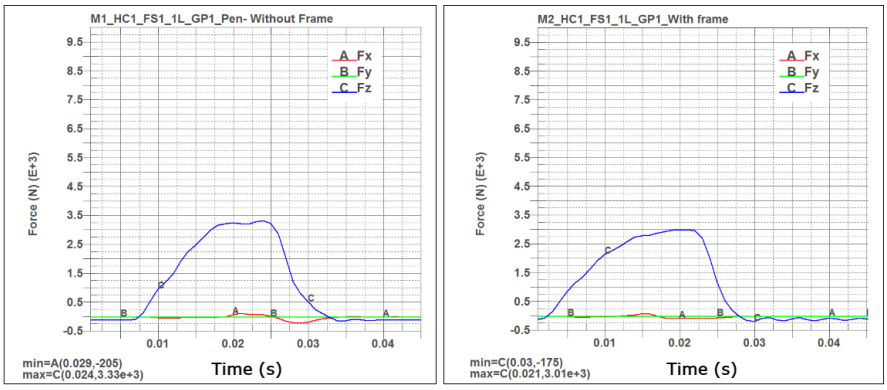

Figure 65: Comparison of maximum force reached by the system on impact. The system setup when considered without frame is on the left and with frame is on the right.

frame is $0.76m/s$ at the end of impact or at the loss of contact from the target. While the bounce off velocity measured for the system with frame at end of impact is also $0.76m/s$. Therefore, it has the same absorption capacity. The frame only prevents the cushion from penetrating into the mass plate. Although the mass of the system with frame is higher the bounce off velocity depends on the residual energy in the system after impact. The amount of energy absorbed in both the condition is the same.

Acceleration:

The figure 64 shows the maximum acceleration reached by the cushion due to the load acting by impact. The maximum acceleration measured for the cushion without frame is depicted on the graph on the left. It is measured to be $323m/s^2$ or $32.3g$. The graph on the right is for the cushion with frame and the maximum acceleration measured is $290m/s^2$ or $29g$ which has higher mass hence lower acceleration. Since the system mass in the condition with frame is slightly higher, acceleration with which the system bounces off is lower than the system without frame

Force:

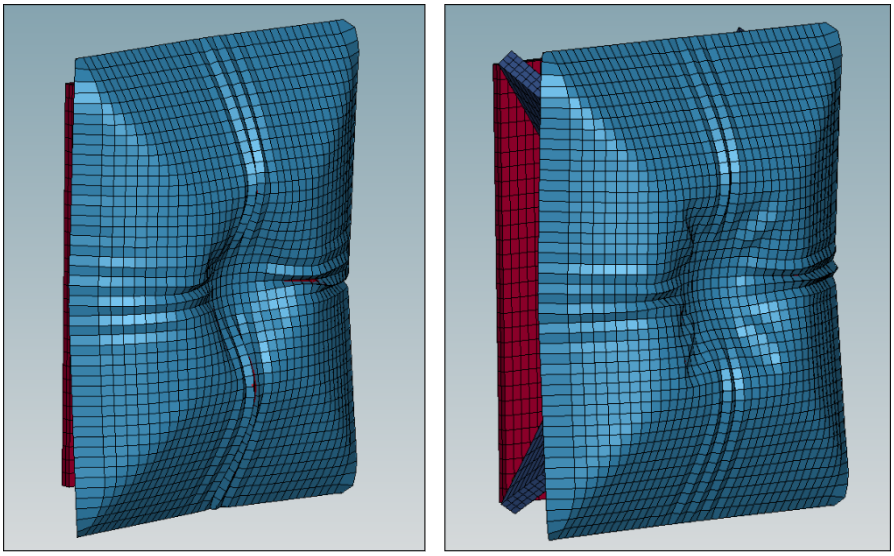

Figure 66: Comparison of distribution of load on the system by impact. The system setup when considered without frame is on the left and with frame is on the right. The load distribution in the in-plane direction is also seen in the face sheet when frame is used.

The figure 65 shows the maximum force taken up by the cushion model. The graph on the left is for the cushion model without frame and the plot on the right is the force measured for the cushion model when frame is given as the interface support. The maximum force measured on the left is $3330N$ and in with frame condition is $3010N$. This shows that some amount of force is being distributed through the face sheet along the in-plane direction when a frame interface is used and some of the force is also taken up by the frame there by transferring a reduced amount of force through the mass plate.

Difference in Impact:
The observation of indentation and also the in-plane distribution of load can be seen in figure 66. The figure on the left is for the cushion model without frame and on the right is for the cushion considered with frame. The wrinkling of the face sheet on the right shows the distribution of the load along the diagonals of the cushion as well. The frame, apart from serving the purpose of interface support, it also acts as a thick face on one side for the sandwich cushion helping in the in-plane distribution of the load. The results predicted for the cushion model when considered with frame without frame evaluates the purpose and effect of using a frame support. Although there is increase in the indentation depth when a frame is used due to increase in system over all mass, The force in the system with a frame is still lower that without the frame condition. When the frame is further analysed, the amount of force taken up by the frame could be further studied.

6 Results and Conclusion

6.1 Discussion on Correlation Results of Cushion Model M1

At the start of this work the data for different impact condition was available only from the laboratory testing. There were no relative data available through FEM. The main requirement for this work was to generate a finite element model for the cushion model 1 that was already laboratory tested through the laboratory testing and to provide with the resulting data. These results were to be correlated to validate the reliability of the finite element model setup for different laboratory tested conditions.

For a FE model setup one of the major task is to formulate the right material parameters for the cushion. The cushion is made of aluminum honeycomb celled core and Dyneema composite face sheet. Since both of these materials are orthotropic and a direct material property data, either by previous studies or laboratory testing was not available, a reliable material parameters were to be generated. Hence these property data were formulated by close approximations. These material property values were to be given as input parameters for the material cards on LS Dyna.

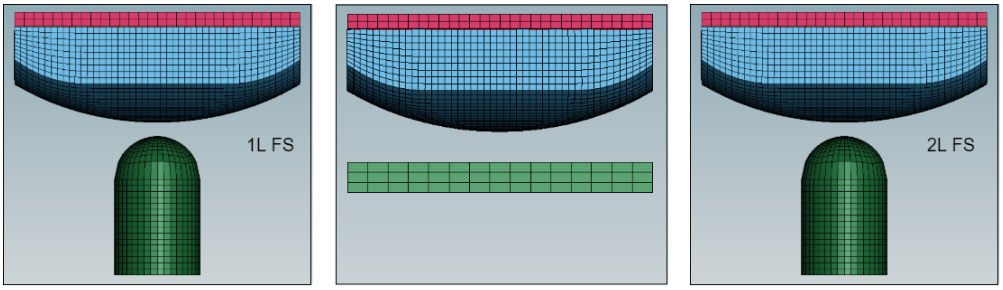

Figure 67: Comparison of model setup for different impact conditions considered for correlation with cushion model 1. The first model setup is the condition with one layer of face sheet impacting on a penetrator target, the second model setup is on a flat target. The third model setup is the condition with two layers of face sheet.

The cushion model 1 that was considered for correlation was meshed and were modelled for different impacting conditions as in the laboratory testing. This model setup is shown in the figure 67. The first condition considered was the cushion model1 with one layer of Dyneema face sheet impacting on a penetrator target. The next condition that was considered was with a change in the target. Hence cushion model 1 with one layer of face sheet impacting on a flat target. The next condition considered is the cushion model 1 with two layers of face sheet impacting on a penetrator target. The results of these conditions were correlated with laboratory testing for indentation depth, acceleration,velocity and force.

In figure68 a comparison of impact pattern for all the three conditions are summarised. On the top are the impact pattern seen in the laboratory tests and the bottom im-

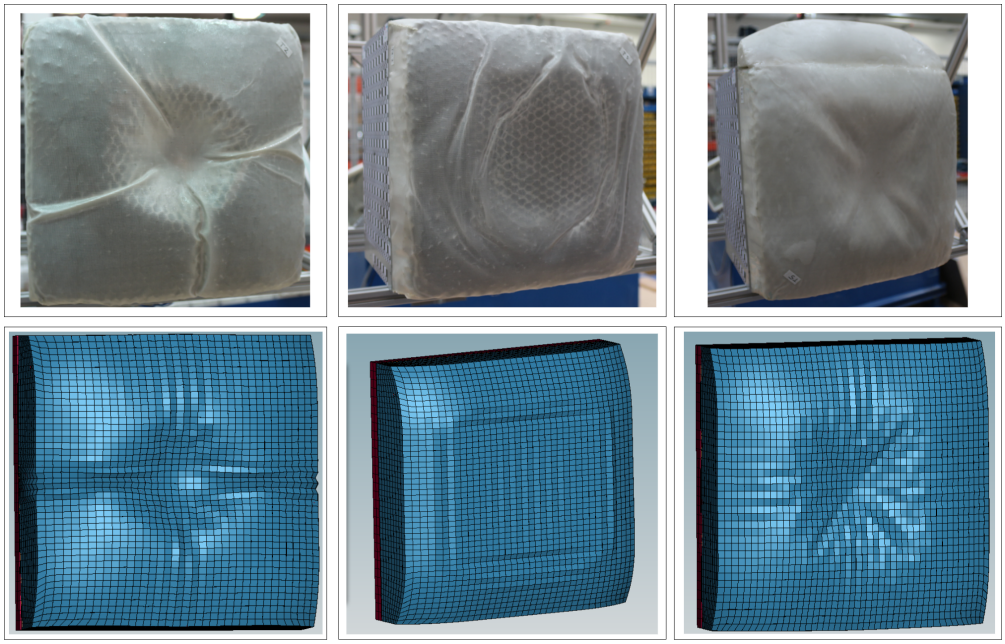

Figure 68: Comparison of impact pattern for the conditions considered for cushion model 1 with one layer face sheet in the first set, flat target in the second set and two layers of face sheet in the third set.

ages are the impact pattern seen through FEM. The first set is for the cushion model 1 with one layer face sheet impacting on the penetrator target. The second set of top and bottom images are for the model impacting on a flat target. The third set is for the cushion model 1 with two layers of face sheet impacting on a penetrator target.

Table 22: Summary of results of Indentation depth, Velocity, Acceleration and Force for different laboratory testing conditions of cushion model 1. The obtained values through FEA are correlated with laboratory test data.

Variation of Model 1 Setup	Impact Depth (mm)		Bounce off Velocity (m/s)		Max. Acceleration (g)		Force (N)	
	laboratory test	FEA	Laboratory test	FEA	Laboratory test	FEA	Laboratory test	FEA
M1_HC1_FS1_1L_GP1- Pen	54	40	0.65	0.76	34	36	3588	3570
M1_HC1_FS1_1L_GP1- Flat	28	21	0.5	0.53	80	88	7331	8360
M1_HC1_FS1_2L_GP1- Pen	43	32	0.8	0.83	43	48	4627	4700

The results seen through FE analysis in relation to the values observed through laboratory testing is summarised in table 22. The values for indentation depth, acceleration, velocity and force is summarised for all the three conditions. The first condition is the cushion model 1 with one layer face sheet. The second condition is with the flat target. The third condition is the cushion model with two layers of face sheet. The deviation in values recorded through FEA from that of laboratory condition for indentation depth shows 26%, 25%, 25.5% decrease respectively. A difference of ± 20 % was taken as a considerable range, since the overall system mass in the laboratory testing is about $15kg$ and in the FEA, the over all system mass is $10.5kg$ which is 30% decrease in mass. The approximation of the material parametric values taken in the formulation

of the material cards are also to be taken into account.

The values for bounce off velocity reached by the system obtained through FEA is correlated with values obtained through the laboratory testing. The bounce off velocity value in laboratory test data are the averaged value of the curve as discussed earlier. These values are in very close agreement with each other as shown in the table. The bounce off velocity reached by the system in the FEA models are higher than laboratory models because of the overall system mass being lower which makes the system bounce off with higher residual energy in the FEA conditions. Higher residual energy with in the system is because of lower dissipation of impact energy. A difference in values observed for the bounce off velocity is 16%, 6%, 4% increase for one layer penetrator condition, one layer flat plate condition and two layer penetrator condition respectively.

The acceleration of the cushion system is measured in the similar way in the FEA as in the laboratory testing. The deviation in measured value for the cushion model in FEA from that of laboratory tests are 6%, 9%, 11% increase respectively. The increase in bounce of velocity and maximum acceleration of the FEA system shows that the cushion has higher residual energy because of lower indentation. The force values obtained through FEA are by multiplying the acceleration values with the overall system mass of $10.5kg$, a percentage change in the values of FE model from that of the laboratory values is 0.5% decrease in the one layer penetrator condition, 14% increase in the one layer flat plate condition and 1.6% increase in the two layer penetrator condition. Although the system overall mass in the FEA condition is less, the measure force value is higher in the flat target condition and the two layer face sheet condition. Which means that the force being distributed in the FEA is higher. The impact forces are distributed in the in-plane direction. The core deformation in the in-plane direction would result in the shear crumbling of the cells. Since the FE formulated core has shear limits lower than the data sheet values and also the face sheet being a little elastic than the laboratory condition. This further helps in higher distribution of in-plane force in the cushion.

For a reduced overall mass of 30% and a cumulative decrease in indentation depth of 25% which depends on overall mass and properties of core and face sheet, a cumulative increase in bounce of velocity and acceleration of 10% shows that the FE model formulated has comparatively close agreement with the laboratory models. Assuming if the core and face sheet properties were to be exact, the indentation depth should have had 30% percentage change in the values. Hence an approximate of 5% error can be regarded as the deviation due to the used properties of the core and face sheet.

A higher energy is absorbed by the cushion when the impact forces are converted into deformation of the cells of the core and deformation of the face sheet. The impact forces are converted into normal forces and shear forces. Normal forces results in bending of the cushion and are taken up by the faces. Shear forces results in buckling and crumbling of the cushion and are taken up by the core. Hence core would be a better energy absorber when the cells are stiffer with lower yield limits. Stiffer core would offer more strength to the face sheet to absorb the normal forces and lower

yield limits buckles the cells quicker. Based on the studies and approximation done throughout the current work, it is observed that a core with thicker foils offers higher stiffness and larger cells will offer lower yield limits, which might be more suitable as an energy absorber.

6.2 Discussion on Evaluation of Frame with Cushion Model M2

The second requirement of the current work was to design a interface frame and to evaluate the cushion model 2. The cushion model 2 was a geometrical development from cushion model 1. The condition of the cushion setup is similar to that considered for cushion model 1 with one layer of face sheet impacting on a penetrator target. The other additional part considered is the frame. The condition with cushion model 2 with one layer face sheet without a frame is modelled with a stand off, as per the requirement, between the ground plate and mass plate to observe the extent of bending of the cushion. The standoffs are then modelled over the frame to observe the depth of penetration of the frame into the housing.

The frame is designed based on all the requirements of it being a simple, light weight interface structure. The provision for accommodating a load cell and attachment points for the frame to cushion and housing are also considered. Standoff points are also provided. Based on these requirements the frame is designed and given for future analysis. The FEA model in this work does not have the actual meshed frame, a simple geometry without any cut outs and a solid X frame is meshed and modelled with cushion model 2 for analysis.

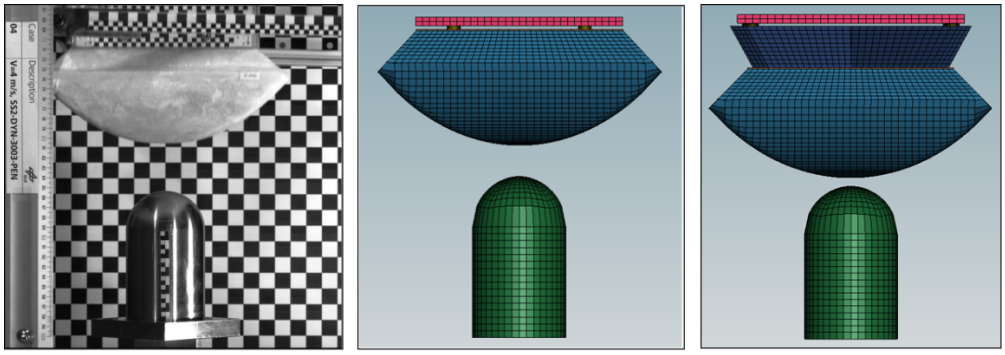

Figure 69: Comparison of model setup for different impact conditions considered for prediction of results with cushion model 2. The first model setup is the condition with one layer of face sheet impacting on a penetrator target without frame and the second model setup is with frame.

The figure 69 shows the model setup of the cushion model 2 with one layer of Dyneema face sheet. The first image is a depiction of the model setup in the laboratory testing for the future. FE model setup of the cushion without frame and with frame condition is compared. The frame mesh is taken for a simple geometry rather the actual frame.

Both the conditions is simulated for impact condition on a penetrator target.

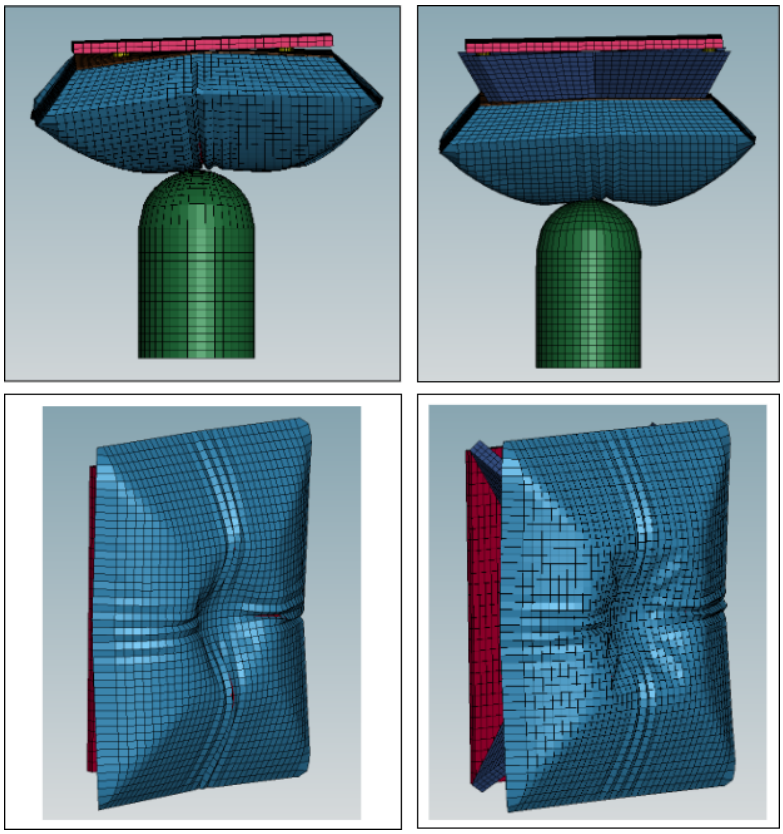

Figure 70: Comparison of bending and impact pattern of the cushion for the conditions of cushion model with one layer face sheet impacting on a penetrator target with frame on the right and without frame on the left.

The figure 70 shows the bending of the cushion on the top images and impact pattern in the bottom images. The bending observed in the cushion on the left is when a frame is not used. The cushion model on right with frame shows reduced bending. The bending of the cushion gets reduced along one edge of the cushion, the edge transverse to this edge still shows considerable bending even when frame is used, since the frame does not support the entire base. Frame offers support and interface connection between the housing and cushion. Frame also acts as an increased height of the face of the sandwich panel. The faces of the sandwich takes up the in-plane load or the bending loads and hence offers larger distribution of in-plane force which is seen in the impact pattern.

The values measured for the cushion model 2 with one layer of face sheet impacting on a penetrator target are tabulated in table 23. The values measured for model without frame and with frame are summarised. The impact depth for the model with frame is higher because of the increased overall system mass due to the additional weight offered by the frame. Minimum velocity reached by the system and maximum acceleration of the system is slightly lower for model with the frame for the same reason.

Table 23: Summary of results of Indentation depth, Velocity, Acceleration and Force for cushion model 2. The obtained values through FEA are compared between without frame and with frame condition.

Cushion Model 2	Impact Depth (mm)	Minimum Velocity (m/s)	Max. Acceleration (g)	Force (N)
Without frame	0.021	-0.76	32.3	3330
With frame	0.039	-0.757	29	3010

Force measured for the model with frame is lower than the model without frame even though the overall mass of the system with frame is higher. This is because of the larger in-plane distribution of force due to the frame.

7 Future Scope

The current work 'Finite Element Model Correlation and Evaluation of a Structural Support for the DLR shell Lander' was carried out beginning with the data that was available from previous works. The models were formulated and improved to match the actual laboratory testing conditions.

As discussed and understood about the approximations considered for the properties of core and face sheet, actual mechanical test to get the exact values of the properties of both core and face sheet can be carried out. Another alternative to mechanical testing could be either to get the values from the manufacturers. Least suggested method of obtaining the right property values would be by analytical calculations as the values would be prone to larger deviation and errors since the number of variables required to define each property is more and a larger approximations and assumptions are to be taken into consideration to get the defined parameters.

The mass plate formulated in this work is 10kg which make the overall system to be about 10.5kg in the FEA models. The actual overall mass of the system in the laboratory testing has been 15kg. This update of mass plate can be carried out for further analysis. Dyneema face sheet as a composite material is adapted based on the known number of layers glued over the core as in the laboratory testing for correlation. Volume fraction of the fibres in the composite is assumed and based on which the laminate thickness is adopted, both of which plays a crucial role in defining the property values. The overall thickness of the face sheet used in each laboratory test conditions can be measured and adapted accordingly to get more closer values.

In this work although the frame is designed for the requirements, only a simple solid frame is meshed for the FE analysis. The actual design of the frame can be meshed and the force transfer from target to core to ground plate to frame and then to mass plate can be studied. A detailed stress analysis could also be performed for a finalised design of frame.

A detailed study on the crash worthiness of the cushion involving behaviour of the core and face sheet thus deciding on the optimised height of the core and faces of the sandwich panel can be performed. Based on the understanding so far, a core of larger cell size would offer lower yield limits and thicker foil thickness would offer higher crush strength thereby increasing the absorption capacity. This understanding could be verified through laboratory tests. A study on composite face sheet based on certain known layup and thickness of the composite can be performed. Face sheet with woven fibres of deformable properties offer larger distribution of in-plane forces. These studies would decide on the thickness of the faces and the core and therefore the design of the cushion could be complete.

Appendix

A1. 2D Computer Aided Drawings (CAD) of the Frame Design

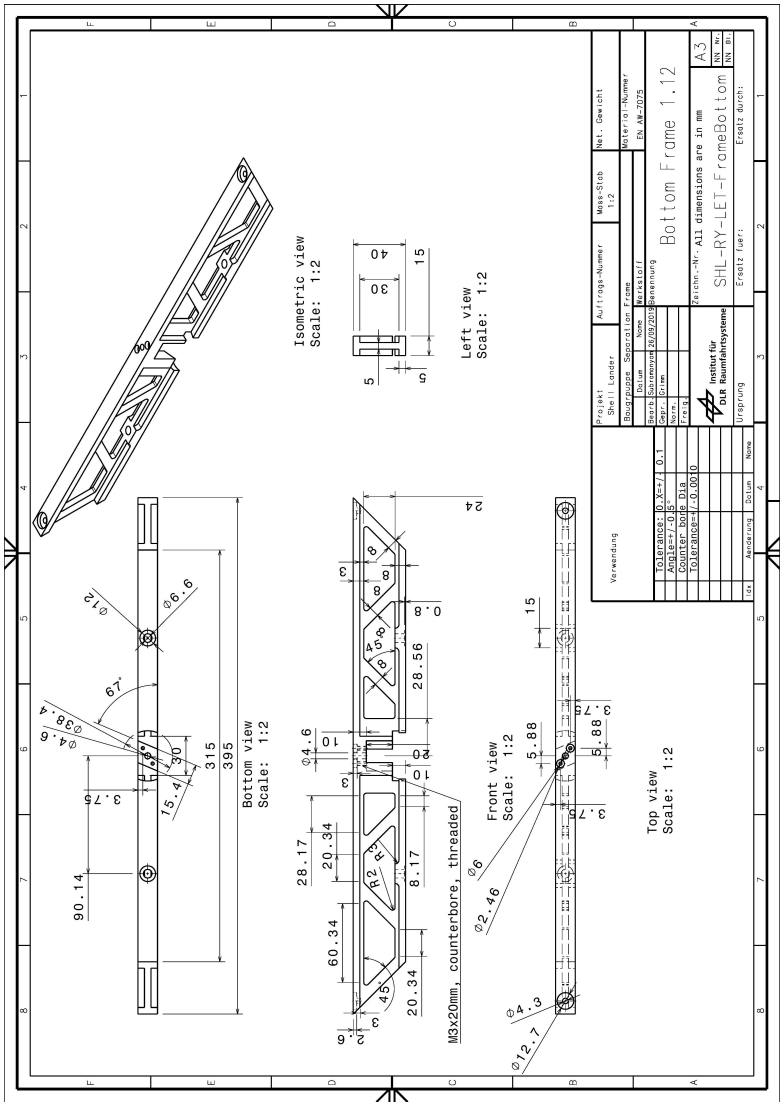

Figure 71: CAD of beam A of the two beam interface frame. The bottom view and top view gives the dimensions of each of the attributes of the beam. Front view shows the dimensions of the through holes and pockets. Left view shows the definition of the I-section of the beam. Also given is the isometric view of the beam. All dimensions are in millimetres (mm) with a scale of 1:2.

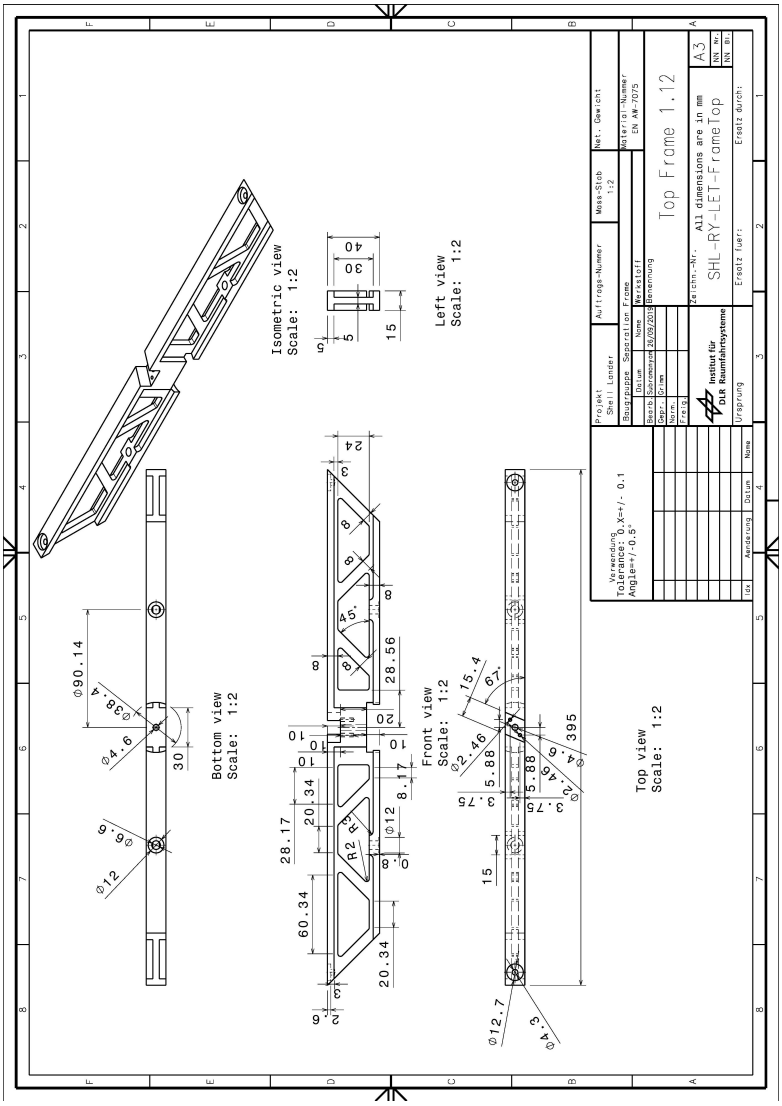

Figure 72: CAD of beam B of the two beam interface frame. The bottom view and top view gives the dimensions of each of the attributes of the beam. Front view shows the dimensions of the through holes and pockets. Left view shows the definition of the I-section of the beam. Also given is the isometric view of the beam. All dimensions are in millimetres (mm) with a scale of 1:2.

A2. LS Dyna: *Section_Shell and Simulation Runs of Model 2

*SECTION_SHELL keyword that defines the face sheet element type. The thickness of the face sheet as a composite laminate is defined in this keyword as discussed in section 3.2.2.

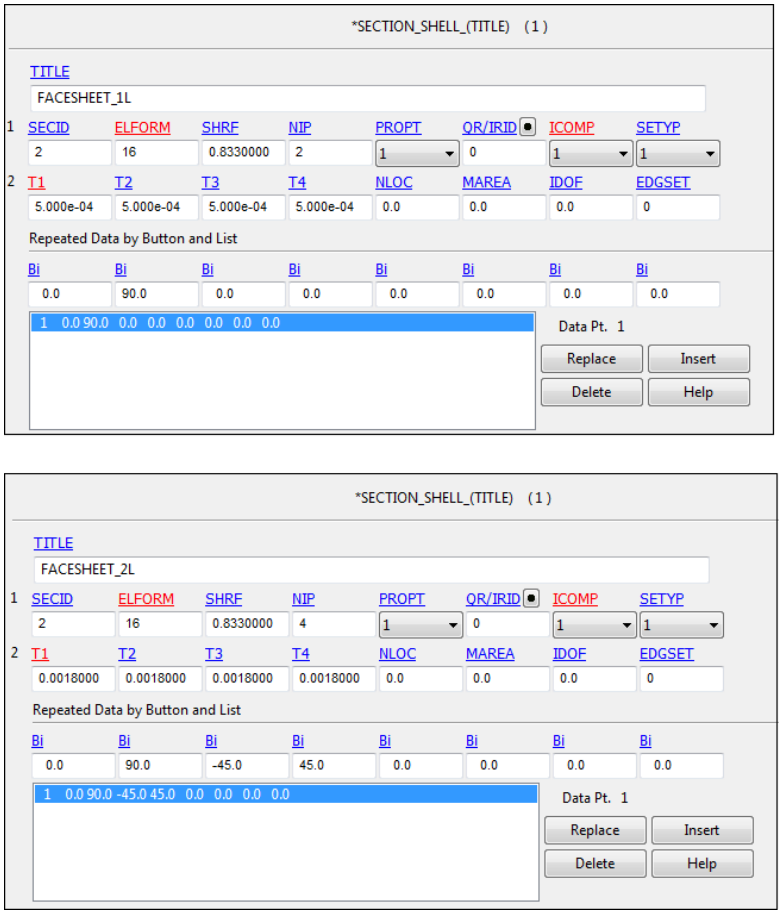

Figure 73: Keyword *SECTION_SHELL that defines the elements of face sheet of the mesh model.

This is an FEA simulation run for cushion model 2 with aluminum honeycomb core over which one layer of Dyneema-Epoxy composite face sheet falling on a penetrator target. The cushion has an aluminum base for the ground plate. Standoffs are screwed to the ground plate that acts as holder to the housing.

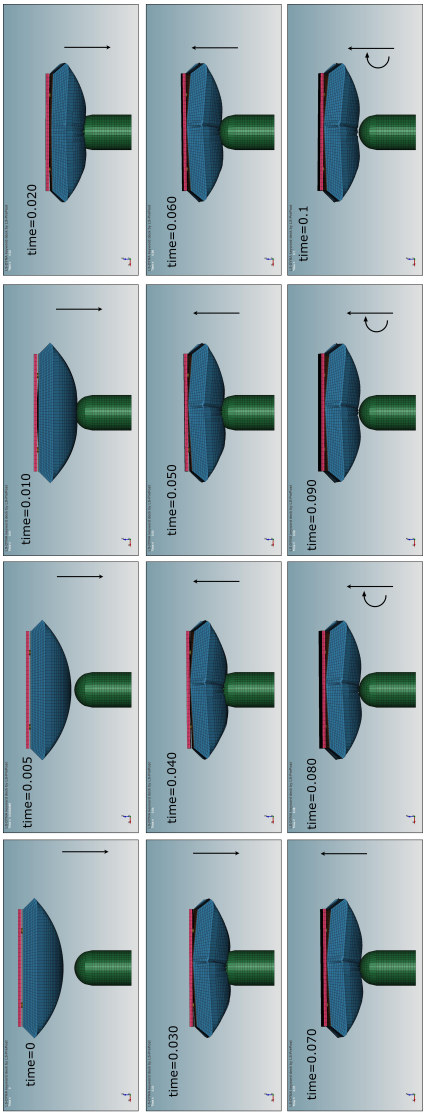

Figure 74: The simulation run for cushion model 2 without the frame support depicting the cushion motion at different instances. The simulation is run between 0s to 0.1s. The first contact is at 0.007s and the loss of contact occurs at 0.025s between which measurements are taken.

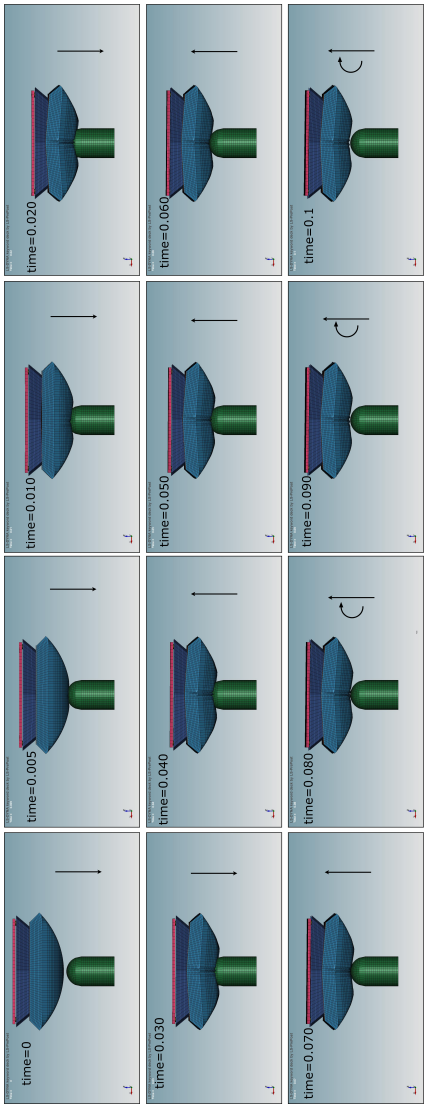

Figure 75: The simulation run for cushion model 2 with the frame support depicting the cushion motion at different instances. The simulation is run between 0s to 0.1s. The first contact is at 0.0026s and the loss of contact occurs at 0.022s between which measurements are taken.

A3. Simulation Keyword Files and The Laminator Results

The run files on LS Dyna are stored as .k files. Three of five k-files are given below.

1. The values recorded for the base model that is the cushion model 1 with one layer of Dyneema face sheet impacting on penetrator target is taken. There after the second condition was only with the change in geometry of the target. Every other value remain same. Hence .k file of the second condition is not given here

2. The third condition of using two layers of face sheet has different values in keyword

that is related to face sheet. Hence only the keyword of face sheet values are given here.

3. The cushion model 2 has mostly the same properties for core and single layered face sheet, only the additional components like the stand offs and frame are to be considered. The keywords describing the properties of only these components are included.

The Laminator: Face sheet values calculated for Dyneema-Epoxy composite for one layer and two layers are given.

1. **Base Model: Keyword file for Cushion Model 1 with one layer face sheet and penetrator target.**

```
$# LS-DYNA Keyword file created by LS-PrePost(R) V4.6.10 - 19Jun2019
$# Created on Dec-18-2019 (06:05:25)
*KEYWORD
*TITLE_TITLE
$#                                                                  title
M1_HC1_FS1_1L-Pen
*CONTROL_ACCURACY
$#     osu       inn    pidosu      iacc
         0         4         0         0
*CONTROL_DYNAMIC_RELAXATION
$#  nrcyck     drtol    drfctr    drterm    tssfdr    irelal     edttl    idrflg
      2501.00000E-4     0.995      0.05       0.0         0      0.04         1
*CONTROL_ENERGY
$#    hgen      rwen    slnten     rylen
         2         1         2         1
*CONTROL_SHELL
$#  wrpang     esort     irnxx    istupd    theory       bwc     miter      proj
      20.0         1        -1         0         2         2         1         0
$# rotascl    intgrd    lamsht    cstyp6    thshel
       1.0         0         1         1         0
$# psstupd   sidt4tu     cntco    itsflg    irquad    w-mode   stretch      icrq
         0         0         0         0         2       0.0       0.0         0
$#  nfail1    nfail4   psnfail    keepcs     delfr   drcpsid    drcprm   intperr
         0         0         0         0         0         0       1.0         0
*CONTROL_TERMINATION
$#  endtim    endcyc     dtmin    endeng    endmas     nosol
       0.1         0      0.05       0.0       0.0         0
*CONTROL_TIMESTEP
$#  dtinit    tssfac      isdo    tslimt     dt2ms      lctm     erode     ms1st
       0.0       0.8         0       0.0       0.0         0         1         0
$#  dt2msf   dt2mslc     imscl    unused    unused     rmscl
       0.0         0         0                           0.0

*DATABASE_DCFAIL
$#      dt    binary      lcur     ioopt
1.00000E-5         1         0         1
*DATABASE_ELOUT
$#      dt    binary      lcur     ioopt   option1   option2   option3   option4
1.00000E-5         1         0         1         0         0         0         0
*DATABASE_GLSTAT
$#      dt    binary      lcur     ioopt
1.00000E-5         1         0         1
*DATABASE_MATSUM
$#      dt    binary      lcur     ioopt
1.00000E-5         1         0         1
*DATABASE_NCFORC
$#      dt    binary      lcur     ioopt
1.00000E-5         1         0         1
*DATABASE_SLEOUT
$#      dt    binary      lcur     ioopt
1.00000E-5         1         0         1
*DATABASE_BINARY_D3PLOT
$#      dt      lcdt      beam     npltc    psetid
     0.001         0         0         0         0
```

```
$#   ioopt
         0
*DATABASE_EXTENT_BINARY
$#   neiph     neips    maxint    strflg    sigflg    epsflg    rltflg    engflg
         0         0         3        11         1         1         1         1
$#  cmpflg    ieverp    beamip     dcomp      shge     stssz    n3thdt   ialemat
         1         0         0         1         2         1         2         1
$# nintsld   pkp_sen      sclp     hydro     msscl     therm    intout    nodout
         0         0       1.0         0         0         0ALL       ALL
$#    dtdt    resplt     neipb     quadr     cubic
         0         0         0         0         0
*LOAD_BODY_Z
$#    lcid        sf    lciddr        xc        yc        zc       cid
         8       1.0         9       0.0       0.0       0.0         0

*CONTACT_TIED_SHELL_EDGE_TO_SURFACE_OFFSET_ID
$#     cid                                                          title
         1 FACESHEET_TO_CORE_BONDING
$#    ssid      msid     sstyp     mstyp    sboxid    mboxid       spr       mpr
         2         1         3         3         0         0         0         1
$#      fs        fd        dc        vc       vdc    penchk        bt        dt
       0.0       0.0       0.0       0.0       0.0         0       0.01.00000E20
$#     sfs       sfm       sst       mst      sfst      sfmt      fsf       vsf
       1.0       1.0       0.0       0.0       1.0       1.0       1.0       1.0
$#    soft    sofscl    lcidab    maxpar     sbopt     depth     bsort    frcfrq
         1       0.1         0     1.025       5.0         2         0         1
$#  penmax    thkopt    shlthk     snlog      isym     i2d3d    sldthk    sldstf
       0.0         0         0         0         0         0       0.0       0.0

*CONTACT_AUTOMATIC_SURFACE_TO_SURFACE_ID
$#     cid                                                          title
         2PENETRATOR_TO_FACESHEET
$#    ssid      msid     sstyp     mstyp    sboxid    mboxid       spr       mpr
         3         2         3         3         0         0         0         1
$#      fs        fd        dc        vc       vdc    penchk        bt        dt
       0.0       0.0       0.0       0.0       0.0         0       0.01.00000E20
$#     sfs       sfm       sst       mst      sfst      sfmt      fsf       vsf
       1.0       1.0       0.0       0.0       1.0       1.0       1.0       1.0
$#    soft    sofscl    lcidab    maxpar     sbopt     depth     bsort    frcfrq
         2       0.1         0     1.025       2.0         2         0         1

*CONTACT_AUTOMATIC_SURFACE_TO_SURFACE_ID
$#     cid                                                          title
         3 PENETRATOR_TO_CORE
$#    ssid      msid     sstyp     mstyp    sboxid    mboxid       spr       mpr
         3         1         3         3         0         0         0         1
$#      fs        fd        dc        vc       vdc    penchk        bt        dt
       0.0       0.0       0.0       0.0       0.0         0       0.01.00000E20
$#     sfs       sfm       sst       mst      sfst      sfmt      fsf       vsf
       1.0       1.0       0.0       0.0       1.0       1.0       1.0       1.0
$#    soft    sofscl    lcidab    maxpar     sbopt     depth     bsort    frcfrq
         2       0.1         0     1.025       2.0         2         0         1

*CONTACT_FORCE_TRANSDUCER_PENALTY_ID
$#     cid                                                          title
         4FORCE_PENETRATOR
$#    ssid      msid     sstyp     mstyp    sboxid    mboxid       spr       mpr
         0         3         0         3         0         0         0         0
$#      fs        fd        dc        vc       vdc    penchk        bt        dt
```

```
       0.0       0.0       0.0       0.0       0.0         0       0.01.00000E20
$#     sfs       sfm       sst       mst      sfst      sfmt       fsf       vsf
       1.0       1.0       0.0       0.0       1.0       1.0       1.0       1.0
*CONTACT_AUTOMATIC_SURFACE_TO_SURFACE_ID
$#     cid                                                                 title
         5PENETRATOR_TO_GP
$#    ssid      msid     sstyp     mstyp    sboxid    mboxid       spr       mpr
         5         3         3         3         0         0         0         1
$#      fs        fd        dc        vc       vdc    penchk        bt        dt
       0.0       0.0       0.0       0.0       0.0         0       0.01.00000E20
$#     sfs       sfm       sst       mst      sfst      sfmt       fsf       vsf
       1.0       1.0       0.0       0.0       1.0       1.0       1.0       1.0
$#    soft    sofscl    lcidab    maxpar     sbopt     depth     bsort    frcfrq
         2       0.1         0     1.025       2.0         2         0         1

*CONTACT_TIED_SURFACE_TO_SURFACE_OFFSET_ID
$#     cid                                                                 title
         6GP-Core
$#    ssid      msid     sstyp     mstyp    sboxid    mboxid       spr       mpr
         5         1         3         3         0         0         0         0
$#      fs        fd        dc        vc       vdc    penchk        bt        dt
       0.0       0.0       0.0       0.0       0.0         0       0.01.00000E20
$#     sfs       sfm       sst       mst      sfst      sfmt       fsf       vsf
       1.0       1.0       0.0       0.0       1.0       1.0       1.0       1.0
$#    soft    sofscl    lcidab    maxpar     sbopt     depth     bsort    frcfrq
         1       0.1         0     1.025       2.0         2         0         1

*CONTACT_TIED_NODES_TO_SURFACE_OFFSET_ID
$#     cid                                                                 title
         7GP_Node-MP
$#    ssid      msid     sstyp     mstyp    sboxid    mboxid       spr       mpr
         1         6         4         3         0         0         2         0
$#      fs        fd        dc        vc       vdc    penchk        bt        dt
       0.0       0.0       0.0       0.0       0.0         0       0.01.00000E20
$#     sfs       sfm       sst       mst      sfst      sfmt       fsf       vsf
       1.0       1.0       0.0       0.0       1.0       1.0       1.0       1.0

*CONTACT_AUTOMATIC_NODES_TO_SURFACE_ID
$#     cid                                                                 title
         8GP_Rest-MP
$#    ssid      msid     sstyp     mstyp    sboxid    mboxid       spr       mpr
         3         6         4         3         0         0         0         0
$#      fs        fd        dc        vc       vdc    penchk        bt        dt
       0.0       0.0       0.0       0.0       0.0         0       0.01.00000E20
$#     sfs       sfm       sst       mst      sfst      sfmt       fsf       vsf
       1.0       1.0       0.0       0.0       1.0       1.0       1.0       1.0

*PART
$#                                                                          title
CORE
$#     pid     secid       mid     eosid      hgid      grav    adpopt      tmid
         1         1         1         0         1         0         0         0
*SECTION_SOLID_TITLE
CORE
$#   secid    elform       aet
         1         1         0
*MAT_MODIFIED_HONEYCOMB_TITLE
HONEYCOMB_CORE-3/8''-1.0-0.0007''-Al5052
$#     mid        ro         e        pr      sigy        vf        mu      bulk
```

```
         1      16.06.895000E7      0.054.050000E8       0.3      0.05       0.0
$#     lca       lcb       lcc       lcs      lcab      lcbc      lcca      lcsr
        -1         2         3         0         0         0         0         7
$#    eaau      ebbu      eccu      gabu      gbcu      gcau      aopt      macf
6.895000E7  206800.0  310300.0   82740.0   48260.0       0.0       2.0         1
$#      xp        yp        zp        a1        a2        a3
       0.0       0.0       0.0       0.0       0.0       1.0
$#      d1        d2        d3      tsef      ssef      vref      tref    shdflg
       0.0       1.0       0.0       0.0       0.0       0.7       0.0       1.0
*HOURGLASS_TITLE
CORE HOURGLASS
$#    hgid       ihq        qm       ibq        q1        q2    qb/vdc        qw
         1         5      0.03         0       1.5      0.06       0.1       0.1

*PART
$#                                                                         title
FACESHEET
$#     pid     secid       mid     eosid      hgid      grav    adpopt      tmid
         2         2         2         0         2         0         0         0
*SECTION_SHELL_TITLE
FACESHEET
$#   secid    elform      shrf       nip     propt   qr/irid     icomp     setyp
         2        16     0.833         2       1.0         0         1         1
$#      t1        t2        t3        t4      nloc     marea      idof    edgset
5.00000E-45.00000E-45.00000E-45.00000E-4       0.0       0.0       0.0         0
$#      bi        bi        bi        bi        bi        bi        bi        bi
       0.0      90.0       0.0       0.0       0.0       0.0       0.0       0.0
*MAT_ENHANCED_COMPOSITE_DAMAGE_TITLE
FS1_1L_Dyneema_Special Weave_Vf=60%
$#     mid        ro        ea        eb      (ec)      prba    (prca)    (prcb)
         2    1030.01.43400E101.43400E10       0.0     0.031     0.028       0.0
$#     gab       gbc       gca      (kf)      aopt      2way
3.914000E9       0.0       0.0       0.0       2.0       0.0
$#      xp        yp        zp        a1        a2        a3    mangle
       0.0       0.0       0.0       1.0       0.0       0.0       0.0
$#      v1        v2        v3        d1        d2        d3    dfailm    dfails
       0.0       0.0       0.0       0.0       1.0       0.0       1.0       1.0
$#   tfail      alph      soft      fbrt     ycfac    dfailt    dfailc       efs
       0.0       0.0       1.0       0.0       2.0       1.0      -1.0       0.0
$#      xc        xt        yc        yt        sc      crit      beta
3.860000E71.191000E83.860000E71.191000E81.904000E7      54.0       0.0
$#     pel      epsf      epsr      tsmd     soft2
       0.0       0.0       0.0       0.9       1.0
$#  slimt1    slimc1    slimt2    slimc2     slims    ncyred     softg
       0.0       0.0       0.0       0.0       0.0       0.0       1.0
*HOURGLASS_TITLE
FACESHEET HOURGLASS
$#    hgid       ihq        qm       ibq        q1        q2    qb/vdc        qw
         2         8       0.1         0       1.5      0.06       0.1       0.1

*PART
$#                                                                         title
PENETRATOR TARGET
$#     pid     secid       mid     eosid      hgid      grav    adpopt      tmid
         3         3         3         0         0         0         0         0
*SECTION_SOLID_TITLE
PENETRATOR TARGET
$#   secid    elform       aet
         3         1         0
```

```
*MAT_RIGID_TITLE
PENETRATOR
$#     mid        ro         e        pr         n    couple         m     alias
         3    7800.02.00000E11       0.3       0.0       0.0       0.0
$#     cmo      con1      con2
       1.0         7         7
$#lco or a1        a2        a3        v1        v2        v3
       0.0       0.0       0.0       0.0       0.0       0.0

*PART
$#                                                                         title
GROUND PLATE
$#     pid     secid       mid     eosid      hgid      grav    adpopt      tmid
         5         5         5         0         0         0         0         0
*SECTION_SOLID_TITLE
GROUND PLATE
$#   secid    elform       aet
         5         1         0
*MAT_PIECEWISE_LINEAR_PLASTICITY_TITLE
GP1-ALUMINUM 5052-O
$#     mid        ro         e        pr      sigy      etan      fail      tdel
         5    2684.97.03300E10      0.335.965000E7       0.01.00000E21       0.0
$#       c         p      lcss      lcsr        vp
       0.0       0.0        10         0       0.0
$#    eps1      eps2      eps3      eps4      eps5      eps6      eps7      eps8
       0.0       0.0       0.0       0.0       0.0       0.0       0.0       0.0
$#     es1       es2       es3       es4       es5       es6       es7       es8
       0.0       0.0       0.0       0.0       0.0       0.0       0.0       0.0

*PART
$#                                                                         title
MASS PLATE
$#     pid     secid       mid     eosid      hgid      grav    adpopt      tmid
         6         6         6         0         0         0         0         0
*SECTION_SOLID_TITLE
MASS PLATE
$#   secid    elform       aet
         6         1         0
*MAT_PIECEWISE_LINEAR_PLASTICITY_TITLE
MP-STEEL CARBON A441 ARMCO HIGH STRENGTH B PLATE BAR .75-1.5 IN
$#     mid        ro         e        pr      sigy      etan      fail      tdel
         6    7833.42.06800E11      0.292.783000E8       0.0       0.0       0.0
$#       c         p      lcss      lcsr        vp
       0.0       0.0        11         0       0.0
$#    eps1      eps2      eps3      eps4      eps5      eps6      eps7      eps8
       0.0       0.0       0.0       0.0       0.0       0.0       0.0       0.0
$#     es1       es2       es3       es4       es5       es6       es7       es8
       0.0       0.0       0.0       0.0       0.0       0.0       0.0       0.0

*DEFINE_CURVE_TITLE
LCA-LT_Angle
$#    lcid      sidr       sfa       sfo      offa      offo    dattyp     lcint
         1         0       1.0       1.0       0.0       0.0         0         0
$#                a1                  o1
                0.0            172369.0
               10.0            158000.0
               20.0            136000.0
               30.0            107000.0
               40.0             65100.0
```

```
                50.0             17200.0
                60.0              5980.0
                70.0              4260.0
                80.0              3750.0
                90.0              3750.0
*DEFINE_CURVE_TITLE
LCB-T_VolStrain_mean_v3
$#    lcid      sidr       sfa       sfo      offa      offo    dattyp     lcint
         2         0       1.0       1.0       0.0       0.0         0         0
$#                a1                 o1
              -0.1                 0.0
          0.175798                 0.0
          0.180692                 0.0
          0.185513                 0.0
          0.190317                 0.0
          0.195125                 0.0
          0.199916                 0.0
          0.204771                 0.0
          0.209583                 0.0
          0.214421                 0.0
          0.219265                 0.0
            0.2241                 0.0
          0.228966                 0.0
          0.233806                 0.0
          0.238638                 0.0
          0.243449                 0.0
          0.248315                 0.0
          0.267821                 0.0
          0.272646                 0.0
          0.277519                 0.0
          0.282293                 0.0
              0.76                 0.0
               0.8                 0.0
          0.815367            379212.0
*DEFINE_CURVE_TITLE
LCC-L_VolStrain_mean_v3
$#    lcid      sidr       sfa       sfo      offa      offo    dattyp     lcint
         3         0       1.0       1.0       0.0       0.0         0         0
$#                a1                 o1
              -0.1                 0.0
               0.0                 0.0
          0.002243                 0.0
          0.006501                 0.0
          0.010795                 0.0
          0.015086                 0.0
          0.019398                 0.0
          0.023631                 0.0
          0.027867                 0.0
          0.032108                 0.0
           0.03646                 0.0
          0.040783                 0.0
          0.045117                 0.0
          0.049394                 0.0
          0.053675                 0.0
           0.05801                 0.0
          0.062313                 0.0
          0.066598                 0.0
          0.070907                 0.0
          0.075201                 0.0
```

```
          0.079444                0.0
          0.083698                0.0
          0.088039                0.0
          0.092332                0.0
          0.096611                0.0
          0.100881                0.0
          0.105206                0.0
          0.109467                0.0
          0.113742                0.0
          0.118033                0.0
          0.122297                0.0
          0.126612                0.0
          0.130907                0.0
          0.135173                0.0
          0.139438                0.0
          0.143711                0.0
          0.148035                0.0
          0.152338                0.0
          0.156683                0.0
          0.161038                0.0
          0.165335                0.0
          0.169639                0.0
          0.173878                0.0
          0.178126                0.0
          0.182451                0.0
          0.186788                0.0
             0.191                0.0
          0.195256                0.0
          0.199549                0.0
            0.2039                0.0
          0.208184                0.0
          0.212474                0.0
          0.216712                0.0
          0.221002                0.0
          0.225284                0.0
          0.229613                0.0
          0.233914                0.0
          0.238176                0.0
          0.242441                0.0
               0.6                0.0
          0.654659           137895.0
*DEFINE_CURVE_TITLE
Strain_Rate
$#    lcid      sidr       sfa       sfo      offa      offo    dattyp     lcint
         7         0       1.0       1.0       0.0       0.0         0         0
$#              a1                  o1
              0.0                 1.0
             40.0                 1.1
*DEFINE_CURVE_TITLE
GRAVITY
$#    lcid      sidr       sfa       sfo      offa      offo    dattyp     lcint
         8         0       1.0       1.0       0.0       0.0         0         0
$#              a1                  o1
              0.0                9.81
          10000.0                9.81
*DEFINE_CURVE_TITLE
DR
$#    lcid      sidr       sfa       sfo      offa      offo    dattyp     lcint
         9         1       1.0       1.0       0.0       0.0         0         0
```

```
$#                a1                  o1
                 0.0                 0.0
                0.03                9.81
                 1.0                9.81
*DEFINE_CURVE_TITLE
Stress-Strain_1047_Mat_024_5052Al
$#    lcid      sidr       sfa       sfo      offa      offo    dattyp     lcint
        10         0       1.0       1.0       0.0       0.0         0         0
$#                a1                  o1
                 0.0    5.9645100000e+07
    5.9230398620e-05    6.0662500000e+07
    1.7769100668e-04    6.2556300000e+07
    3.5538201337e-04    6.5110800000e+07
    5.9230398620e-04    6.8109104000e+07
    8.8845600840e-04    7.1375400000e+07
           0.0012438    7.4783600000e+07
           0.0016584    7.8249104000e+07
           0.0021323    8.1718096000e+07
           0.0026654    8.5157200000e+07
           0.0032577    8.8546600000e+07
           0.0039092    9.1875000000e+07
             0.00462    9.5136600000e+07
             0.00539    9.8329000000e+07
           0.0062192    1.0145200000e+08
           0.0071076    1.0450700000e+08
           0.0080553    1.0749500000e+08
           0.0090623    1.1042000000e+08
           0.0101284    1.1328300000e+08
           0.0112538    1.1608700000e+08
           0.0124384    1.1883500000e+08
           0.0136822    1.2152900000e+08
           0.0149853    1.2417300000e+08
           0.0163476    1.2676700000e+08
           0.0177691    1.2931500000e+08
           0.0192499    1.3181800000e+08
           0.0207899    1.3427900800e+08
           0.0223891    1.3669900800e+08
           0.0240475    1.3908099200e+08
           0.0257652    1.4142499200e+08
           0.0275421    1.4373400000e+08
           0.0293783    1.4600800000e+08
           0.0312736    1.4825000000e+08
           0.0332282    1.5046000000e+08
           0.0352421    1.5264000000e+08
           0.0373151    1.5479100800e+08
           0.0394474    1.5691400000e+08
            0.041639    1.5901000000e+08
           0.0438897    1.6107900800e+08
           0.0461997    1.6312400000e+08
           0.0485689    1.6514400000e+08
           0.0509974    1.6714099200e+08
            0.053485    1.6911500800e+08
           0.0560319    1.7106700800e+08
           0.0586381    1.7299800000e+08
           0.0613034    1.7490800000e+08
            0.064028    1.7679800000e+08
           0.0668119    1.7866899200e+08
           0.0696549    1.8052099200e+08
           0.0725572    1.8235400000e+08
```

```
          0.0755187    1.8417000000e+08
          0.0785395    1.8596899200e+08
          0.0816195    1.8775100800e+08
          0.0847587    1.8951600000e+08
          0.0879571    1.9126600000e+08
          0.0912148    1.9300000000e+08
          0.0945317    1.9471900800e+08
          0.0979078    1.9642300800e+08
           0.101343    1.9811299200e+08
           0.104838    1.9978899200e+08
           0.108392    2.0145200000e+08
           0.112005    2.0310099200e+08
           0.115677    2.0473600000e+08
           0.119408    2.0636000000e+08
           0.123199    2.0797000000e+08
           0.127049    2.0956899200e+08
           0.130958    2.1115600000e+08
           0.134927    2.1273100800e+08
           0.138954    2.1429400000e+08
           0.143041    2.1584700800e+08
           0.147187    2.1738899200e+08
           0.151393    2.1892000000e+08
           0.155657    2.2044000000e+08
           0.159981    2.2195000000e+08
           0.164364    2.2345000000e+08
           0.168807    2.2494099200e+08
           0.173308    2.2642099200e+08
           0.177869    2.2789200000e+08
           0.182489    2.2935400000e+08
           0.187168    2.3080700800e+08
           0.191906    2.3225100800e+08
           0.196704    2.3368600000e+08
           0.201561    2.3511200000e+08
           0.206477    2.3653000000e+08
           0.211452    2.3793900800e+08
           0.216487    2.3934000000e+08
           0.221581    2.4073299200e+08
           0.226734    2.4211900800e+08
           0.231946    2.4349600000e+08
           0.237218    2.4486600000e+08
           0.242548    2.4622800000e+08
           0.247938    2.4758300800e+08
           0.253388    2.4893100800e+08
           0.258896    2.5027100800e+08
           0.264464    2.5160400000e+08
           0.270091    2.5293100800e+08
           0.275777    2.5425000000e+08
           0.281522    2.5556300800e+08
           0.287327    2.5686899200e+08
            0.29319    2.5816899200e+08
              0.297    2.5881800000e+08
*DEFINE_CURVE_TITLE
Stress-Strain_593_STEEL CARBON A441 ARMCO HIGH STRENGTH B PLATE BAR .75-1.5 IN
$#    lcid      sidr       sfa       sfo      offa      offo    dattyp     lcint
        11         0       1.0       1.0       0.0       0.0         0         0
$#              a1                  o1
             0.0    2.7831600000e+08
    5.5250900914e-05    2.7988000000e+08
    1.6575299378e-04    2.8285500800e+08
```

3.3150499803e-04	2.8698300800e+08
5.5250898004e-04	2.9197200000e+08
8.2876300439e-04	2.9754800000e+08
0.0011603	3.0348499200e+08
0.001547	3.0961100800e+08
0.001989	3.1580198400e+08
0.0024863	3.2197299200e+08
0.0030388	3.2806800000e+08
0.0036466	3.3405100800e+08
0.0043096	3.3990201600e+08
0.0050278	3.4560800000e+08
0.0058013	3.5116400000e+08
0.0066301	3.5656899200e+08
0.0075141	3.6182598400e+08
0.0084534	3.6693798400e+08
0.0094479	3.7191001600e+08
0.0104977	3.7674700800e+08
0.0116027	3.8145500800e+08
0.012763	3.8604000000e+08
0.0139785	3.9050800000e+08
0.0152492	3.9486400000e+08
0.0165753	3.9911299200e+08
0.0179565	4.0326000000e+08
0.0193931	4.0731001600e+08
0.0208848	4.1126899200e+08
0.0224319	4.1513900800e+08
0.0240341	4.1892499200e+08
0.0256917	4.2263200000e+08
0.0274044	4.2626201600e+08
0.0291725	4.2981798400e+08
0.0309957	4.3330499200e+08
0.0328743	4.3672400000e+08
0.0348081	4.4008000000e+08
0.0367971	4.4337299200e+08
0.0388414	4.4660800000e+08
0.0409409	4.4978598400e+08
0.0430957	4.5290899200e+08
0.0453057	4.5598000000e+08
0.047571	4.5900000000e+08
0.0498916	4.6197100800e+08
0.0522673	4.6489600000e+08
0.0546984	4.6777500800e+08
0.0571847	4.7061100800e+08
0.0597262	4.7340400000e+08
0.062323	4.7615699200e+08
0.064975	4.7887001600e+08
0.0676823	4.8154499200e+08
0.0704449	4.8418300800e+08
0.0732627	4.8678499200e+08
0.0761357	4.8935299200e+08
0.079064	4.9188700800e+08
0.0820476	4.9438800000e+08
0.0850864	4.9685798400e+08
0.0881804	4.9929699200e+08
0.0913297	5.0170598400e+08
0.0945343	5.0408601600e+08
0.0977941	5.0643801600e+08
0.101109	5.0876300800e+08
0.104479	5.1106099200e+08

```
            0.107905    5.1333200000e+08
            0.111386    5.1557900800e+08
            0.114922    5.1780099200e+08
            0.118513    5.1999801600e+08
             0.12216    5.2217299200e+08
            0.125862    5.2432400000e+08
            0.129619    5.2645299200e+08
            0.133431    5.2856099200e+08
            0.137298    5.3064700800e+08
            0.141221    5.3271200000e+08
            0.145199    5.3475699200e+08
            0.149233    5.3678300800e+08
            0.153321    5.3878899200e+08
            0.157465    5.4077600000e+08
            0.161664    5.4274400000e+08
            0.165918    5.4469401600e+08
            0.170228    5.4662700800e+08
            0.174593    5.4854201600e+08
            0.179013    5.5044102400e+08
            0.183488    5.5232198400e+08
            0.188019    5.5418803200e+08
            0.192605    5.5603699200e+08
            0.197246    5.5787097600e+08
            0.201942    5.5968902400e+08
            0.206694    5.6149196800e+08
              0.2115    5.6328102400e+08
            0.216362    5.6505497600e+08
             0.22128    5.6681497600e+08
            0.226252    5.6856102400e+08
             0.23128    5.7029299200e+08
            0.236363    5.7201203200e+08
            0.241502    5.7371801600e+08
            0.246695    5.7540998400e+08
            0.251944    5.7708998400e+08
            0.257248    5.7875801600e+08
            0.262607    5.8041299200e+08
            0.268022    5.8205702400e+08
            0.273492    5.8368800000e+08
              0.2776    5.8450099200e+08

*INITIAL_VELOCITY_NODE
$#     nid        vx        vy        vz       vxr       vyr       vzr      icid
   2971094       0.0       0.0      -4.0       0.0       0.0       0.0         0
   2971095       0.0       0.0      -4.0       0.0       0.0       0.0         0
   2971096     .........
*END
```

2. Keyword file for Cushion Model 1 with two layers of face sheet and penetrator target.

```
$# LS-DYNA Keyword file created by LS-PrePost(R) V4.6.10 - 19Jun2019
$# Created on Dec-18-2019 (04:25:37)
*KEYWORD
*TITLE_TITLE
$#                                                                  title
M1_HC1_FS1_2L_-Pen
*CONTROL_ACCURACY
$#     osu       inn    pidosu      iacc
         0         4         0         0
*CONTROL_DYNAMIC_RELAXATION
$#  nrcyck     drtol    drfctr    drterm    tssfdr    irelal     edttl    idrflg
      2501.00000E-4     0.995      0.05       0.0         0      0.04         1
*CONTROL_ENERGY
$#    hgen      rwen    slnten     rylen
         2         1         2         1
*CONTROL_SHELL
$#  wrpang     esort     irnxx    istupd    theory       bwc     miter      proj
      20.0         1        -1         0         2         2         1         0
$# rotascl    intgrd    lamsht    cstyp6    thshel
       1.0         0         1         1         0
$# psstupd   sidt4tu     cntco    itsflg    irquad    w-mode   stretch      icrq
         0         0         0         0         2       0.0       0.0         0
$#  nfail1    nfail4   psnfail    keepcs     delfr   drcpsid   drcprm   intperr
         0         0         0         0         0         0       1.0         0
.
.
.
*PART
$#                                                                  title
FACESHEET_2L
$#     pid     secid       mid     eosid      hgid      grav    adpopt      tmid
         2         2         2         0         2         0         0         0
*SECTION_SHELL_TITLE
FACESHEET
$#   secid    elform      shrf       nip     propt   qr/irid     icomp     setyp
         2        16     0.833         4       1.0         0         1         1
$#      t1        t2        t3        t4      nloc     marea      idof    edgset
    0.0018    0.0018    0.0018    0.0018       0.0       0.0       0.0         0
$#      bi        bi        bi        bi        bi        bi        bi        bi
       0.0      90.0     -45.0      45.0       0.0       0.0       0.0       0.0
*MAT_ENHANCED_COMPOSITE_DAMAGE_TITLE
FS1_Dyneema_2L
$#     mid        ro        ea        eb      (ec)      prba    (prca)    (prcb)
         2    1030.01.70800E102.42000E10       0.0     0.312     0.441       0.0
$#     gab       gbc       gca      (kf)      aopt      2way
7.335000E9       0.0       0.0       0.0       2.0       0.0
$#      xp        yp        zp        a1        a2        a3    mangle
       0.0       0.0       0.0       1.0       0.0       0.0       0.0
$#      v1        v2        v3        d1        d2        d3    dfailm    dfails
       0.0       0.0       0.0       0.0       1.0       0.0       1.0       1.0
$#   tfail      alph      soft      fbrt     ycfac    dfailt    dfailc       efs
       0.0       0.0       1.0       0.0       2.0       1.0      -1.0       0.0
$#      xc        xt        yc        yt        sc      crit      beta
2.535000E74.146000E72.390000E76.549000E72.045000E7      54.0       0.0
$#     pel      epsf      epsr      tsmd     soft2
```

```
       0.0       0.0       0.0       0.9       1.0
$#  slimt1    slimc1    slimt2    slimc2     slims    ncyred     softg
       0.0       0.0       0.0       0.0       0.0       0.0       1.0
*HOURGLASS_TITLE
FACESHEET HOURGLASS
$#    hgid       ihq        qm       ibq        q1        q2    qb/vdc        qw
         2         8       0.1         0       1.5      0.06       0.1       0.1
.
.
.
*END
```

3. Keyword file for Cushion Model 2 with one layer face sheet with standoffs, frame and penetrator target.

```
$# LS-DYNA Keyword file created by LS-PrePost(R) V4.6.10 - 19Jun2019
$# Created on Jan-20-2020 (04:25:37)
*KEYWORD
*TITLE_TITLE
$#                                                                  title
M2_HC1_FS1_1L_Frame-Pen
*CONTROL_ACCURACY
$#     osu       inn    pidosu      iacc
         0         4         0         0
*CONTROL_DYNAMIC_RELAXATION
$#  nrcyck     drtol    drfctr    drterm    tssfdr    irelal     edttl    idrflg
      2501.00000E-4     0.995      0.05       0.0         0      0.04         1
*CONTROL_ENERGY
$#    hgen      rwen    slnten     rylen
         2         1         2         1
*CONTROL_SHELL
$#  wrpang     esort     irnxx    istupd    theory       bwc     miter      proj
      45.0         0        -1         0         2         2         1         0
$# rotascl    intgrd    lamsht    cstyp6    thshel
       1.0         0         1         1         0
$# psstupd   sidt4tu     cntco    itsflg    irquad    w-mode   stretch      icrq
         0         0         0         0         2       0.0       0.0         0
$#  nfail1    nfail4   psnfail    keepcs     delfr   drcpsid    drcprm   intperr
         0         0         0         0         0         0       1.0         0
*CONTROL_TERMINATION
$#  endtim    endcyc     dtmin    endeng    endmas     nosol
       0.1         0      0.05       0.0       0.0         0
.
.
.
*CONTACT_TIED_NODES_TO_SURFACE_ID
$#     cid                                                          title
         5Standoffs_Frame
$#    ssid      msid     sstyp     mstyp    sboxid    mboxid       spr       mpr
         2         7         4         3         0         0         0         0
$#      fs        fd        dc        vc       vdc    penchk        bt        dt
       0.0       0.0       0.0       0.0       0.0         0  0.01.00000E20
$#     sfs       sfm       sst       mst      sfst      sfmt      fsf       vsf
       1.0       1.0       0.0       0.0       1.0       1.0       1.0       1.0
*CONTACT_TIED_NODES_TO_SURFACE_ID
$#     cid                                                          title
         6Standoffs_MP
$#    ssid      msid     sstyp     mstyp    sboxid    mboxid       spr       mpr
         1         6         4         3         0         0         0         0
$#      fs        fd        dc        vc       vdc    penchk        bt        dt
       0.0       0.0       0.0       0.0       0.0         0  0.01.00000E20
$#     sfs       sfm       sst       mst      sfst      sfmt      fsf       vsf
       1.0       1.0       0.0       0.0       1.0       1.0       1.0       1.0
*CONTACT_AUTOMATIC_NODES_TO_SURFACE_ID
$#     cid                                                          title
         9Frame-MP
$#    ssid      msid     sstyp     mstyp    sboxid    mboxid       spr       mpr
         3         6         4         3         0         0         0         0
$#      fs        fd        dc        vc       vdc    penchk        bt        dt
       0.0       0.0       0.0       0.0       0.0         0  0.01.00000E20
```

```
$#     sfs       sfm       sst       mst      sfst      sfmt       fsf       vsf
       1.0       1.0       0.0       0.0       1.0       1.0       1.0       1.0
*CONTACT_TIED_NODES_TO_SURFACE_ID
$#     cid                                                                 title
         8FS_GP
$#    ssid      msid     sstyp     mstyp    sboxid    mboxid       spr       mpr
         5         5         4         3         0         0         0         0
$#      fs        fd        dc        vc       vdc    penchk        bt        dt
       0.0       0.0       0.0       0.0       0.0         0       0.01.00000E20
$#     sfs       sfm       sst       mst      sfst      sfmt       fsf       vsf
       1.0       1.0       0.0       0.0       1.0       1.0       1.0       1.0
*CONTACT_TIED_NODES_TO_SURFACE_ID
$#     cid                                                                 title
        10Frame_GP
$#    ssid      msid     sstyp     mstyp    sboxid    mboxid       spr       mpr
         4         5         4         3         0         0         0         0
$#      fs        fd        dc        vc       vdc    penchk        bt        dt
       0.0       0.0       0.0       0.0       0.0         0       0.01.00000E20
$#     sfs       sfm       sst       mst      sfst      sfmt       fsf       vsf
       1.0       1.0       0.0       0.0       1.0       1.0       1.0       1.0
.
.
.
*PART
$#                                                                      title
STANDOFFS
$#     pid     secid       mid     eosid      hgid      grav    adpopt      tmid
         4         4         4         0         0         0         0         0
*SECTION_SOLID_TITLE
STANDOFFS
$#   secid    elform       aet
         4         1         0
*MAT_PIECEWISE_LINEAR_PLASTICITY_TITLE
Standoffs~GP_10_47
$#     mid        ro         e        pr      sigy      etan      fail      tdel
         4    2684.97.03300E10      0.335.965000E7       0.0       0.0       0.0
$#       c         p      lcss      lcsr        vp
       0.0       0.0        10         0       0.0
$#    eps1      eps2      eps3      eps4      eps5      eps6      eps7      eps8
       0.0       0.0       0.0       0.0       0.0       0.0       0.0       0.0
$#     es1       es2       es3       es4       es5       es6       es7       es8
       0.0       0.0       0.0       0.0       0.0       0.0       0.0       0.0
.
.
.
*PART
$#                                                                      title
FRAME
$#     pid     secid       mid     eosid      hgid      grav    adpopt      tmid
         7         7         7         0         0         0         0         0
*SECTION_SOLID_TITLE
FRAME
$#   secid    elform       aet
         7         1         0
*MAT_PIECEWISE_LINEAR_PLASTICITY_TITLE
Frame_Al_7075_102
$#     mid        ro         e        pr      sigy      etan      fail      tdel
         7    2795.77.17100E10      0.335.178000E8       0.0       0.0       0.0
```

```
$#       c         p      lcss      lcsr        vp
       0.0       0.0        12         0       0.0
$#    eps1      eps2      eps3      eps4      eps5      eps6      eps7      eps8
       0.0       0.0       0.0       0.0       0.0       0.0       0.0       0.0
$#     es1       es2       es3       es4       es5       es6       es7       es8
       0.0       0.0       0.0       0.0       0.0       0.0       0.0       0.0

*DEFINE_CURVE_TITLE
.
.
.
*DEFINE_CURVE_TITLE
Stress-Strain_102_ALUMINUM 7075-T651 PLATE
$#    lcid      sidr       sfa       sfo      offa      offo    dattyp     lcint
        12         0       1.0       1.0       0.0       0.0         0         0
$#                a1                  o1
                  0.0    5.1784163200e+08
    2.4435643354e-05    5.1798972800e+08
    7.3306931881e-05    5.1828460800e+08
    1.4661386376e-04    5.1872352000e+08
    2.4435642990e-04    5.1930259200e+08
    3.6653463030e-04    5.2001673600e+08
    5.1314849406e-04    5.2085993600e+08
    6.8419799209e-04    5.2182537600e+08
    8.7968312437e-04    5.2290560000e+08
           0.0010996    5.2409270400e+08
            0.001344    5.2537846400e+08
           0.0016128    5.2675462400e+08
            0.001906    5.2821283200e+08
           0.0022236    5.2974492800e+08
           0.0025657    5.3134300800e+08
           0.0029323    5.3299948800e+08
           0.0033232    5.3470710400e+08
           0.0037387    5.3645910400e+08
           0.0041785    5.3824908800e+08
           0.0046428    5.4007123200e+08
           0.0051315    5.4192006400e+08
           0.0056446    5.4379065600e+08
           0.0061822    5.4567840000e+08
           0.0067442    5.4757932800e+08
           0.0073307    5.4948960000e+08
           0.0079416    5.5140595200e+08
           0.0085769    5.5332544000e+08
           0.0092367    5.5524537600e+08
           0.0099209    5.5716339200e+08
           0.0106295    5.5907737600e+08
           0.0113626    5.6098553600e+08
           0.0121201    5.6288627200e+08
            0.012902    5.6477811200e+08
           0.0137084    5.6665990400e+08
           0.0145392    5.6853049600e+08
           0.0153945    5.7038905600e+08
           0.0162741    5.7223475200e+08
           0.0171783    5.7406700800e+08
           0.0181068    5.7588512000e+08
           0.0190598    5.7768876800e+08
           0.0200372    5.7947744000e+08
           0.0210391    5.8125094400e+08
           0.0220654    5.8300902400e+08
```

```
            0.0231161    5.8475148800e+08
            0.0241913    5.8647820800e+08
            0.0252909    5.8818905600e+08
            0.0264149    5.8988403200e+08
            0.0275634    5.9156313600e+08
            0.0287363    5.9322636800e+08
            0.0299337    5.9487385600e+08
            0.0311554    5.9650553600e+08
            0.0324017    5.9812160000e+08
            0.0336723    5.9972217600e+08
            0.0349674    6.0130732800e+08
            0.0362869    6.0287724800e+08
            0.0376309    6.0443200000e+08
            0.0389993    6.0597190400e+08
            0.0403921    6.0749696000e+08
            0.0418094    6.0900742400e+08
            0.0432511    6.1050348800e+08
            0.0447172    6.1198534400e+08
            0.0462078    6.1345312000e+08
            0.0477228    6.1490700800e+08
            0.0492623    6.1634726400e+08
            0.0508261    6.1777408000e+08
            0.0524145    6.1918758400e+08
            0.0540272    6.2058796800e+08
            0.0556644    6.2197555200e+08
             0.057326    6.2335040000e+08
            0.0590121    6.2471270400e+08
            0.0607226    6.2606272000e+08
            0.0624575    6.2740064000e+08
            0.0642169    6.2872659200e+08
            0.0660007    6.3004076800e+08
            0.0678089    6.3134336000e+08
            0.0696416    6.3263462400e+08
            0.0714987    6.3391462400e+08
            0.0733802    6.3518361600e+08
            0.0752862    6.3644166400e+08
            0.0772166    6.3768908800e+08
            0.0791715    6.3892595200e+08
            0.0811508    6.4015244800e+08
            0.0831545    6.4136870400e+08
            0.0851827    6.4257497600e+08
            0.0872352    6.4377132800e+08
            0.0893123    6.4495788800e+08
            0.0914137    6.4613491200e+08
            0.0935396    6.4730246400e+08
              0.09569    6.4846080000e+08
            0.0978647    6.4960992000e+08
             0.100064    6.5075001600e+08
            0.1022876    6.5188121600e+08
            0.1045357    6.5300371200e+08
            0.1068082    6.5411756800e+08
            0.1091051    6.5522297600e+08
            0.1114265    6.5632000000e+08
            0.1137724    6.5740876800e+08
            0.1161426    6.5848947200e+08
            0.1185373    6.5956217600e+08
            0.1209564    6.6062700800e+08
               0.1294    6.6115782400e+08
*END
```

```
*****************************************************************************
*                                The Laminator                                *
*                  Analysis of Composite Laminates Based on                   *
*                      Classical Laminated Plate Theory                       *
*****************************************************************************
```

Material 1: Dyneema-Epoxy, Vf=60%,1L

Engineering Properties
****

Matl	E1	E2	G12	v12
1	7.129e+010	3.465e+009	3.913e+009	0.330

Thermal and Moisture Properties
****

Matl	CTE1	CTE2	CME1	CME2
1	0.000e+000	0.000e+000	0.000e+000	0.000e+000

Stacking Sequence
****

Layer	Matl	Ply Angle	Ply Thickness
1	1	0.0	2.250e-001
2	1	90.0	2.250e-001

Total Laminate Thickness :			4.500e-001

Laminate Matrices
****

'ABD' Matrix

1.691e+010	5.173e+008	1.996e-006	-1.726e+009	0.000e+000	2.246e-007
5.173e+008	1.691e+010	2.279e-005	0.000e+000	1.726e+009	2.564e-006
1.996e-006	2.279e-005	1.761e+009	2.246e-007	2.564e-006	0.000e+000
-1.726e+009	0.000e+000	2.246e-007	2.853e+008	8.729e+006	3.369e-008
0.000e+000	1.726e+009	2.564e-006	8.729e+006	2.853e+008	3.846e-007
2.246e-007	2.564e-006	0.000e+000	3.369e-008	3.846e-007	2.971e+007

'ABD' Inverse

1.549e-010	-4.740e-012	-2.339e-025	9.372e-010	1.195e-026	-1.825e-024
-4.740e-012	1.549e-010	-6.354e-025	-6.462e-027	-9.372e-010	-1.203e-024
-2.339e-025	-6.354e-025	5.679e-010	-1.825e-024	-1.203e-024	7.423e-038
9.372e-010	3.231e-027	-1.825e-024	9.182e-009	-2.809e-010	-1.386e-023
2.389e-026	-9.372e-010	-1.203e-024	-2.809e-010	9.182e-009	-3.765e-023
-1.825e-024	-1.203e-024	7.423e-038	-1.386e-023	-3.765e-023	3.365e-008

Apparent Laminate Stiffness Properties
****

EX	EY	GXY	EXB	EYB
1.434e+010	**1.434e+010**	**3.913e+009**	1.434e+010	1.434e+010

Apparent Laminate Coupling Coefficients
(Poisson and Shear Coupling)
****

vXY	vYX	nXY,X	nXY,Y	nX,XY	nY,XY
0.031	**0.028**	0.000	0.000	0.000	0.000

Apparent Laminate Thermal and Moisture Properties
****

CTEX	CTEY	CTEXY	CMEX	CMEY	CMEXY
0.000e+000	0.000e+000	0.000e+000	0.000e+000	0.000e+000	0.000e+000

Apparent Laminate Strength for First Ply Failure
Under Unidirectional Loading: +/-NX, +/-NY, NXY
****

Failure Theory	X-Axis Tension	X-Axis Compression	Y-Axis Tension	Y-Axis Compression	XY Shear
Max Stress	1.215e+008	-3.855e+007	1.215e+008	-3.855e+007	1.904e+007
Max Strain	1.215e+008	-3.870e+007	1.215e+008	-3.870e+007	1.904e+007
Tsai-Hill	1.197e+008	-3.877e+007	1.197e+008	-3.877e+007	1.904e+007
Hoffman	1.194e+008	-3.855e+007	1.194e+008	-3.855e+007	1.904e+007
Tsai-Wu	**1.191e+008**	**-3.863e+007**	**1.191e+008**	**-3.863e+007**	**1.904e+007**

```
*****************************************************************************
*                                The Laminator                                *
*                  Analysis of Composite Laminates Based on                   *
*                      Classical Laminated Plate Theory                       *
*****************************************************************************

Material 1: Dyneema-Epoxy, Vf=60%,2L

Engineering Properties
**********************

Matl          E1           E2          G12         v12

  1      7.129e+010   3.465e+009   3.913e+009    0.330

Thermal and Moisture Properties
*******************************

Matl         CTE1         CTE2         CME1         CME2

  1      0.000e+000   0.000e+000   0.000e+000   0.000e+000

Stacking Sequence
*****************

 Layer     Matl      Ply Angle      Ply Thickness

   1         1           0.0         2.250e-001
   2         1          90.0         2.250e-001
   3         1         -45.0         2.250e-001
   4         1          45.0         2.250e-001
                                     ----------
Total Laminate Thickness :           9.000e-001

Laminate Matrices
*****************
                                 'ABD' Matrix

  2.738e+010   7.470e+009   1.907e-006   -3.174e+009   1.448e+009   8.630e+008
  7.470e+009   2.738e+010   2.289e-005    1.448e+009   2.780e+008   8.630e+008
  1.907e-006   2.289e-005   9.957e+009    8.630e+008   8.630e+008   1.448e+009

 -3.174e+009   1.448e+009   8.630e+008    2.625e+009   5.042e+008   3.883e+008
  1.448e+009   2.780e+008   8.630e+008    5.042e+008   1.072e+009   3.883e+008
  8.630e+008   8.630e+008   1.448e+009    3.883e+008   3.883e+008   6.721e+008

                                 'ABD' Inverse

  6.505e-011  -2.026e-011   1.217e-011    1.212e-010  -1.186e-010  -8.525e-011
 -2.026e-011   4.590e-011   6.981e-012   -5.537e-011   5.272e-011  -4.643e-011
  1.217e-011   6.981e-012   1.515e-010    1.676e-011  -2.206e-011  -3.479e-010

  1.212e-010  -5.537e-011   1.676e-011    6.669e-010  -3.710e-010  -2.916e-010
 -1.186e-010   5.272e-011  -2.206e-011   -3.710e-010   1.450e-009  -4.914e-010
 -8.525e-011  -4.643e-011  -3.479e-010   -2.916e-010  -4.914e-010   2.859e-009

Apparent Laminate Stiffness Properties
**************************************
```

EX	EY	GXY	EXB	EYB
1.708e+010	**2.421e+010**	**7.335e+009**	2.468e+010	1.135e+010

Apparent Laminate Coupling Coefficients
(Poisson and Shear Coupling)
****

vXY	vYX	nXY,X	nXY,Y	nX,XY	nY,XY
0.312	**0.441**	0.187	0.152	0.080	0.046

Apparent Laminate Thermal and Moisture Properties
****

CTEX	CTEY	CTEXY	CMEX	CMEY	CMEXY
0.000e+000	0.000e+000	0.000e+000	0.000e+000	0.000e+000	0.000e+000

Apparent Laminate Strength for First Ply Failure
Under Unidirectional Loading: +/-NX, +/-NY, NXY
****

Failure Theory	X-Axis Tension	X-Axis Compression	Y-Axis Tension	Y-Axis Compression	XY Shear
Max Stress	3.252e+007	-3.252e+007	5.267e+007	-2.397e+007	2.011e+007
Max Strain	3.252e+007	-3.252e+007	5.267e+007	-2.397e+007	2.011e+007
Tsai-Hill	3.243e+007	-3.923e+007	5.256e+007	-2.393e+007	2.010e+007
Hoffman	4.132e+008	-2.529e+007	6.532e+007	-2.390e+007	2.064e+007
Tsai-Wu	**4.146e+007**	**-2.535e+007**	**6.549e+007**	**-2.390e+007**	**2.045e+007**

References

[1] A.S.M.Ayman Ashab. "Finite Element Analysis of Aluminum Honeycomb Subjected to Dynamic Indentation and Compression Loads". In: (2016).

[2] Michael F Ashby. *Materials Selection in Mechanical Design*. 3rd ed. Elsevier Butterworth-Heinemann: Amsterdam, Boston, 2005.

[3] TN Bitzer. *Honeycomb technology: materials, design, manufacturing, applications and testing*. Springer Science & Business Media, 1997.

[4] Issac M. Daniel and Ori Ishai. *Engineering Mechanics of Composite Materials*. second. 2006.

[5] Lorna J Gibson and Michael F Ashby. *Cellular solids: structure and properties*. Cambridge university press, 1999.

[6] Christian D Grimm et al. "Size matters – The shell lander concept for exploring medium-size airless bodies". In: *Acta Astronautica* (2020).

[7] Gurit. *Guide to composites*. 2020. URL: https://www.gurit.com/Our-Business/Composite-Materials.

[8] Hexcel. *Honeycomb sandwich design technology. Technology manuals*. 2020. URL: https://www.hexcel.com/Resources/Technology-Manuals.

[9] Verena Knappe. "Correlation and evalution of a finite element model using solid Elements for the Virtual Testing of the Touchdown Behaviour of a Robotic Landing Platform with a Crushable Shock Absorber". Diplomarbeit. RWTH, DLR, 2013.

[10] Livermore Software Technology Corporation (LSTC). *LS-DYNA Keyword User's Manual, Volume-I, R11*. Ed. by editor. 2018. URL: https://www.dynasupport.com/manuals (visited on 2020).

[11] Livermore Software Technology Corporation (LSTC). *Livermore Software Technology Corporation (LSTC), LS-DYNA Theory Manual*. Ed. by editor. 2006. URL: https://www.dynasupport.com/manuals (visited on 2020).

[12] Livermore Software Technology Corporation (LSTC). *LS-DYNA Keyword User's Manual, Volume-II, Material Models, R6.1.0*. Ed. by editor. 2012. URL: https://www.dynasupport.com/manuals (visited on 2020).

[13] Material Science Coperation. *Composite Material Handbook, Polymer Matrix Composite Materials Usage Design and Analysis*. Vol. 3. MIL-HDBK-17. 1997.

[14] Frank Meyer. "Korrelation und Bewertung eines FE-Modells zum virtuellen Testen des Crashverhaltens von Aluminium-Honigwaben-Sandwichstrukturen innerhalb des Marslander-Projektes". Masterarbeit. TU Braunschweig, DLR, 2014.

[15] Achilles Petras. "Design of sandwich structures". Ph.D Dissertation. Cambridge University, 1998.

[16] Bianca Reihnhardt. "Touchdown Simulation, Testing and Validation of a Marslander Demonstrator". Master Thesis. University of Bremen, Faser institute, Bremen, 2014.

[17] Bianca Reinhardt. "Experimental investigation and evaluation of crash behaviour of a planetary landing platform using crushable layers of Aluminum Honeycombs". Bachelor Thesis. DLR, Astrium, 2012.

[18] Silvio Schröder. "A Crushable Shell for Small Body Landers". In: *CEAS Space Journal 12 65-72* (2019).

[19] Magda Stanczak. "Numerical Modelling of honeycomb structure subjected to blast loading". In: *12th European LS-Dyna Conference, Koblenz, Germany* (Koblenz, Germany). DYNAmore GmbH. 2019.